Subspace-based damage detection in engineering structures considering reference uncertainties and temperature effects

Eva Viefhues

DOCTORAT BRETAGNE LOIRE / MATHSTIC

UNIVERSITÉ DE RENNES 1

THÈSE DE DOCTORAT DE

L'UNIVERSITÉ DE RENNES 1

ÉCOLE DOCTORALE N° 601
Mathématiques et Sciences et Technologies de l'Information et de la Communication
Spécialité : *signal, image, vision*

Par
Eva VIEFHUES

Subspace-based damage detection in engineering structures considering reference uncertainties and temperature effects

Thèse présentée et soutenue à Rennes, le 14/12/2021
Unité de recherche : Inria Rennes

Rapporteurs avant soutenance :

Peter KRAEMER	Professeur, University of Siegen, Allemagne
Julien WAEYTENS	Chargé de recherche, Université Gustave Eiffel

Composition du Jury :

Président :	Maria Pina LIMONGELLI	Professeur, Politecnico di Milano, Italie
Rapporteurs :	Peter KRAEMER	Professeur, University of Siegen, Allemagne
	Julien WAEYTENS	Chargé de recherche, Université Gustave Eiffel
Examinateurs :	Michael DÖHLER	Chargé de recherche, Inria Rennes
	Falk HILLE	Chercheur, BAM Federal Institute for Materials Research and Testing, Allemagne
Dir. de thèse :	Laurent MEVEL	Directeur de recherche, Inria Rennes

Acknowledgement

This thesis was written during my scientific work in the Division *Buildings and Structures* at the Federal Institute for Materials Research and Testing (BAM) and in very close cooperation with the research institute Inria Rennes (France). I would like to express my sincere thanks for the financial support from BAM - especially to my superiors Matthias Baeßler and Andreas Rogge, who offered me the opportunity to do research in this exciting field. Gratitude is also owed to the DAAD for the mobility grant within the Procope program making two research trips to Inria Rennes possible.

I am particularly grateful to my supervisor Laurent Mevel from the I4S team at Inria Rennes. In many fruitful discussions I could learn from his comprehensive knowledge in the field of statistics which enabled me to do research in this borderline area between statistics and civil engineering. To my co-supervisor Michael Döhler from the I4S team I would like to express my heartfelt thanks for his great support and mentoring. He not only inspired the research proposal, but also provided guidance through the challenges of the research process and was open for discussions at any time. The very frequent and reliable exchange with him has enabled me to take a critical yet constructive look at my results. With his wide knowledge in the research field, his ability to make complex things simple, and his openness and positivity it was always a great pleasure to work with him. Thanks also go to Julien Waeytens and Yann Lecieux who, as jury members of the CSID, encouraged me in my development as a PhD student.

Furthermore, I would like to thank my colleagues at BAM. Especially my supervisor Falk Hille helped me in many constructive discussions with his great experience to always look at the problems and results also from the user's point of view. I would like to thank Fred Ziegler for his support in implementing the experiments on the test bridge. Likewise, I am very thankful to Patrick Simon for putting up with extra work during his experiments in the climate chamber to make it possible to provide experimental data for my purposes. I thank my colleagues in the SHM group for the interesting technical and personal exchange. It was a great pleasure to be able to learn from their experiences, some of them of many years, and to get involved in some of their exciting projects. I also enjoyed the many friendly conversations with the other colleagues and especially with my roommate Borana

Kullolli. I would like to thank Simone Morawietz and Margrit Kaiser for their great organizational support.

I am very grateful to my reviewers, Peter Kraemer from the University of Siegen and Julien Waeytens from the University Gustave Eiffel, for their high interest in my work. Through their constructive comments also in the run-up to the defense and in the exciting discussions about the results, I was able to learn further from their great experience. I would like to thank them and Maria Pina Limongelli very much for taking the time to be the jury for my thesis defense. It is a great pleasure to have had the opportunity to meet them.

Finally, I would like to thank my family and friends for their support and words of encouragement. A special thanks is due to my parents who have always encouraged me in my life choices. Their personal commitment, especially in the last two years during the pandemic, made it possible for me to finish this work. Likewise, I would like to extend a very special thank you to my husband and children. Without their tireless support, patience, understanding and cheerfulness, I would never have been able to complete this work.

Table of Contents

Table of Contents iii

List of figures vii

List of tables x

Notation xiii

Introduction 1

Context of the work . . . 1
Chosen method . . . 2
Contribution to the research field . . . 3
Outline of the work . . . 5

I Preliminaries 7

1 State of the art 9

1.1 Introduction . . . 9
1.2 Vibration-based damage diagnosis concepts . . . 10
1.3 Feature evaluation and related uncertainties . . . 16
1.4 Data-based damage detection under changing environmental conditions . . . 20
1.4.1 Methods with relation to measured environmental parameters . . . 21
1.4.2 Methods with unmeasured environmental conditions . . . 22

2 Background theory 27

2.1 Introduction . . . 27
2.2 Structural dynamics of output-only systems . . . 28
2.3 System identification . . . 29
2.3.1 Concept of stochastic subspace identification . . . 29
2.3.2 Covariance-driven subspace identification . . . 31

2.3.3 Identification of the eigenstructure 31
2.4 Stochastic subspace-based damage detection 32
2.4.1 Subspace-based residual function 33
2.4.2 Statistical damage testing 34
2.4.3 Asymptotic residual covariance 36
2.4.4 Decision making from test results 37
2.5 Considerations for uncertainty computation 39
2.5.1 Mathematical remarks 39
2.5.2 Concept of uncertainty propagation 40
2.5.3 Relevant uncertainty computations from literature 41
2.6 Model interpolation of linear parameter varying systems 44
2.6.1 Concept 45
2.6.2 Model interpolation 45
2.7 Summary 46

II Contribution to theory 47

3 Stochastic subspace-based damage detection with uncertain reference null space 49
3.1 Introduction 49
3.2 Damage detection with uncertain reference 50
3.2.1 Formalized problem statement 50
3.2.2 Asymptotic distribution of the residual 52
3.2.3 Asymptotic covariance of the residual 54
3.2.4 Test statistic 58
3.3 Proof of concept and discussion 59
3.3.1 Study setup 60
3.3.2 Statistical properties and test performance 61
3.3.3 Data length in the reference state 63
3.3.4 Data length of the testing data set 66
3.3.5 System parametrization 68
3.3.6 Reference null space computed from observability matrix 70
3.4 Summary 71
3.5 Dissemination 72

4 Stochastic subspace-based damaged detection under changing environmental conditions 75
4.1 Introduction . . . 75
4.2 Damage detection robust to temperature effects . . . 76
4.2.1 Formalized problem statement . . . 76
4.2.2 Parameter adapted reference null space . . . 79
4.2.3 Residual function and statistical evaluation . . . 83
4.2.4 Residual covariance . . . 84
4.2.5 Discussion and comparison to previous approaches . . . 86
4.3 Proof of concept and discussion . . . 87
4.3.1 Study setup . . . 88
4.3.2 Damage detection under changing temperatures . . . 89
4.3.3 Covariance computation from test data . . . 93
4.3.4 Considerations for reference setup . . . 94
4.3.5 Effects of changes in the excitation covariance . . . 96
4.4 Summary . . . 97
4.5 Dissemination . . . 98

III Applications 101

5 Damage detection of a steel frame considering uncertainties in the reference matrix 103
5.1 Introduction . . . 103
5.2 Experimental setup and dynamical properties . . . 104
5.3 Damage detection with uncertain reference null space . . . 106
5.4 Summary . . . 109
5.5 Dissemination . . . 109

6 Damage detection of a temperature affected laboratory beam structure 111
6.1 Introduction . . . 111
6.2 Experimental setup and dynamical properties . . . 112
6.3 Damage detection with temperature effects . . . 113
6.4 Summary . . . 119
6.5 Dissemination . . . 119

7 Damage detection of a testing bridge exposed to ambient temperature variations **121**
7.1 Introduction . . . 121
7.2 Experimental setup and dynamical properties of the structure . . . 122
7.3 Damage detection with temperature effects . . . 125
7.3.1 General settings and temperature effect . . . 125
7.3.2 Robust damage detection . . . 127
7.3.3 Effect of reference setup . . . 128
7.4 Summary . . . 131
7.5 Dissemination . . . 132

Conclusion **133**
Considered aspects . . . 133
Summary, improvements and limits . . . 133
Outlook . . . 136

Resume in French **139**

Bibliography **151**

List of Figures

1 Westend bridge and excitation device of EMPA [Roh+00b]. 1

1.1 Damage detection procedure. 11
1.2 Classification concept. 12

2.1 χ^2-distribution for different parameters (left) and definition of threshold (right). 38
2.2 Typical receiver operating characteristic curve. 39

3.1 Mass-spring chain with four sensors. 60
3.2 Theoretical χ^2-distribution and histograms of the new test statistics and the conventional test with $\Sigma_1 = 0$, $M = 50{,}000$, $N = 100{,}000$. 61
3.3 Histogram in the reference and the damaged state of the conventional (left) and the new test (right), $M = 50{,}000$, $N = 100{,}000$, damage = 2%. 62
3.4 POD (left) and ROC diagram with damage of 2% (right) of the conventional and the new test, $M = 50{,}000$, $N = 100{,}000$. 63
3.5 Empirical mean of conventional and new tests for different data lengths M, $N = 100{,}000$. 64
3.6 Histogram in the reference and the damaged state of the conventional (left) and the new test (right) for different M, $N = 100{,}000$, damage = 2%. . . . 65
3.7 POD of conventional and new test for different M, $N = 100{,}000$, damage = 1.4%. 65
3.8 POD (left) and ROC diagram with damage of 2% (right) of the conventional and the new test, $M = 500{,}000$, $N = 100{,}000$. 66
3.9 Histogram in the reference and the damaged state of the conventional (left) and the new test (right) for different N, $M = 100{,}000$, damage = 2%. . . . 67
3.10 POD of conventional and new test for different N, $M = 100{,}000$, damage = 2%. 67

3.11 Empirical mean of conventional and new tests for different data lengths M for a system parametrized with respect to structural parameters, N = 100,000. 69
3.12 POD of conventional and new test for a system parametrized with respect to structural parameters for M = 50,000 (left) and M = 500,000 (right), N = 100,000. 69
3.13 POD of conventional and new test with non parametric test for M = 50,000 (left) and M = 500,000 (right), N = 100,000. 69
3.14 Empirical mean of conventional and new tests for different data lengths M when the reference null space is computed from observability matrix, N = 100,000. 70
3.15 POD of conventional and new test when the reference null space is computed from observability matrix for M = 50,000 (left) and M = 500,000 (right), N = 100,000. 71

4.1 Determination of weights at parameter working points for any P from a Gaussian function. 80
4.2 Mass-spring chain and temperature dependent stiffness. 88
4.3 Test values at different testing temperatures computed from a single reference data set at 10°C for the whole temperature range (left) and with zoom on the temperatures close to the reference temperature (right). . . . 89
4.4 Test values at different testing temperatures computed with the *average approach* [Bal+08a]. 90
4.5 Test values at different testing temperatures computed with the three strategies of the new method. 91
4.6 Test performance of the average method and the three strategies of the new method. Probability of detection (left) and ROC curves for 0.8 % stiffness reduction (right). 92
4.7 Test values at different testing temperatures when the uncertainties of the reference null space are neglected (left) and ROC curves for 0.8 % stiffness reduction computed with S(H) strategy. 93
4.8 Test values at different testing temperatures when the covariance is computed from the testing data (left) and ROC curves for 0.8 % stiffness reduction computed with S(H) strategy. 94
4.9 Test values at different testing temperatures for different reference setups. 96

4.10 Test values when reference and testing data sets have different excitation covariance, computed with S(H) interpolation (left) and S(O) interpolation (right) strategies. 97

5.1 Laboratory testing structure (left) and sensor positions (right). 104
5.2 Reversible damage detail (left) and screw configuration (right). 105
5.3 Test values of the conventional (left) and the new test (right) in the undamaged reference state computed with different reference data lengths M. 107
5.4 Test values of the conventional (left) and the new test (right) in the reference and at different damaged states. 107
5.5 Test values of the conventional (left) and the new test (right) in the reference and at different damaged states for different N. 108

6.1 Test setup of the concrete beam with locations of geophones, shaker, and loading for the damage introduction. 112
6.2 Concrete beam in the climate chamber. 113
6.3 1st to 4th eigenfrequencies at different system states and at different temperatures. The y-axis is scaled to about 5 % of each frequency. 114
6.4 Fixed reference null space and covariance matrix. Test values at different testing temperatures in the undamaged and damaged states. Reference data at 5°C. 116
6.5 Averaged reference null space and covariance matrix. Test values at different testing temperatures in the undamaged and damage states. Reference data at -25°C, 5°C, and 40°C. 116
6.6 Interpolated reference null space and covariance matrix. Test values at different testing temperatures in the undamaged and damage states. Reference data at -25°C, 5°C, and 40°C. 116
6.7 Effect of weighting function in interpolated reference null space and covariance matrix. Sharp weighting function (top) and wide weighting function (bottom). Test values at different testing temperatures in the undamaged and damaged states. Reference data at -25°C, 5°C, and 40°C. 118

7.1 Testing bridge. 122
7.2 Static system of the testing bridge. 123

7.3 Pre-stressing facility (left) and encased shaker (right). 123
7.4 Test setup testing bridge with geophones and shaker for excitation. 124
7.5 Stabilization diagram at 15°C. 125
7.6 First four modeshapes of the testing bridge. 125
7.7 Temperature effect to the first four eigenfrequencies of the testing bridge. 126
7.8 Test values with reference data from one fixed reference temperature. . . . 127
7.9 Test values of the 4 algorithms for different testing temperatures in the undamaged and the damaged case, computed for reference setup A. 128
7.10 Test values of the 4 algorithms for different testing temperatures in the undamaged case, computed for reference setup B, C, D and E from top to bottom. 129
7.11 Weights for different reference setups with weighting function W1 (left) and with optimized weighting functions (right). 130
7.12 Effect of optimized weighting function to false positives for the interpolation approach in reference setups C, D, and E. 131
1 Histogrammes du test dans les états de référence et endommagé, pour le test conventionnel (gauche) et le nouveau test (droite). 144
2 Probabilité de détection (gauche) and dépendance du test de la longueur de données M dans l'état de référence (droite). 144
3 Valeurs du test pour toutes les strategies développées, ainsi que pour l'approche existante [Bal+08a] aux températures de test variées et les références prises à 0, 5, 10, 15 and 20°C. 145
4 Valeurs du test conventionnel (gauche) et du nouveau test (droite) dans l'état de réference et plusieurs états endommagés. 146
5 Valeurs du test avec la stratégie d'interpolation des matrices Hankel (en haut), et avec l'approche existante [Bal+08a] (en bas). Les données de référence ont été utilisées à -25°C, 5°C, et 40°C. 147
6 Testing bridge. 148
7 Test values of the 4 algorithms for different testing temperatures in the undamaged and the damaged case, computed for reference setup A. 148

List of Tables

4.1 Reference setups 95

5.1 Frequencies of the steel frame in Hz from [Hil18] 106

7.1 Frequencies and damping ratios at 15°C. 125
7.2 Reference setups for testing bridge 128

NOTATION

List of variables

A	state transition matrix
b	bias
C	observation matrix
$\mathbf{C}$	damping matrix
$\mathcal{C}$	controllability matrix
c	ratio of N and M
D_1	diagonal matrix of n singular values of a matrix
D_2	diagonal matrix of noise singular values very close to zero of a matrix
E	selection matrix
e	selection vector
F	selection matrix
f	eigenfrequency
G	cross-covariances between states and output
$\mathcal{H}$	Block Hankel matrix, data matrix in general for SSI
I	identity matrix
$\mathcal{J}_{X1,X2}$	sensitivity of $X1$ with respect to $X2$
$\mathbf{K}$	stiffness matrix
$\mathbf{k}$	stiffness of elements in simulation
L	selection matrices position sensor
M	number of data samples in reference data
$\mathbf{M}$	mass matrix
m	DOF of dynamical system
$\mathbf{m}$	masses of elements in simulation
N	number of data samples in test data
N_b	block length for covariance estimation
n	model order
n_b	number of blocks for covariance estimation

$\mathcal{O}$	observability matrix
P	scheduling parameter
$\mathcal{P}$	permutation matrix
q	displacement at DOF
R	output covariances
r	number of sensors
S	reference null space
T	temperature
t	in the context of system representations: continuous time
t	in the context of hypothesis testing: test statistics
U_1	column space of a matrix
U_2	left null space of a matrix
u	number of available reference data sets / scheduling parameters P
u_i	left singular vector of the Hankel matrx
V_1	row space of a matrix
V_2	null space of a matrix
v	measurement noise
v_i	right singular vector of the Hankel matrix
W	invertible weighting matrix in SSI
w	state noise
x	system state
$\mathcal{Y}$	set of output data
y	output data column vector at one time instance at all sensor locations
Z	SSI algorithm depending factor matrix

γ	change in the residual
Δ	diagonal matrix of Λ
δ	parameter change
ϵ	perturbation magnitude in Taylor approximation
ζ	subspace-based residual (see also explanation of $\tilde{\boxdot}$)
θ	parameter vector, contains e.g. the modal parameters
θ^*	parameter vector in the reference state
Λ	vector of eigenvalues λ
λ	in the context of system identification: eigenvalue of A in discrete state-space system

λ	in the context of hypothesis test: non-centrality parameter
μ	eigenvalue of system in continuous time
ν	in the context of equation of motion: excitation function
ν	in the context of χ^2-distribution: degree of freedom
ξ	damping ratio
ρ	weighting function for interpolation
Σ_X	covariance matrix of random variable X
σ_i	singular value of the Hankel matrix
σ^2	variance of the Gaussian weighting function
τ	time increment
Φ	matrix with eigenvectors ϕ
ϕ	eigenvector of A in discrete state-space system
φ	mode shape
χ	left eigenvector of A in discrete state-space system
Ψ	matrix with mode shapes φ
ω	angular frequency

List of indices

a	acceleration
c	separated into conjugate complex pairs
d	displacement
i	counting variable
j	counting variable
k	time index
l	counting variable
p	size parameter, e.g. p+1 is number of block rows in Hankel matrix $\mathcal{H}$
q	size parameter, e.g. number of block columns in Hankel matrix $\mathcal{H}$
(s)	counting variable
s	number of columns of S
t	number of rows of S
v	velocity

List of symbols

^{T}	transposed
†	pseudoinverse
Δ	perturbation
$\otimes$	Kronecker product
$\mathcal{N}$	Normal distribution
cov	covariance
vec	stacking operator
E	expectation
Re	real part of a complex number or matrix
Im	imaginary part of a complex number or matrix
$\widehat{\boxdot}$	estimate of $\boxdot$
$\dot{\boxdot}$	derivation of $\boxdot$ with respect to time
$\boxdot'$	derivation of $\boxdot$ with respect to variable
$\bar{\boxdot}$	mean of $\boxdot$
$\underline{\boxdot}$	interpolated version of $\boxdot$
$\tilde{\boxdot}$	variable $\boxdot$ belongs to residual with consideration of uncertainty in the reference null space

List of acronyms

AR	autoregressive
ARMA	autoregressive moving average
ARX	autoregressive model with exogenous inputs
CCP-VARX	constant coefficient pooled vector autoregressive with exogenous variables
COMAC	coordinate modal assurance criterion
DOF	degrees of freedom
ERA	eigensystem-realization-algorithm
EMPA	Eidgenössische Materialprüfungs- und Forschungsanstalt
FE	finite element
FP-VARX	functionally pooled vector autoregressive with exobenous variables
FRF	frequency response function
GMM	Gaussian mixture model
GLR	generalized likelihood ratio

IDDM	interpolated damage detection method
LPV	linear parameter varying system
LSWT	lag shifted whiteness test
LTI	linear time-invariant
MAC	modal assurance criterion
MAF	moving average filter
MCD	minimum covariance determinant
MD	Mahalanobis distance
MEWMA	multivariate exponentially weighted moving average
MMSE	minimum mean square error
MPC	modal phase collinearity
MVEE	maximum volume enclosing ellipsoid
PCA	principle component analysis
PCE	polynomial chaos expansion
PFA	probability of false alarms
POD	probability of detection
PSD	power spectral density
ROC	receiver operating characteristic
SDDLV	stochastic dynamic damage locating vector
SHM	structural health monitoring
SSDD	stochastic subspace-based damage detection
SSI	stochastic subspace identification
SVD	singular value decomposition

INTRODUCTION

Context of the work

Structural health monitoring (SHM) can be understood as the strategy to provide periodically updated information on the condition or damage state of a mechanical structure. Since the 1990s research on vibration-based methods for automated damage diagnosis of engineering structures increased rapidly. Some effort was made in continuous monitoring strategies, since many structures reached the end of their calculated life cycle and construction methods from the 1960s with insufficient evaluation of their critical details led to deteriorating conditions. One example is the long-term monitoring of the highway Westend bridge in Berlin (Germany) in Fig. 1 that was started in 2000 by the German Federal Institute for Materials Research and Testing (BAM) and is still ongoing [BHS16; Hu+15].

The vibration-based methods are inspired by the developments in condition monitoring from aerospace and offshore oil industries. The principle is based on the fact that the dynamical behavior of a structure is affected by damage altering its stiffness, mass

Figure 1 – Westend bridge and excitation device of EMPA [Roh+00b].

or damping properties, which is reflected in the measured vibration response of the system. Following the Fundamental Axioms of Structural Health Monitoring introduced by Worden et al. in [Wor+07], the structure condition is monitored by extracting damage sensitive features from vibration measurements and comparing the feature value in a (healthy) reference state to the value in the current testing state. Such automated SHM procedures can complement and partly replace the obligatory visual inspections of engineering structures by possibly continuous information, also at locations that are difficult to reach, and thus help to guarantee high infrastructure integrity.

However, special conditions have to be considered for the application of vibration-based damage diagnosis to engineering structures. On one hand, the monitoring setup must consider rough environmental conditions and poor accessibility requiring new sensor techniques [Leo06; SSS10]. It must be designed for a limited number of sensors that can be placed on a large-scale and often complex structure, employing optimal sensor placement and clustering approaches [Bal+08b; All+19; Men+20].

On the other hand the measured data must be processed with methods which are adequate for engineering structures. Since the structure excitation usually is unmeasured and always affected by e.g. wind, output-only methods are particularly interesting in this context. They are based on the assumption of ambient excitation, and the dynamic properties can be evaluated under normal operating conditions and without human interaction. It has to be taken into account that the damage sensitive features are usually computed from noisy data and thus are subject to statistical variability. Hence, the statistical properties of the feature need to be considered properly when comparing the testing data to the reference data, in order to decide if a change is significant, i.e. if there is damage or not. Moreover, when significant changes are detected it must be distinguished between changes due to damage and changes due to variability in the environmental conditions [Soh07], otherwise high false alarm rates may occur. These requirements to robust data processing are in the scope of the present work and the developments are based on the following methodology.

Methodology

Inspired by the covariance-driven stochastic subspace identification (SSI) the stochastic subspace-based damage detection (SSDD) method was introduced in [BAB00]. It is formulated for the output-only state-space representation of the dynamical system and is

based on estimates of the output covariances. A reference model represented by the left null subspace of a Hankel matrix built from output covariances is confronted to the corresponding data Hankel matrix of the current system in a residual function. The residual is asymptotically Gaussian distributed and due to orthogonality it has zero mean if the tested system equals the reference system. If the system has changed the residual will be different from zero. In a subsequent hypothesis test, it is evaluated if the change is statistically significant, which is done by means of generalized likelihood ratio test considering the asymptotic local approach [BBM87]. The test takes into account the uncertainties of the tested data resulting from measurement and excitation noise by means of the residual covariance matrix. Thus, the statistical properties of the damage detection test can be characterized precisely in the healthy and the damaged scenarios. The test statistic is used as damage indicator, where a threshold is derived from empirical studies on reference data.

Such methods based on direct model-data matching are particularly appealing for automated damage diagnosis, since the model estimation step is avoided in the testing state. Successful applications in the field of vibration monitoring are reported e.g. in [JMM12; DM13b; Döh+14; Ven+14]. Moreover, the approach provides solutions for damage localization and quantification in connection with finite element model-based sensitivities in the same framework [Bal+08b; DMZ16; All+19]. While having a strong theoretical background, some robustness under real application is still missing in this framework, which is the subject of this work.

Contributions to the research field

The developments in this thesis aim at robust and automated methods for vibration-based SHM of engineering structures. The output-only damage detection with SSDD has been proven to be suitable for this task, since on one hand the dynamical model building part is performed only in the reference state and avoided during the monitoring phase, which enables fast performance. On the other hand the statistical properties of the damage indicator can be described precisely for the reference and the testing system state. However, some fundamental requirements for robust application are not met in the existing method, namely regarding the treatment of uncertainties related to the reference data, as well as the consideration of changes in the environmental variables that may perturb damage detection. Appropriate developments are in the scope of this work. The

contribution to the research field can be summarized as follows:

(1) Damage detection with uncertain reference The stochastic character of the vibration data leads to natural variability in the residual and consequently in the resulting damage indicator. So far in the stochastic subspace-based residual the uncertainties related to the testing data are considered, and it is assumed that the reference is perfectly known without uncertainties. This is true in ideal cases but does not hold in real world applications, since the reference usually is estimated from data and thus can contain considerable uncertainties. When neglecting these uncertainties in the residual evaluation, the observed statistical properties do not match the theoretical expectations and the test behavior becomes unpredictable. Since a correct statistical characterization is missing in this case, thresholds can only be set empirically from studies on reference data.

To close this gap, the statistical properties of the residual function is evaluated for the more realistic case when the reference is estimated from data. A theory-based formulation of the statistical properties is derived leading to a residual covariance, which considers both the uncertainties related to the reference and the testing data. The associated hypothesis test shows very good accordance to the theoretical expected behavior. The results are predictable and independent from data length in the reference and the testing state.

The impact of these developments is not only of academic value. The crucial part of defining a threshold is emphasized repeatedly in the literature, e.g. [BB15; GN09]. With the new residual evaluation for SSDD a threshold now can be derived apriori based on theoretical considerations without extensive empirical studies on reference data. Moreover, neglecting the uncertainty of the reference null space in the previous procedure leads to an inherent bias in the test. This is eliminated with the new formulation leading to a significantly higher test sensitivity.

(2) Damage detection under changing environmental parameters A very important part of the monitoring procedure is the formulation of a reference model adequate for the testing situation, in particular when environmental conditions are changing. Many automated vibration-based damage detection methods fail due to such variability, since it affects the dynamical behavior of the structures in a similar way as damages [Soh07]. As a consequence either the damage detection becomes insensitive to damages due to masking effects or high false alarm rates occur.

The basic residual in the SSDD is sensitive to changes in the dynamical system and

so far in this context only few works [Bal+08a; FMG03; FKB13] have been made to consider if these changes are due to damages or result from environmental effects such as temperature. However, these methods are developed empirically. Some of them are not optimal when the temperature in the testing state deviates from the mean temperature of the reference data sets, or they require reference data sets at as many temperature scenarios as possible.

In this work a robust approach is derived based on system theoretic considerations that is inspired by a model interpolation approach for linear parameter varying (LPV) systems from [Zha18], assuming that the dynamical behavior of an engineering structure under changes in an external parameter (temperature) can be approximated as a linear time-invariant system at a fixed temperature point. The new approach provides the possibility to compute a parameter value adapted reference null space for any testing parameter value from data in the undamaged state at only few reference parameter values. Three strategies are derived, which are based on interpolation or regression analysis. The corresponding damage detection test is developed, considering the uncertainties related to the reference null space based on interpolation or regression. The resulting test is shown to be robust and still sensitive to damages.

For the experimental validation a multi-sensor equipped testing bridge is constructed within this thesis on an outside testing field of the Federal Institute for Material Research and Testing Germany (BAM).

Outline of the work

The present thesis comprises three parts, I Preliminaries, II Contribution to theory, and III Applications.

Part I provides the background for the developments within this work. First, the state of the art is presented in chapter 1 proposing a classification concept for vibration-based damage detection procedures and introducing developments that were made (a) in the context of uncertainty considerations in the damage detection procedure and (b) for methods robust to changes in the environmental conditions. In chapter 2 the background theory is summarized comprising in particular the background of the SSDD and also theory on uncertainty computation and model interpolation.

Part II presents the contributions of this thesis to the methodology. In chapter 3 the damage detection test based on the residual for the SSDD with estimated reference is

derived. The concept is proven in a numerical study of a simple structure and the results are discussed with respect to the strengths and limits. In chapter 4 the development of the method robust to changes in environmental conditions is carried out considering three different strategies for the reference computation. Again, the theoretical part is followed by a proof of concept on the basis of numerical simulations. The considerations of the reference setup, from which the reference null spaces can be derived, are discussed.

Finally, the approaches are validated in three application studies in part III. The behavior of the new SSDD with estimated reference evaluated under stable environmental conditions is discussed in chapter 5. The damage detection approach robust to temperature changes is evaluated in chapters 6 and 7 on a concrete beam tested in a climate chamber as well as on an outdoor testing bridge that was constructed related to this thesis on an outside testing field and is exposed to realistic environmental conditions.

Part I

Preliminaries

In this part the reader is introduced to the subject of the thesis. An overview of the existing research in the field of vibration-based damage detection is given, in particular regarding the consideration of uncertainties and the effects of changing environmental conditions. In a second chapter, the theoretical background of the chosen methods is summarized.

Chapter 1

State of the art

1.1 Introduction

In the past decades many vibration-based structural health monitoring (SHM) techniques have been proposed that aim at automated damage diagnosis procedures in engineering structures. Classically, the procedure comprises the following steps [FDN01]: the definition of the monitoring task and observation of the structural vibration data, the extraction of damage sensitive data features, and the evaluation of the features to classify the structure into undamaged and damaged. The latter is equivalent to the task of finding feature deterioration and is often considered as a pattern recognition process [SF01; CF04; FW12].

In the present work developments are made on the feature extraction and evaluation part within SHM. Based on the fact that damage affects the stiffness, mass or damping properties of the structure, and consequently its dynamic properties [FW07], a damage sensitive feature is extracted from the vibration data and evaluated subsequently in four stages with increasing complexity: (1) damage detection, (2) damage localization, (3) damage quantification, and (4) lifetime prediction [Ryt93]. The detection of damage is the fundamental task for SHM, before further levels of the damage diagnosis can be reached. What follows is a summary of the literature mainly related to the damage detection task on linear time-invariant systems that this thesis deals with, although some methods may provide the possibility to be modified for the localization, quantification, or prediction stage. Due to the usually unmeasured excitation of engineering structures, such as wind and traffic, output-only methods are of particular interest.

After a brief overview on vibration-based damage diagnosis concepts and the associated damage sensitive features, evaluation techniques and their capability to consider uncertainties is given. Subsequently methods are collected that are proposed to handle changes in the environmental conditions.

1.2 Vibration-based damage diagnosis concepts

Many overviews on vibration-based damage diagnosis methods can be found that use different classification strategies for the methods, e.g. distinguishing between parametric and non-parametric methods [FK13] with or without machine learning basis [Avc+21], or categories such as basic modal properties, dynamical flexibility, and updating structural model parameters [DFP98; CF04]. Others discriminate between model-based and response-based techniques [Lim19] where the latter are classified in a comprehensive overview in [Lim+21] into modal-based methods, time series methods, and time-frequency methods. The authors in [FW12] propose to furthermore distinguish between feature extraction and feature evaluation step, pointing out the important property of the dimension of the extracted feature, where small dimensions simplify the subsequent evaluation step.

Following the Fundamental Axioms of SHM in [Wor+07] and the data-based decision making in [FKK13], the damage detection procedure can be described as illustrated in Fig. 1.1. First, the feature is extracted from data by some feature extraction operation **FE**. Then, usually an additional metric **ME** is applied with the purpose of quantifying the difference between features in the undamaged reference state and the current monitoring state. Subsequently the comparable quantity is evaluated, where either the quantity itself is considered to be the damage indicator or a statistical evaluation procedure **SE** leads to such an indicator. In the latter case it is possible to take into account uncertainties that are inherent in the damage feature due to the underlying noisy data. For decision making the distribution properties of the damage indicator under undamaged conditions are derived or computed empirically by means of a Monte Carlo study **MC** leading to a threshold to which the damage indicator in the testing state is compared.

This leads to the classification scheme in Fig. 1.2 for the following literature overview listing some prominent categories, but without claim on completeness. The extraction of the feature from data can be interpreted as a compression process of the vibration data with different complexity, similarly to the compression effect in system identification described in [CF04]. There the system model in the time or frequency domain is considered as a compression of the initial time history, and the modal representation is the compressed version of the system model. The feature extraction approaches are directly inspired by the available information at a particular system identification stage. Not all existing methods may fit into the scheme and since the boundaries are blurred some of the presented feature metrics may be meant to be part of the feature extraction or feature evaluation.

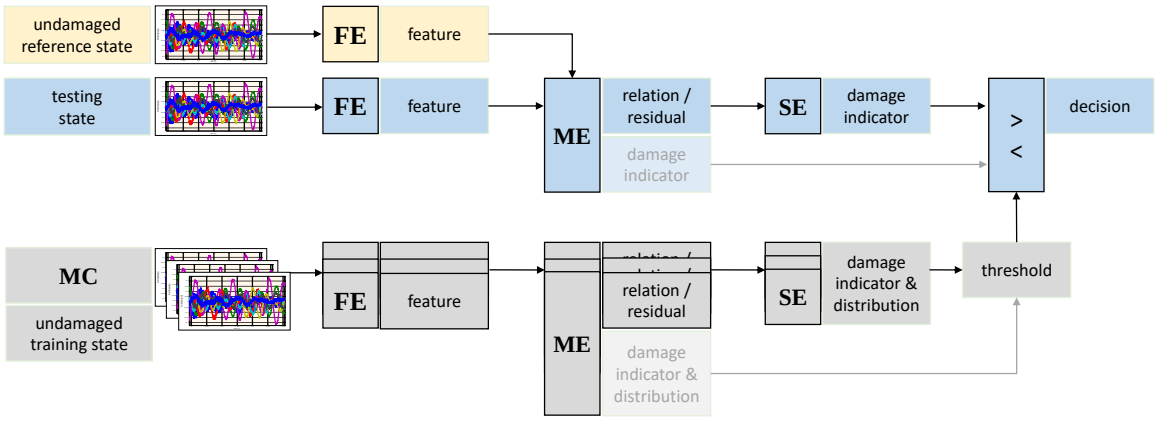

Figure 1.1 – Damage detection procedure.

Modal parameters and associated parameters Initially, damage detection approaches were proposed using modal parameters such as frequency [Ada+78], mode shapes, and modal damping, since they are functions of the physical properties of the structure [DFP98] which are affected by damage. Those features are derived e.g. by non-parametric methods like peak picking in the simplest form or parametric methods like polyreference least-squares complex frequency-domain (LSCF) [Pee+04] or subspace identification methods [VD96; PD99; DM12]. Many approaches and application studies exist that are based on these fundamental dynamical characteristics even in recent publications. A shortcoming of modal parameter based damage detection is the requirement to identify the modal parameters in each analyzed data set, and to track and match them, which can be difficult in the presence of weakly excited or close modes.

An application to wind turbines can be found in [Oli+18] using the difference of the system frequencies and it is emphasized that characteristic situations of such structures can be taken into account. The authors of [RF10] provide a damage detection algorithm that uses frequencies and mode shapes, which are less sensitive to environmental effects [Der+08]. The mode shapes are estimated with an automated modal parameter identification procedure deploying the modal assurance criterion (MAC). The MAC is introduced in [AB82] aiming at a better comparability of mode shapes through a measure of correlation where a value close to 1 shows good correlation. It is pointed out that with the MAC and the modal scale factor the quality of the modal vector can be evaluated [All03]. The MAC is also used in [Ram+10] to discriminate the physical modal parameters of masonry structures. A finite element (FE) model updating method is applied for comparison

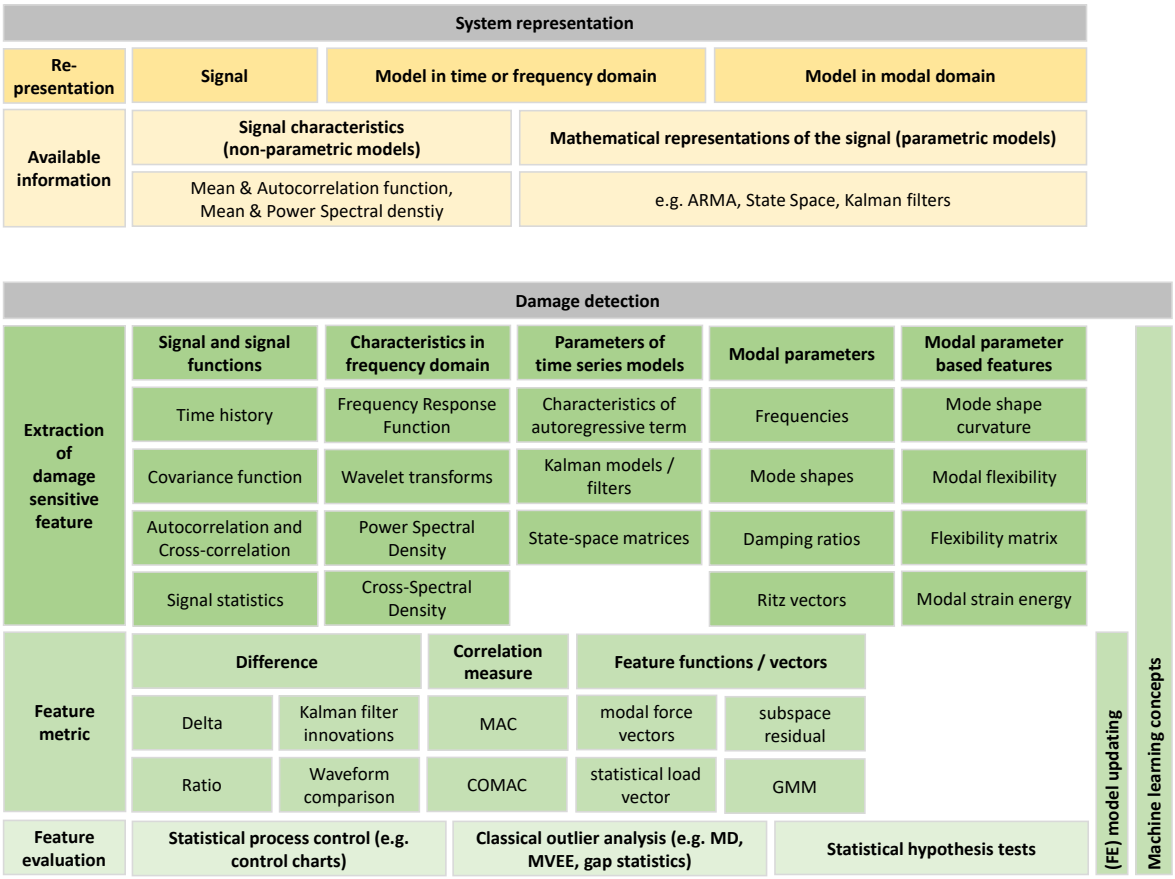

Figure 1.2 – Classification concept.

of system states. In [PBS91] a damage detection method is derived that evaluates the changes in curvature modes shapes, since they are known to be more sensitive to damage than the MAC and the coordinate modal assurance criterion (COMAC). The procedure carries the potential to be expanded to damage localization and even quantification.

Damage detection based on modal curvatures is applied e.g. in [Ad99] to detect damage in a pre-stressed concrete bridge introducing the curvature damage factor, which summarizes the difference in curvature mode shape for all modes in one quantity at each sensor point.

Changes in the flexibility matrix estimated from modal parameters are used in [PB94]. Another approach that is based on those changes is derived in [Ber02] and enhanced to the Stochastic Dynamic Damage Locating Vector (SDDLV) for output-only data in [Ber10].

Damaged detection is done by considering the internal forces under a set of load vectors, which are zero at the damaged elements. In [Döh+15] the test performance could be improved by taking the uncertainties of the underlying identified modal parameters into account. The flexibility and mode shape based methods provide the possibility to be used for the damage localization step.

Parameters of time series models Features that are derived from the parameters of time series models methods are usually of higher dimension than the basic modal parameters and require some effort to provide comparability between the reference and a testing state. However, the modal identification step is avoided, making the methods more suitable for automated procedures.

One group of such features are based on autoregressive (AR) models such as the AR coefficients or autoregressive moving average (ARMA). In [SCF00] and [FSF01] a one dimensional feature projected from AR model coefficients using principal component analysis (PCA) is proposed, where the projection is mentioned to improve the subsequent evaluation procedure with control charts. In [CB08] time series responses are fitted with ARMA models. The resulting ARMA coefficients are fed to a classifier, which is capable of learning in an unsupervised manner and of forming new classes when the structural response exhibits change. The authors in [NK07] use the vector of AR coefficients and apply the method of Gaussian Mixture Models (GMM) evaluating the significance of a distances with gap statistic. The method provides also information on the damage extend from the Mahalanobis distance (MD) of GMMs and is found to be a useful framework for data fusion.

Features based on Kalman filter [Kál63] are capable to include statistical noise and other inaccuracies. The damage detection in [YDG04] is based on a Kalman filter using stochastic subspace identification (SSI). A prediction error is derived from the filter and testing data and its MD is evaluated. When a Kalman filter fits to the assumptions differences between measurements and filter prediction, denoted as innovations, are realization of white noise. An purely data-driven approach based on this property is proposed by [Ber13] evaluating the whiteness of the innovations in a hypothesis test. The authors of [Gre+21a] propose an approach that is capable to reject the influence of the periodic input by estimating the periodic information with a non-steady state Kalman filter.

Characteristics in the frequency domain When models in the frequency domain are used the associated model characteristics such as the Frequency Response Functions (FRF) may be applied for damage detection. The authors of [FC03] propose an approach where a single FRF measured at several frequencies is used together with an analytic model of the reference structure to detect damage. In [SMS99] a FRF curvature method is developed that is an extension of the method in [PBS91] to all frequencies in the measurement range. Similarly, the authors of [Lim10] propose the interpolated damage detection method (IDDM) that uses the deviation of the deformed shape from smooth behavior expressed by the variation of an interpolation error. This method is shown to be appropriate when changes in environmental conditions are supposed enjoying that curvature characteristics are less effected by environmental conditions [Der+08].

The Power Spectral Density (PSD) is used in [WMF00], where the PSD peaks are evaluated with outlier analysis of their MD. The authors of[VSF14] show in a comparative study together with other time series methods that features based on PSD are quite sensitive. In [TA18] an approach is introduced that relies on the vibration energy in acceleration records using the normalized cumulative PSD. The method is able to account for deviations from perfect stationary white noise excitation.

Some research is made on the application of wavelet transforms, which decomposes a function into a set of wavelets helping to extract local spectral and temporal information simultaneously. [Ulr+16] introduce an approach for continuous wavelet transform that captures local mode shape irregularities by significantly magnified transform coefficients leading to a damage indicator inspired by MAC that expresses the similarity wavelet transforms in the reference and the testing state.

Signal and its characteristics and associated signal processing functions The simplest form is to use the signal directly without any compression procedure which leads to high feature dimension and difficult comparability. A method based on Moving Average Filter (MAF) is used in [KXY18] smoothing the signal with MAF to make deviations measurable. Many approaches that rely directly on the signal are based on machine learning concepts, to which some remarks are made in the following section.

An easier comparability is reached when signal statistics are used. In [FW12] some of them are evaluated in a numerical study presenting damage induced changes in the signal peak amplitude, signal mean and variance, and other signal statistics. It is pointed out that their sensitivity towards outliers limits the direct application.

With the goal to reduce the dimension of large data sets for easier interpretation PCA is applied providing a procedure with minimized loss of information. The data is projected to a lower dimensional space creating new uncorrelated variables, the principal components [JC16]. Using PCA e.g. in [Tan05] a feature extraction/de-noising method is developed that is based on frequency response signals. The authors of [Kul03] used PCA for dimensionality reduction of the modal parameters for the subsequent evaluation in control charts.

The application of functions from signal processing allows a different perspective on the data and is widely used. The authors of [FJ97] prove that the cross-correlation functions of the responses excited by ambient noise have similar characteristics as the structural impulse response functions and can be adopted for identifying structural dynamic properties. An approach based on the MD of autocorrelation coefficients is used in [HO14].

Another group of damage sensitive features is based on the data covariance. In [BAB00] an approach is proposed that is inspired by the covariance-driven SSI [BF85], which identifies the state-space representation of the observed system from the covariance Hankel matrix. For damage detection, a Gaussian-distributed residual is computed by confronting a covariance Hankel matrix in the testing state to the left null subspace of the covariance Hankel matrix in the reference state. Together with the statistical evaluation in a hypothesis test the method is referred to as stochastic subspace-based damage detection (SSDD). Based on the concept of SSDD further developments have been made to meet specific requirements for the application to engineering structures: the authors of [Bal+08a] derive an approach that considers changes in the environmental conditions. In [DM13b; DMH14] a residual robust to changes in the excitation covariance is derived and the authors of [DMZ16] enhance the method for damage localization and quantification. Other residual formulations on the basis of the covariance-driven SSI are derived in [YG06] considering that the relevant structural responses are comprised in the active subspace of the covariance Hankel matrix. An approach that uses the MD of the output covariance Hankel matrices can be found in [Gre+21b], where it is shown to be robust to changes in excitation. Comparison of the SSDD to other methods is made in [KF16] and [ZR09]. In the first, the sensitivity of the classical SSDD is compared to a method that considers modal parameters identified with SSI applying an automated mode identification algorithm to find stable poles. The latter compares the SSDD method to damage detection using modal parameters.

1.3 Feature evaluation and related uncertainties

When the damage sensitive feature is extracted and a comparable quantity is derived, the value of this quantity is evaluated with respect to its nominal value in an undamaged reference state. Since the feature usually is computed from noisy data, it is subject to statistical variability and so is the considered damage indicator (cf. Fig. 1.1). In the evaluation the statistical properties must be taken into account in order to define a threshold, from which it is decided if a change in the dynamical system is significant or results from natural variations due to noise. The threshold is based on the distribution properties of the damage indicator and an allowed false positive error probability. When the distribution is not known, it is a common procedure to determine it empirically from several reference data sets in the healthy state in a Monte Carlo study.

However, recently the proper consideration and quantification of the feature uncertainties have become an important part of research on vibration-based damage detection. When the statistical properties of the underlying feature are known, the properties of the resulting damage indicator can often be derived from them, e.g. with a first-order perturbation approach using the Delta Method [CB02]. In the following uncertainty quantification approaches for modal parameters, system matrices and related damage indicators are recalled and some groups of evaluation techniques are presented.

Uncertainty quantification First, the statistical distribution properties of a feature need to be derived for its uncertainty quantification. When the distribution is (asymptotically) Gaussian uncertainty quantification boils down to computation of the respective covariance. For example, computation procedures for uncertainty quantification of modal parameters estimated with SSI are in the focus in [RPD08; PGS07; MDM16] enhanced by efficient algorithms in [DM13a]. For modal parameters computed with an Eigensystem-Realization-Algorithm (ERA) the corresponding uncertainties are derived in [LM11] and when they are computed on the basis of Bayesian spectral density an approach can be found in [YK19]. In [Bro+18] the prior computation of the expected modal parameter uncertainty is used to optimize the measurement setups and their necessary duration. It is pointed out in [BB15] that the proper uncertainty quantification becomes particularly difficult when only few or short data sets are available.

Approaches computing the uncertainty of system matrices estimated with output-only and input-output subspace identification procedures and the resulting transfer function are derived in [DM13a; GDM20]. Formulations of the dominant parts of the estimation

errors of system matrices in a shift invariance and a state approach are presented in [Ike14].

Uncertainty bounds related to the MAC estimates are derived in [GDM21], discriminating between the MAC computed from the same mode shape and the one computed from two different mode shape. Distribution properties of the Modal Phase Collinearity (MPC), which is used to discriminate between real and complex-valued mode shape vectors, are computed in [Gre+21c].

Uncertainty in data-driven residuals is treated e.g. in [DVG12] in the context of null space-based additive fault detection. Statistical properties of a Hankel matrix-based Mahalanobis distance for damage detection are investigated from the authors of [Gre+21b]. An approach for uncertainty computation of updated model parameters in the context of a FE model updating procedure is proposed in [Gau+17]. Other authors focus on explicit uncertainty quantification models of damage sensitive features such as Frequency Response Functions and modal parameters [Mao12; CM11].

Control charts In order to monitor the damage indicator with respect to its expected nominal value and nominal distribution, control charts developed for statistical process control by Walter Shewhart in the 1920s are used as graphical tools. The quantity of interest is evaluated in real-time by illustrating its current value in relation to the expected statistics. Applications can be found e.g. in [SCF00; YDG04; FSF01], where the mean of one-dimensional damage indicators are monitored by means of the X-Bar chart.

When the feature dimension is greater than one, multi-variate charts can be used, e.g. Hotelling T^2 or Multivariate Exponentially Weighted Moving Average (MEWMA) charts, which combine information from several variables in one scalar. The authors of [Kul03] evaluate the sensitivity of univariate versus multivariate control charts. They emphasize that in cases where it is not known in advance which parts of the damage sensitive feature are relevant it can be advantageous to use high-dimensional feature vectors and reduce the dimension subsequently by PCA, providing higher sensitivity of the control charts.

Classical outlier or novelty analysis Feature evaluation based on classical outlier or novelty analysis investigates the statistical properties of the damage sensitive feature. A widely used approach for multivariate quantities is the Mahalanobis Distance (MD), which is the distance between a point and a distribution accounting for the respective variance in the direction of the evaluated point by considering the covariance matrix. The

authors of [WMF00] introduce a systematic study on the application of outlier analysis by MD pointing out that this approach assumes at least near-Gaussian distribution of the undamaged feature and refers the reader to Kernel Density Estimation approaches if the distribution is multi-modal.

In [Der+15] several outlier analysis concepts are studied comparing the MD to the Minimum Covariance Determinant (MCD) and the Maximum Volume Enclosing Ellipsoid (MVEE), emphasizing that the MCD is more robust to outliers in the training data.

The goal of the work in [BB15] is to investigate the MD with different versions of the covariance matrix and the authors of [Gre+17] compare a damage evaluation approach using the MD with statistical hypothesis testing in the context of SSDD.

The application of gap statistics as in [NK07] may belong to this group of evaluation techniques. Usually applied to measure the variation of data within a cluster, in this approach the difference between GMM is evaluated to derive the number of existing mixtures.

Statistical hypothesis tests Statistical hypothesis testing is another evaluation technique that is widely used to classify a monitored system. In fact, it is tested whether a given sample of data is drawn from a given probability distribution. Therefore, two hypotheses are defined assuming different underlying distributions. The null hypothesis holds when the tested data belongs to the unchanged reference system, the alternate hypothesis applies when the data is recorded from a changed system. Various test statistics exist, which take the covariance of the tested feature into account, and the choice depends on the feature properties.

A hypothesis test for change detection in is derived in [BAB00] using the asymptotic local approach to change detection from [BBM87]. The test is designed for the subspace-based residual introduced in the previous section. Since the residual is asymptotically Gaussian, general statistical framework, namely Generalized Likelihood Ratio (GLR) test, can be applied and the resulting test statistic follows a χ^2-distribution. The test is able to take into account the variability of the evaluated feature due to noisy test data by means of the feature covariance matrix. Assuming that a dynamical system can be described by a set of system parameters, the damage detection can be done with respect to these system parameters, without determining the parameter anew in the testing state. This parametric version has the benefit that the theoretical distribution of the test statistic can be described precisely in the undamaged and in the damaged state.

Other hypothesis tests are proposed e.g. in [SF01] where the standard deviation ratio of residual errors from an ARMA model is evaluated statistically in a Box-Andersen test; in [Ber13] where a Lag Shifted Whiteness Test (LSWT) is designed that evaluates the whiteness of the Kalman filter innovations; in [SM13] where Bayesian tests are used deriving the uncertainties in the detection, localization, and quantification step; in [Döh+15] where a statistical χ^2-test was used in a damage localization procedure; in [DVG12] where data-driven residuals are evaluated in a χ^2-test providing an analytic design of the damage detection procedure considering measurement noise as well as identification uncertainty. Some applications to engineering structures can be found e.g. in [Döh+14; GK17; Ven+14].

For generalization of hypothesis testing for multiclass classification problems the authors of [FW12] provide suggestions.

Model updating When model updating procedures [FM95] are applied, the metric formulation and the evaluation step in Fig. 1.2 often are combined. Such approaches are inverse methods [Fri07] deriving updated FE models from data measured in the testing state. A function representing the distance between the measured data or data feature and the predicted data from the FE model is minimized by means of optimization methods. Many model updating methods are developed in the past decades. In [Wae+16] three techniques are compared that are based on the classical Tikhonov regularization, Constitutive Relation Error and a Bayesian approach using physical parameters such as the Young modulus as updating parameter. The Bayesian model updating is a suitable method handling uncertainties as emphasized by the authors of [SDL15]. They give an overview how to consider the uncertainties of the measurements and those related to the numerical model properly in the damage detection procedure on the basis of Bayesian and fuzzy approaches. Others provide approaches for uncertainty considerations, which use automated fault estimation based on interval arithmetic [KWA19] or which are based on the covariance estimation procedure for the updated model parameters [Gau+17]. More detailed overviews can be found in [Bro+01] or [FW12].

Supervised learning An increasing number of approaches come from the vibrant field of supervised learning methods, such as artificial neural networks, where the steps of the damage detection as displayed in Fig. 1.1 usually are hidden within the end-to-end algorithms. The stochastic character of the data is considered within the algorithms. These methods process the raw data of the time history itself or even plots of them

[Tan+19], as well as previously derived features requiring some classification information of the already processed features [Mig+12]. A more detailed discussion of some concepts for vibration-based damage detection can be found in [FW12] and [Avc+21].

1.4 Data-based damage detection under changing environmental conditions

The application of automated vibration-based damage diagnosis methods often fails due to changing environmental conditions. This is e.g. observed by the authors of [Far+94; PD00; Roh+00a] applying such SHM methods over long time periods to bridge structures. The dynamical behavior of the structures is significantly affected by environmental effects such as temperature, changes in the excitation statistics, humidity, mass loading, or soil conditions [Soh07; Ube+17; WSF02].

Since the impact of these effects to the dynamics is quite high compared to small damages [PMD01; LD07; Far+00], automated methods are perturbed in two ways. Either the data that is considered for the baseline contains several environmental nominal states. In this case high variability of the damage indicator in the normal state is assumed, which masks the effect of damages leading to poor sensitivity of the test. In the other case, when the testing data is recorded at a normal state with fixed environmental conditions, changes in the structural dynamics due to new conditions during the testing phase lead to high false alarm rates.

Several approaches exist that aim at robust damage detection procedures by data normalization in the sense of separating signal changes caused by environmental variations from structural changes [Soh07]. The normalization step can be performed at several stages of the damage detection procedure, i.e. during the feature extraction by choosing environmental insensitive features or prepare them adequately, during the computation of the damage indicator, or during the evaluation step. In the following, two groups of concepts are distinguished: The first group is based on the assumption that the environmental conditions are measured and the other group works without further knowledge about the detailed environmental conditions.

1.4.1 Methods with relation to measured environmental parameters

In this section methods are recalled, which assume that the environmental conditions can be characterized uniquely by measurable external parameters and the related changes of the feature or damage indicator distribution can be expressed as a function of this parameter. Concepts that are based on regression or interpolation are widely used. Also approaches exist that consider classification of the testing situation or parameter dependent sensitivities.

Regression and Interpolation In [PD00] a study on one-year data from the Z24 bridge in Switzerland is presented showing a strong dependency of the frequencies from temperature while other environmental conditions have no significant impact. The temperature dependency is not linear over time, but has a declination gradient change at a temperature of 0°C. To model the temperature dependency a black-box autoregressive model with exogenous terms (ARX) is fitted to the frequency-temperature relation obtained from data using temperatures as input and delivering the frequencies. The prediction error is used as damage indicator and compared to an expected distribution property. Similarly in [Soh+98] a linear adaptive model is used to reproduce the natural variability of the frequencies of a bridge leading to a baseline for discrimination of deviations in data sets at new testing temperatures. In [Hu+15] regression functions are used to remove the temperature effects on the frequencies and the residual is evaluated by outlier analysis. The authors of [Oli+18] propose a SHM procedure for application to wind turbines with removing environmental effects with regression from modal parameters. An approach considering a SSI for modal identification is presented in [KF16], deriving regression models for the modal parameters and their distribution properties. The authors of [MCC12] apply static and dynamic regression models complemented by a PCA. In [Ram+10] masonry structures are evaluated regarding the modal parameters and MAC using regression analysis to reject changes in environmental conditions.

Approaches in [WSF02] use AR coefficients as damage sensitive features, where different dimensions of the AR model are considered. A regression analysis is performed on the damage indicator – the MD of the coefficients – on each component of its statistics. It turned out that with this approach the eigenvalues of covariance matrix become negative in some cases, hence an interpolation approach is also derived. In this interpolation the statistics of the damage indicator is computed from the neighbored statistics applying

linear interpolation. The approach provides some capability for generalization for multi-parameter situations. The results are compared to a previous approach when large training data sets spanning all environmental conditions of interest were used, showing that the regression method is much more sensitive.

Classification Some approaches rely on the idea to classify the current testing feature to one particular reference feature of classification. In [FMG03] an approach is derived within the setup of a smart structure concept. It is based on the SSDD that uses a reference null space to set up a comparable residual. Several references are stored in a data base and for a particular testing temperature the closest reference is used. The method is developed further in [FKB13] computing a reference model based on weighted references.

An approach based on Bayesian system identification and model class selection is proposed in [Sim+20], where a set of competing parameterized probabilistic structural models are postulated, which explicitly account for the effect of varying ambient temperatures on the mechanical properties of the system. Information provided by the structural models and by recorded vibration data leads to the parameters of the temperature-dependent structural models. From this the plausible state of the system is obtained.

Parameter dependent sensitivities Statistical rejection approaches using parameter dependent sensitivities to compute residuals that are tested subsequently in hypothesis tests are derived e.g. in [Bal+09]. From data sets at some reference temperatures a combined system and temperature effect model is obtained and changes due to temperature are rejected as nuisance by using corresponding sensitivities. A temperature adjusted reference that is based on temperature related modal parameters computed from temperature models is derived in [Bas+10].

In [Bhu+19] an approach based on load vectors is proposed, where a sensitivity-based correction of the identified modal parameters in the damaged state is performed with respect to the temperature field and the temperature dependent parameters of the finite element model in the reference state.

1.4.2 Methods with unmeasured environmental conditions

In cases where the environmental conditions are unmeasured or cannot be described uniquely robust features that can be formulated insensitive to changes in the environmental conditions or large normal condition models are applied.

Robust feature or damage indicator It is found that e.g. mode shapes are less sensitive to changes in the environmental conditions than frequencies are [Der+08]. This motivates for approaches that are based on features or damage indicators which can be formulated insensitive to such changes.

In the first stage, features can be employed that are less affected by environmental conditions. This includes e.g. the IDDM in [Lim10] that is based on FRF and uses the deviation of the deformed shape from smooth behavior, and is shown to be adequate for damage detection under changes in the environmental conditions.

In other approaches the damage sensitive features are processed to be insensitive to changes in the environmental parameters. E.g. PCA is used to remove the temperature affected parts of a feature. In [Yan+05a] PCA is used for linear cases, where the environmental parameters are taken into account as embedded variables. The same authors [Yan+05b] propose a two-step procedure for non-linear cases – clustering of the data space into several regions and application of PCA to each local region – which allows performing a piecewise linearization. In another publication [KBD13] PCA is used to project the data into a subspace where the variance from the environment is small. Nonlinear PCA with autoassocative neural networks (AANN) is proposed in [Kra91] generalizing the mapping into feature space to allow arbitrary nonlinear functionalities for multivariate data analysis. The authors of [Der+08] propose a feature that is based on modal filtering tuned to a particular mode observed in frequency domain output. In the damage detection the fact is used that damage produces spurious peaks in the frequency domain output of the modal filter while environmental changes shift the peak in the frequency domain without changing the general shape. The authors of [Van+05] introduce damage detection based on robust singular value decomposition (SVD), which distinguishes between changes in the working conditions and damage by evaluating changes in the rank of a feature vector matrix. In [Cro+12] also a strategy is proposed that prepares the data for robust feature extraction by using cointegration, which is based on finding a stationary linear combination of non-stationary time series to purge the data set of its common trends leading to a robust residual.

In the context of robustness towards changes in the excitation the authors of [DM13b] and [Gre+21b] propose robust residuals which are based on output covariance Hankel matrices either using insensitive subspaces of the Hankel matrix or normalizing them before the damage indicator is computed.

The intention in [Man02] is to derive univariate damage indicators. The method is

based on MD, where the approach is applied to lamb-wave data. Similarly the authors of [Der+15] introduce a robust outlier analysis that uses the MCD, which is able to remove the masking effect and search inclusively for multiple outliers. An approach based on GMM is explained in [Kul14]. Non-linear effects from environmental variations can be removed by considering Minimum Mean Square Error (MMSE) and applying PCA.

Large normal condition models Another concept when no information is available on the current environmental state is based on large normal condition models. One vibrant field is the application of machine learning approaches to environmentally affected engineering structures, such as in [GGW17; Tan+19]. In [SW10] a negative selection algorithm is used for cases of damage detection where the data under normal conditions is significantly non-Gaussian or environmental conditions lead to variability. A combination of time series analysis, neural networks, and statistical inference approaches is developed in [SWF02]. The effect of damage on the extracted feature is separated from environmental effects by means of an AR model and AR-ARX model.

Other methods derive global models that represent the effect of the environmental parameters to the statistical properties of damage sensitive features. The authors of [RWD14] propose an approach that identifies damage sensitive features in a reference state from each part of a training data broken up into time sequences that are short compared to the time of parameter variations. Using kernel PCA a data-driven global nonlinear system model is derived from the identified features. The features in the testing state are then compared to the feature predicted from the global model. In [SCS16] polynomial chaos expansion (PCE) is used to find a model that represents the extracted features in relation to the measured operational conditions.

Approaches that are based on average models are developed e.g. in [Bal+08a]. Here a global reference model is built from a merged data set smoothing out the temperature effect by the averaging operation. In fact, this can be understood as a kind of interpolation with no respect to the testing temperature. Similarly, the authors of [HF09] provide an approach that uses Constant Coefficient Pooled Vector Autogressive with Exogenous Variables (CCP–VARX) representations, which provide averaged descriptions of the structural dynamics over temperature, while the functionally pooled FP-VARX counterparts consider the explicit modeling of temperature dependence of the dynamics.

These approaches provide some robustness in practice, since they do not require explicit measurements of the environmental conditions. However, if the reference measure-

ments are not representative the approaches may fail, since no further relation between the current measurement in the testing state and the large normal model is taken into account.

Chapter 2

Background theory

2.1 Introduction

The developments in this thesis are based on the stochastic subspace-based damage detection (SSDD) and the associated residual vector. The residual uses subspace properties of an output covariance Hankel matrix. It is defined as the product of the left null space of the Hankel matrix in the reference state and the Hankel matrix estimated from current measurement data in the test state [BAB00; DMH14]. The statistical evaluation of the residual in a hypothesis test yields a damage detection test statistic that considers the uncertainties of the residual.

In the context of this thesis the theory on complete consideration of the residual uncertainties is developed, using perturbation theory, and a SSDD approach robust to changes in the environmental conditions is derived from local model interpolation. This chapter recalls the used theories and methods.

After introducing the models that describe the dynamics of a mechanical structure in section 2.2, section 2.3 gives an overview on how those models and its modal parameters can be extracted from vibration data in time domain by means of the stochastic system identification (SSI). Then, the current state of the SSDD method is presented in section 2.4. The mathematical perturbation theory including the delta method and the basics of a local model interpolation approach for linear parameter varying (LPV) systems are summarized in sections 2.5 and 2.6.

2.2 Structural dynamics of output-only systems

The dynamics of a linear time-invariant (LTI) mechanical structure can be described in continuous time t by the following equation of motion

$$\mathbf{M}\ddot{q}(t) + \mathbf{C}\dot{q}(t) + \mathbf{K}q(t) = \nu(t). \tag{2.1}$$

The vector $q \in \mathbb{R}^m$ collects the displacements at the m degrees of freedom (DOF) of the system and $\dot{}$ and $\ddot{}$ denote the derivatives with respect to time. $\mathbf{M}$, $\mathbf{C}$, and $\mathbf{K} \in \mathbb{R}^{m\times m}$ are the mass, damping, and stiffness matrices of the system, respectively. ν is the excitation function that is represented by a white noise term in output-only systems with unknown excitation.

With the system state

$$x(t) = \begin{bmatrix} q(t) \\ \dot{q}(t) \end{bmatrix} \in \mathbb{R}^n, \tag{2.2}$$

where $n = 2m$ is the model order, a first-order system in state space can be derived from (2.1) [Jua94]. Sampled at rate $1/\tau$ such that $t = k\tau$, the stochastic state-space model of an output-only system at time step k writes as

$$\begin{cases} x_{k+1} = Ax_k + w_k \\ y_k = Cx_k + v_k. \end{cases} \tag{2.3}$$

$y_k \in \mathbb{R}^r$ is the output of the system measured at r sensor positions with measurement noise $v_k \in \mathbb{R}^r$. The state noise term $w_k \in \mathbb{R}^n$ is related to the unknown excitation. Both noise terms are unmeasured, and usually assumed to be stationary, centered, white, and having finite fourth moment. A and C are the state transition matrix and the observation matrix of the discrete time system. They are directly linked to the mechanical system matrices from (2.1) with

$$A = \exp\left(\begin{bmatrix} 0 & I \\ -\mathbf{M}^{-1}\mathbf{K} & -\mathbf{M}^{-1}\mathbf{C} \end{bmatrix}\tau\right) \in \mathbb{R}^{n\times n}$$

$$C = \begin{bmatrix} L_d - L_a\mathbf{M}^{-1}\mathbf{K} & L_v - L_a\mathbf{M}^{-1}\mathbf{C} \end{bmatrix} \in \mathbb{R}^{r\times n}. \tag{2.4}$$

L_d, L_v, and $L_a \in \{0,1\}^{r\times m}$ are selection matrices denoting the sensor locations at the

corresponding DOF in q, where displacements d, velocities v, and accelerations a are recorded.

2.3 System identification

Several approaches exist that are used to identify the systems in (2.1) and (2.3) from data. The determination of the particular system matrices in (2.1) from data only is impossible and is usually treated in the context of FE model updating [FM95]. Nevertheless, the dynamic properties of the system can be retrieved by the identification of its eigenstructure, namely the eigenfrequencies, damping ratios, and mode shapes. The state-space matrices in (2.3) can be identified directly from data, e.g. with subspace identification methods. From the identified matrices the eigenvalues, the eigenvectors, and the corresponding modal parameters can be derived in a subsequent step.

It has to be stated that the matrices and parameters, which are identified from data, are estimates and usually afflicted with uncertainties. This is due to the stochastic character of the measured data caused by the noise terms in (2.3). The estimates of the true variable are denoted by $\hat{}$ in the following.

In this thesis a SSI algorithm is used to identify modal parameters from data. The concept of the SSI and in particular the covariance-driven subspace identification [BF85] are recalled in the following and it is shown how to derive the eigenstructure of the dynamical systems. The theoretical background gives some context for the later introduced SSDD method.

2.3.1 Concept of stochastic subspace identification

The following concept of the SSI is inherent in many algorithms, as e.g. in [VD96; PD99; BM07]. It is based on a matrix $\mathcal{H}_{p+1,q}$ computed from data projections and/or data covariances, whose column space is the observability matrix $\mathcal{O}$ of the system arising in the context of control theory [Kál63]. The observability matrix writes as

$$\mathcal{O}_{p+1} = \begin{bmatrix} C \\ CA \\ \vdots \\ CA^p \end{bmatrix} \in \mathbb{R}^{(p+1)r \times n}, \tag{2.5}$$

where p is a size parameter denoting the block rows, and A and C are the state-space matrices introduced in section 2.2. For system identification the two matrices have to be derived from the observability matrix. C follows as the first block-row of (2.5). Due to the shift invariance property of $\mathcal{O}_{p+1}$, which states that A is the over the time steps consistent term in $\mathcal{O}_{p+1}$, the state transition matrix can be approximated with a least square approach from

$$\mathcal{O}_{p+1}^{\uparrow} A = \mathcal{O}_{p+1}^{\downarrow}, \tag{2.6}$$

where

$$\mathcal{O}_{p+1}^{\uparrow} = \begin{bmatrix} C \\ CA \\ \vdots \\ CA^{p-1} \end{bmatrix} \quad , \quad \mathcal{O}_{p+1}^{\downarrow} = \begin{bmatrix} CA \\ CA^{2} \\ \vdots \\ CA^{p} \end{bmatrix} \quad \in \mathbb{R}^{pr \times n}. \tag{2.7}$$

The observability matrix is derived in the SSI as follows. The matrix $\mathcal{H}_{p+1,q}$ holds the factorization property

$$\mathcal{H}_{p+1,q} = W \mathcal{O}_{p+1} Z_q \quad \in \mathbb{R}^{(p+1)r \times qr}. \tag{2.8}$$

Herein W is an invertible weighting function, often defined to be the identity matrix. The definition of Z_q depends on the chosen SSI algorithm and the corresponding type of $\mathcal{H}_{p+1,q}$. q denotes the block columns, with usually $q = p + 1$, and it is $\min\{pr, qr\} > n$. The observability matrix can be computed from the image subspace of the matrix $\mathcal{H}_{p+1,q}$ with

$$\mathcal{O}_{p+1} = W^{-1} U_1 D_1^{1/2}, \tag{2.9}$$

Image U_1 and the singular values in D_1 are computed by a singular value decomposition (SVD) of matrix $\mathcal{H}_{p+1,q}$, truncated at the assumed model order n, leading to

$$\mathcal{H}_{p+1,q} = U D V^T = \begin{bmatrix} U_1 & U_2 \end{bmatrix} \begin{bmatrix} D_1 & 0 \\ 0 & D_2 \end{bmatrix} \begin{bmatrix} V_1^T \\ V_2^T \end{bmatrix}. \tag{2.10}$$

$D_1 \in \mathbb{R}^{n \times n}$ denotes the diagonal matrix of n singular values and $D_2 \in \mathbb{R}^{(p+1)r-n \times qr-n}$ is assumed to be zero, or containing noise in the case of the matrix estimate. $U_1 \in \mathbb{R}^{(p+1)r \times n}$ and $U_2 \in \mathbb{R}^{(p+1)r \times (p+1)r-n}$ are the column space and the left null space, respectively. $V_1 \in \mathbb{R}^{qr \times n}$ spans the row space and $V_2 \in \mathbb{R}^{qr \times qr-n}$ denotes the null space of matrix $\mathcal{H}_{p+1,q}$.

A consistent estimate of the observability matrix is obtained, when $\mathcal{H}_{p+1,q}$ is replaced

by an estimate $\widehat{\mathcal{H}}_{p+1,q}$.

2.3.2 Covariance-driven subspace identification

A well-known SSI algorithm is the covariance-driven subspace identification [BF85]. It uses the output covariances to built matrix $\mathcal{H}_{p+1,q}$ and is applied in this work.

Let $\mathcal{Y}_N = \{y_1, y_2, ..., y_N\}$ be a set of N output data samples at r sensor locations. The cross-covariances between the states and the output are $G = \mathbf{E}(x_{k+1} y_k^T)$ and the output covariances are computed to [VD96]

$$R_i = \mathbf{E}(y_{k+i}\, y_k^T) = C A^{i-1} G. \tag{2.11}$$

Matrix $\mathcal{H}_{p+1,q}$ is the block Hankel matrix of output covariances with

$$\mathcal{H}_{p+1,q} \stackrel{\text{def}}{=} \begin{bmatrix} R_1 & R_2 & \dots & R_q \\ R_2 & R_3 & \dots & R_{q+1} \\ \vdots & \vdots & \ddots & \vdots \\ R_{p+1} & R_{p+2} & \dots & R_{p+q} \end{bmatrix} \stackrel{\text{def}}{=} \text{Hank}(R_i)\,. \tag{2.12}$$

The factorization property in (2.8) and $W = I$ yield

$$\mathcal{H}_{p+1,q} = \mathcal{O}_{p+1} \mathcal{C}_q, \tag{2.13}$$

since it becomes $Z_q = \begin{bmatrix} G & AG & \dots & A^{q-1}G \end{bmatrix}$, which is exactly the well-known controllability matrix $\mathcal{C}_q$.

A consistent estimate of the block Hankel matrix $\widehat{\mathcal{H}}_{p+1,q} \stackrel{\text{def}}{=} \text{Hank}(\widehat{R}_i)$ can be obtained from data by using the empirical output covariances

$$\widehat{R}_i = \frac{1}{N} \sum_{k=i+1}^{N} y_{k+i} y_k^T. \tag{2.14}$$

2.3.3 Identification of the eigenstructure

With the previous SSI algorithm the state transition and the observation matrix can be derived on the basis of (2.5). From them the eigenstructure of system (2.3) follows with the eigenvalue problem of A

$$A\phi_l = \lambda_l \phi_l, \tag{2.15}$$

where λ_l and ϕ_l denote the l-th eigenvalue and eigenvector, respectively.

The l-th eigenfrequency f_l and damping ratio ξ_l of the system in continuous time in (2.1) are computed from λ_l of the discrete time system as follows. The relation between λ_l and the eigenvalue of the continuous-time system μ_l is defined by

$$\lambda_l = e^{\mu_l \tau}. \tag{2.16}$$

From this and regarding $\omega_l = 2\pi f_l$ and the damping ratio ξ_l it holds

$$\mu_l = -\omega_l \xi_l \pm \omega_l \sqrt{1 - \xi_l^2}\mathrm{i}, \tag{2.17}$$

leading to

$$f_l = \frac{|\mu_l|}{2\pi} \ , \ \xi_l = \frac{-\mathbf{Re}(\mu_l)}{|\mu_l|} \tag{2.18}$$

The observable eigenvectors or mode shapes φ_l can be derived with the observation matrix

$$\Psi = C\Phi, \tag{2.19}$$

with $\Psi = [\varphi_1 \ \varphi_2 \ ... \ \varphi_n]$ and $\Phi = [\phi_1 \ \phi_2 \ ... \ \phi_n]$ being matrices that contain the mode shapes and the eigenvectors in its columns, respectively.

Consistent estimates of the modal parameters can be derived by using estimates of $\widehat{A}$ and $\widehat{C}$, which result from an observability matrix that is computed on a Hankel matrix estimate in (2.10).

2.4 Stochastic subspace-based damage detection

The stochastic subspace-based damage detection (SSDD) method as presented in [BAB00] makes use of the previous described covariance-driven SSI. With a data-driven, asymptotically Gaussian residual changes in a parameter vector are uncovered. The parameter vector is a collection of system parameters, which describe the dynamical behavior of a system completely. Changes in the parameters may be caused by damages [FW07] and can be detected by evaluating the residual statistically. The evaluation is done by means of the asymptotic local approach to change detection. In the following, the theoretical background is recalled, introducing the residual function and its statistical properties first, followed by a summary of the statistical damage testing.

2.4.1 Subspace-based residual function

It is assumed that the dynamical properties of the system in (2.1) or (2.3) can be completely described by some system parameters, collected in a parameter vector θ. Common parametrizations of mechanical structures are physical parameters such as mass, damping, and stiffness parameters, or the eigenstructure. The nominal value of the parameter vector in the undamaged state is denoted by θ^* and detecting changes in θ becomes the monitoring task. In the following notation it is assumed that theta contains the modal parameters and is defined as

$$\theta = \begin{bmatrix} \Lambda \\ \mathrm{vec}(\Phi) \end{bmatrix}, \tag{2.20}$$

where $\Lambda = [\lambda_1 \, , \lambda_2 \, , \ldots \, , \lambda_n]^T$ is a vector containing all eigenvalues.

In accordance to the covariance-driven SSI in section 2.3.2 a block Hankel matrix $\mathcal{H}^*_{p+1,q}$ (2.12) is considered that is built from the output covariances R_i in an undamaged reference state. $\mathcal{H}^*_{p+1,q}$ can be factorized into the observability and the controllability matrix (2.13), which contain the state-space matrices A and C (2.5) and implicitly parameter vector θ. Consequently, a residual function on the basis of $\mathcal{O}_{p+1}$ allows for monitoring the parameter vector θ. The observability matrix in the modal basis can be built from the system parameters in θ^* with

$$\mathcal{O}_{p+1}(\theta^*) = \begin{bmatrix} \Phi \\ \Phi\Delta \\ \vdots \\ \Phi\Delta^{p-1} \end{bmatrix} \in \mathbb{C}^{(p+1)r \times n}, \tag{2.21}$$

with the diagonal matrix $\Delta \stackrel{\mathrm{def}}{=} \mathrm{diag}(\Lambda)$.

The residual function is based on the left null space $S(\theta^*)$ of $\mathcal{O}_{p+1}(\theta^*)$ that is obtained from a SVD analogous to (2.10) with $S(\theta^*) = U_2$. It holds

$$S(\theta^*)^T \mathcal{O}_{p+1}(\theta^*) = 0. \tag{2.22}$$

Due to factorization property (2.13), $\mathcal{H}^*_{p+1,q}$ and $\mathcal{O}_{p+1}(\theta^*)$ share the same left null space. Thus, with a Hankel matrix that is computed under $\theta = \theta^*$ it also holds

$$S(\theta^*)^T \mathcal{H}^*_{p+1,q} = 0. \tag{2.23}$$

In the residual function a covariance Hankel matrix estimated from a data set $\mathcal{Y}_N$ of length N of the current monitoring state is confronted to the reference matrix $S(\theta^*)$. The residual function is defined by

$$\zeta(\theta^*, \mathcal{Y}_N) \stackrel{\text{def}}{=} \sqrt{N}\,\text{vec}(S(\theta^*)^T \widehat{\mathcal{H}}_{p+1,q}), \tag{2.24}$$

with

$$\mathbf{E}_\theta(\zeta(\theta^*, \mathcal{Y}_N)) = 0 \quad \text{iff} \quad \theta = \theta^*. \tag{2.25}$$

$\mathbf{E}_\theta$ denotes the expectation when $\mathcal{Y}_N$ is recorded from a system with system parameter θ. Hence, the residual mean is zero when the system is in the reference state, since the testing Hankel matrix has the same left null space that was determined in the reference state. The mean value deviates from zero when the system is damaged.

Although the idea for the residual relies on (2.22), usually the reference matrix $S(\theta^*)$ is computed directly as the left null space of the covariance Hankel matrix in the reference state. This avoids the system identification step to derive θ^*. In this case, condition (2.25) still applies, since $\mathcal{H}_{p+1,q}$ and $\mathcal{O}_{p+1}$ share the same left null space, as remarked in the context of (2.23).

2.4.2 Statistical damage testing

The statistical evaluation of the residual in (2.24) requires its distribution properties, which are unknown in general. To solve this problem, the asymptotic local approach to change detection [BBM87] is used. This approach is based on the concept of local asymptotic normality [Le 56] and compares the statistical distributions under close hypotheses.

The close hypotheses are formulated as

$$\begin{array}{ll} \mathbf{H}_0 : \ \theta = \theta^* & \text{(reference system)} \\ \mathbf{H}_1 : \ \theta = \theta^* + \delta/\sqrt{N} & \text{(damaged system)}, \end{array} \tag{2.26}$$

and discriminate between the parameter vector in the undamaged and the damaged state. The parameter change δ is unknown but fixed and consequently very small damages can be detected by increasing the number of data samples N.

With the close hypotheses, the central limit theorem applies for the residual function, i.e. the residual is asymptotically Gaussian distributed as shown in [BAB00]. For $N \to \infty$

it holds

$$\zeta(\theta^*, \mathcal{Y}_N) \xrightarrow{d} \begin{cases} \mathcal{N}(0, \Sigma_\zeta(\theta^*)) & \text{under } \mathbf{H}_0 \\ \mathcal{N}(\mathcal{J}_\zeta(\theta^*)\,\delta, \Sigma_\zeta(\theta^*)) & \text{under } \mathbf{H}_1, \end{cases} \tag{2.27}$$

where "d" denotes convergence in distribution. $\mathcal{J}_\zeta(\theta^*)$ is a Jacobian matrix and denotes the asymptotic sensitivity of the residual with respect to the system parameters in the reference state. For a system that is parametrized with respect to its modal parameters, the asymptotic residual sensitivity was derived in [BAB00; BMG04]. It is written as

$$\mathcal{J}_\zeta(\theta^*) = (\mathcal{O}_{p+1}(\theta^*)^\dagger \mathcal{H}_{p+1,q} \otimes S(\theta^*))^T \mathcal{O}'_{p+1}(\theta^*). \tag{2.28}$$

The computation of the derivative $\mathcal{O}'_{p+1}$ is recalled in section 2.5. $\Sigma_\zeta(\theta^*)$ is the residual covariance. When it can be assumed that the noise properties in the dynamical system do not change, there is no need to recompute the covariance in the testing state [BAB00]. A detailed computation procedure of the residual covariance $\Sigma_\zeta(\theta^*)$ is presented in the subsequent section.

With the residual being asymptotically Gaussian distributed (2.27) the damage detection task is to decide if the mean of a Gaussian variable is significantly different from zero. Assuming $\mathcal{J}_\zeta(\theta^*)$ to be of full rank, the residual can be tested in a generalized likelihood ratio test [BAB00]. The test writes as

$$t = \zeta(\theta^*, \mathcal{Y}_N)^T \Sigma_\zeta(\theta^*)^{-1} \mathcal{J}_\zeta(\theta^*) \left(\mathcal{J}_\zeta(\theta^*)^T \Sigma_\zeta(\theta^*)^{-1} \mathcal{J}_\zeta(\theta^*) \right)^{-1} \mathcal{J}_\zeta(\theta^*)^T \Sigma_\zeta(\theta^*)^{-1} \zeta(\theta^*, \mathcal{Y}_N). \tag{2.29}$$

The Gaussian distribution properties of the residual yield an asymptotically χ^2-distributed test statistic t. The Gaussian residual with zero mean in the reference state leads to a central χ^2-distribution. From the mean value $\mathcal{J}_\zeta \delta$ in the damaged case a non-central χ^2-distribution follows and it holds

$$t \xrightarrow{d} \begin{cases} \chi^2(\nu, 0) & \text{under } \mathbf{H}_0 \\ \chi^2(\nu, \lambda) & \text{under } \mathbf{H}_1. \end{cases} \tag{2.30}$$

For a full rank $\mathcal{J}_\zeta(\theta^*)$, the degree of freedom ν and the non-centrality parameter λ in the damaged case are computed with

$$\nu = \operatorname{rank}(\mathcal{J}_\zeta(\theta^*)) \;\;,\;\; \lambda = \delta^T (\mathcal{J}_\zeta^T(\theta^*) \Sigma_\zeta^{-1}(\theta^*) \mathcal{J}_\zeta(\theta^*)) \delta. \tag{2.31}$$

For cases, where the sensitivity matrix is not of full rank, the reader is referred to [Men20].

A special case are the non-parametric tests [Bal+08b], which are applied without focusing on a particular system parametrization θ. This corresponds to a direct detection of changes in the residual and $\mathcal{J} = I$ [DMH14; MDV21]. They are attractive due to their simplicity, since they avoid a detailed system identification even in the reference state. The central limit theorem from (2.27) becomes

$$\zeta(\theta^*, \mathcal{Y}_N) \longrightarrow \begin{cases} \mathcal{N}(0, \Sigma_\zeta(\theta^*)) & \text{under } \mathbf{H}_0 \\ \mathcal{N}(\gamma, \Sigma_\zeta(\theta^*)) & \text{under } \mathbf{H}_1, \end{cases} \tag{2.32}$$

where γ is a change in the residual mean due to damage. The test writes as

$$t = \zeta(\theta^*, \mathcal{Y}_N)^T \Sigma_\zeta(\theta^*)^{-1} \zeta(\theta^*, \mathcal{Y}_N), \tag{2.33}$$

and ν and λ become

$$\nu = \text{rank}(\Sigma_\zeta(\theta^*)) \ , \ \ \lambda = \gamma^T \Sigma_\zeta(\theta^*)^{-1} \gamma. \tag{2.34}$$

2.4.3 Asymptotic residual covariance

For the statistical evaluation of the residual in (2.29) its covariance is required. This covariance cannot be calculated directly, but has to be derived from the covariance of the underlying Hankel matrix $\Sigma_\mathcal{H}$. The computation algorithm for $\Sigma_\mathcal{H}$ depends on the computation method for $\mathcal{H}$. For the covariance-driven SSI an efficient computation algorithm of the Hankel covariance is given in [DM13a], taking problems due to small number of data sets into account. This algorithm is recalled in the following.

Let $\widehat{\mathcal{H}}_{p+1,q}$ be estimated on a data set of length N. The asymptotic covariance of the vectorized Hankel matrix $\Sigma_\mathcal{H}$ is defined as

$$\Sigma_\mathcal{H} \overset{\text{def}}{=} \lim_{N\to\infty} \text{cov}(\sqrt{N}\text{vec}\widehat{\mathcal{H}}_{p+1,q}). \tag{2.35}$$

To estimate the covariance from one reference data set, the data is cut into n_b blocks, each of length N_b such that $N = N_b \cdot n_b$. From each data block of length N_b a Hankel matrix $\widehat{\mathcal{H}}^{(s)}_{p+1,q}$, with $s = 1, ..., n_b$ is computed. With $\widehat{\bar{\mathcal{H}}}_{p+1,q} = \frac{1}{n_b}\sum_{s=1}^{n_b} \widehat{\mathcal{H}}^{(s)}_{p+1,q}$ the well-known computation procedure of the sample covariance leads to

$$\widehat{\Sigma}_\mathcal{H} = \frac{N_b}{n_b - 1} \sum_{s=1}^{n_b} \text{vec}(\widehat{\mathcal{H}}^{(s)}_{p+1,q} - \widehat{\bar{\mathcal{H}}}_{p+1,q})\text{vec}(\widehat{\mathcal{H}}^{(s)}_{p+1,q} - \widehat{\bar{\mathcal{H}}}_{p+1,q})^T. \tag{2.36}$$

The asymptotic residual covariance is derived from $\widehat{\Sigma}_{\mathcal{H}}$ using the statistical delta method to propagate the uncertainties of the underlying Hankel matrix to the residual. The residual covariance estimate writes as [DMH14]

$$\widehat{\Sigma}_{\zeta}(\theta^*) = (I \otimes S^T(\theta^*))\, \widehat{\Sigma}_{\mathcal{H}}\, (I \otimes S(\theta^*)). \tag{2.37}$$

In case of the non-parametric test (2.33) the parameter θ^* is omitted.

2.4.4 Decision making from test results

To draw conclusions from the statistical tests in (2.29) or (2.33) the distribution of t in the undamaged state is considered in order to define a threshold for decision making.

In theory t follows a χ^2-distribution defined by two parameters, ν denoting the DOF and the non-centrality parameter λ (which is 0 in the undamaged state). The number of DOF of the distribution is affected by the system parametrization considered in parameter vector θ. From (2.31) it follows that for a system parametrized with respect to its modal parameters, it holds $\nu = 2mr$. When e.g. a number of $\bar{m}$ structural parameters are used for a full parametrization of the system, it becomes $\nu = \bar{m}$. The non-centrality parameter λ in (2.31) depends on the damage (changed parameter and extent of change), as it is affected by δ only [MDV21]. In the undamaged state δ is zero and the distribution of the test is the central χ^2-distribution. However, a theoretical value of λ cannot be derived, since the residual covariance cannot be obtained from theory but is estimated from data.

In applications the statistical properties usually are evaluated empirically on the basis of a Monte Carlo study. From the empirical distribution of the test values a threshold is derived such that false alarms occur with a desired probability, e.g. with less than 1% as illustrated in Fig.2.1 (left). A test value in the testing phase above the threshold will classify the structure to be damaged.

Fig. 2.1 (right) shows the probability density function (pdf) for a χ^2-distributed random variable for two different DOF in the central case and for $\lambda = 50$. For a small number of DOF the distribution is narrow. The spread increases with larger DOF resulting in a more significant overlap of the central and the non-central distribution. In the context of damage detection based on the test statistic t this means that the smaller the dimension of the parametrization, the smaller damages can be detected [MDV21].

Very common characteristics for the evaluation of the damage detection test perfor-

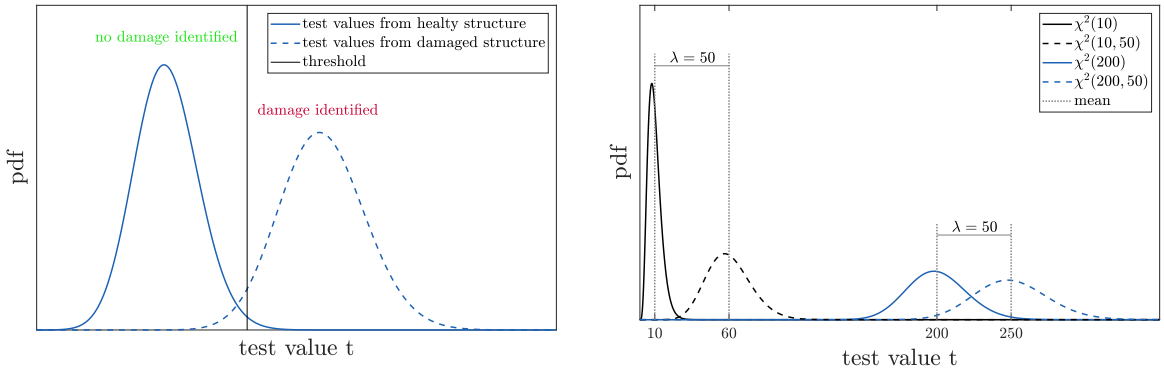

Figure 2.1 – χ^2-distribution for different parameters (left) and definition of threshold (right).

mance are the probability of detection (POD) as a measure of the test sensitivity, and the probability of false alarms (PFA), which usually is part of the conceptualization on the damage detection task and leads to the choice of the damage detection threshold. They are defined as

$$\text{POD} = \frac{\text{true positives detected}}{\text{total true positive}} \quad , \quad \text{PFA} = \frac{\text{false positive detected}}{\text{total true negative}} \, . \tag{2.38}$$

The PFA depends on the spread of the test values in the reference state and the chosen threshold, but not on the damage size. The POD is affected by the spread of the test values, the threshold, and the damage size, where big damages lead to high POD. Consequently, a high threshold avoids false alarms, but depending on the damage size many damages will be undetected. A low threshold leads to a higher sensitivity, but also results in a higher PFA.

To evaluate the test performance independently from the choice of threshold, the relation between POD and PFA can be considered in a receiver operating characteristic (ROC) curve, e.g. described in [SCN09] in the context of noisy non-destructive testing devices. For this curve, couples of POD and PFA are computed for different thresholds at a fixed damage size. A typical ROC curve is demonstrated in Fig. 2.2. Hence, the best performance of a test is when no false alarms occur and the POD is 100%. The more the curve approaches this point, the better it performs. When the curve approaches 100% POD for any PFA, this can be considered as a indication of decoupled POD and PFA. The line of no performance denotes the cases, where POD equals the PFA.

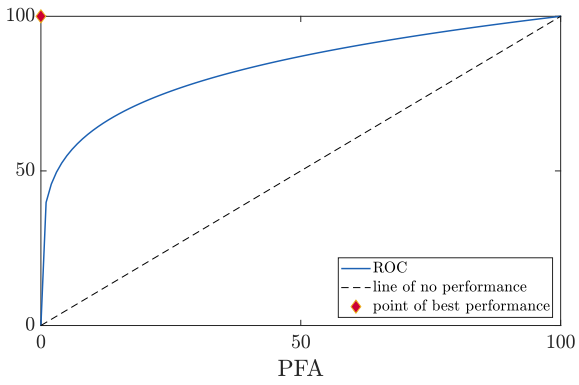

Figure 2.2 – Typical receiver operating characteristic curve.

2.5 Considerations for uncertainty computation

In the previously described damage detection methodology the decision over the structure's state to be damaged or undamaged relies on a statistical test (2.29). In the test the uncertainties related to the residual are considered in terms of the residual covariance $\Sigma_\zeta(\theta^*)$. The covariance is of particular importance for the test behavior. In general, the covariance can be estimated by the sample covariance. However, the direct computation of such a sample covariance is often inconvenient, and instead a sensitivity-based propagation of the (sample) covariance of an underlying random vector is performed. In this thesis such sensitivities are derived by means of perturbation theory. In this section the concept of perturbation propagation is introduced referring to the delta method. Some relevant uncertainty computations from literature are recalled subsequently.

2.5.1 Mathematical remarks

In the following, some mathematical considerations are summarized that are used in the subsequent developments.

Let A, B, C, and D be matrices, such that the matrix multiplication in the following equations applies. For the Kronecker product "$\otimes$" it holds

$$AC \otimes BD = (A \otimes B)(C \otimes D). \tag{2.39}$$

With "vec" denoting the column stacking operator it is

$$\mathrm{vec}(ABC) = (C^T \otimes A)\ vec(B). \tag{2.40}$$

Permutation matrix $\mathcal{P}$ A vectorized matrix $X \in \mathbb{R}^{a\times b}$ can be linked to the vectorization of its transposed by a permutation matrix $\mathcal{P}_{a,b}$ such that

$$\operatorname{vec}(X^T) = \mathcal{P}_{a,b} \operatorname{vec}(X). \tag{2.41}$$

The permutation matrix $\mathcal{P}_{a,b}$ is defined as

$$\mathcal{P}_{a,b} \overset{\text{def}}{=} \sum_{k=1}^{a}\sum_{k=1}^{b} E_{k,l}^{a,b} \otimes E_{l,k}^{b,a} = \left[I_a \otimes e_1 \; I_a \otimes e_2 \; ... \; I_a \otimes e_b\right], \tag{2.42}$$

with properties

$$\mathcal{P}_{a,b}^T \mathcal{P}_{a,b} = \mathcal{P}_{a,b}\mathcal{P}_{a,b}^T = I_{ab}$$
$$\mathcal{P}_{a,b}^T = \mathcal{P}_{b,a}.$$

$E_{k,l}^{a,b} \in \mathbb{R}^{a\times b}$ are matrices which are equal to 1 at entry (k,l) and zero elsewhere, I_a is the identity matrix of size $a \times a$, and $e_i \in \mathbb{R}^b$ are unit vectors with the entry 1 at position i and zero elsewhere. With matrix $H \in \mathbb{R}^{c\times d}$ it holds

$$(X \otimes H)\mathcal{P}_{b,d} = \mathcal{P}_{a,c}(H \otimes X). \tag{2.43}$$

2.5.2 Concept of uncertainty propagation

The perturbation of a function of a random vector is computed from the perturbation of its underlying random vector by means of the delta method. Let $\widehat{X}$ be a random vector whose true value is X and with covariance $\Sigma(\widehat{X})$. The first-order Taylor approximation of vector valued functions $g(\widehat{X})$ yields

$$g(\widehat{X}) \approx g(X) + \Delta g(X) = g(X) + \mathcal{J}_{g,X}(\widehat{X} - X), \tag{2.44}$$

where the derivative or sensitivity $\mathcal{J}_{g,X}$ is the Jacobian matrix in the multivariate case. The Jacobian writes as

$$\mathcal{J}_{g,X} = \frac{\partial g}{\partial X} = \begin{bmatrix} \frac{\partial g_1}{\partial x_1} & \cdots & \frac{\partial g_1}{\partial x_k} \\ \vdots & \ddots & \vdots \\ \frac{\partial g_j}{\partial x_1} & \cdots & \frac{\partial g_j}{\partial x_k} \end{bmatrix} \tag{2.45}$$

for function $g : \mathbb{R}^k \to \mathbb{R}^j$, and is evaluated at X. $\Delta g(X)$ is the perturbation of the function and thus the covariance of the vector valued function follows from $\text{vec}\Delta g\,(\text{vec}\Delta g)^T$. It can be approximated with

$$\Sigma(g(\widehat{X})) \approx \mathcal{J}_{g,X}\,\Sigma(\widehat{X})\,\mathcal{J}_{g,X}^T. \tag{2.46}$$

With the delta method [CB02] it is shown that the approximated covariance of a function of a random variable is correct at the limit, i.e. when the number of samples N goes to infinity. For a sequence of random vectors $\widehat{X}_N$ converging to a true value X for $N \to \infty$ and satisfying the central limit theorem

$$\sqrt{N}(\widehat{X}_N - X) \xrightarrow{d} \mathcal{N}(0, \Sigma) \tag{2.47}$$

it holds

$$\sqrt{N}(g(\widehat{X}_N) - g(X)) \xrightarrow{d} (0, \mathcal{J}_{g,X}\,\Sigma\,\mathcal{J}_{g,X}^T). \tag{2.48}$$

In most cases $g(X)$ is unknown and the Jacobian (2.45) has to be derived by means of mathematical perturbation theory using first-order perturbations denoted by Δ. This is convenient for asymptotic Gaussian variables, e.g. [MDM16]. The basic idea is that $\mathcal{J}_{g,X}$ can be obtained from the relation between $\Delta g(X)$ and ΔX, due to $\Delta g(X) \approx \mathcal{J}_{g,X}\,\Delta X$ (2.44), where $\Delta X = \widehat{X} - X$ for $\widehat{X}$ close to X. In the application case, a perturbation Δ is introduced to the vector valued function. The Δ-terms are isolated, leading to the needed sensitivity by the remaining part of the perturbed function.

2.5.3 Relevant uncertainty computations from literature

This section recalls some uncertainty computation procedures from literature, which are used later in the contribution part of the thesis.

Residual sensitivity $\mathcal{J}_{\zeta,\mathcal{H}}$ related to the testing Hankel matrix The concept of uncertainty propagation is firstly applied to a simple example deriving the sensitivity of the residual as it is used in (2.37). The distribution properties of the conventional residual are derived from the distribution of the underlying Hankel estimate $\widehat{\mathcal{H}}_{p+1,q}$. The index denoting the block row and block column sizes is dropped in the following for simplicity. The distribution of the Hankel matrix is not exactly known but is shown to be

asymptotically Gaussian [Han70] and writes as

$$\sqrt{N}\text{vec}(\widehat{\mathcal{H}} - \mathcal{H}) \xrightarrow{d} \mathcal{N}(0, \Sigma_{\mathcal{H}}). \tag{2.49}$$

With the delta method for a function $f(\widehat{\mathcal{H}}) = \text{vec}(S^T\widehat{\mathcal{H}})$ it follows

$$\sqrt{N}\text{vec}(f(\widehat{\mathcal{H}}) - f(\mathcal{H})) \xrightarrow{d} \mathcal{N}(0, \mathcal{J}_f\Sigma_{\mathcal{H}}\mathcal{J}_f^T). \tag{2.50}$$

Due to the definition of S as the left null space of $\mathcal{H}$ and assuming it is deterministic, the function f is zero at the true value of $\mathcal{H}$. (2.50) becomes

$$\sqrt{N}\text{vec}(S^T\widehat{\mathcal{H}}) \xrightarrow{d} \mathcal{N}(0, \mathcal{J}_f\Sigma_{\mathcal{H}}\mathcal{J}_f^T), \tag{2.51}$$

which is exactly the residual (2.24) and its distribution in the undamaged state. Derivative $\mathcal{J}_f$ is derived by introducing a perturbation into function f and with (2.40) it yields

$$\Delta f(\mathcal{H}) = \text{vec}(S^T\Delta\mathcal{H}) = (I \otimes S^T)\text{vec}(\Delta\mathcal{H}) = \mathcal{J}_f\text{vec}(\Delta\mathcal{H}). \tag{2.52}$$

Perturbation propagation to modal parameters from SSI An algorithm for perturbation propagation from the estimated Hankel matrix to the modal parameters with the SSI procedure is given in [PGS07; RPD08]. A numerical efficient computation is derived in [DM13a]. The computation of the sensitivities is recalled in the following.

The propagation follows the computation procedure of the modal parameters from the Hankel matrix that was described in section 2.3. With a SVD of the covariance Hankel matrix $\mathcal{H}$ the observability matrix $\mathcal{O}$ is derived (2.9) leading to the state-space matrices A and C (2.5). Subsequently, the modal parameters λ and φ in θ^* are computed from A and C (section 2.3.3). The same procedure is considered for the propagation of the perturbations from the Hankel matrix to the identified modal parameters, leading to the associated sensitivity $\mathcal{J}_{\theta^*,\mathcal{H}} = \mathcal{J}_{\theta^*,A|C}\,\mathcal{J}_{A|C,\mathcal{O}}\,\mathcal{J}_{\mathcal{O},\mathcal{H}}$.

Let I_a denote a $a \times a$ identity matrix and $0_{a,b}$ be the $a \times b$ zero matrix. $\mathcal{P}$ is the permutation matrix in (2.42). The sensitivity $\mathcal{J}_{\mathcal{O},\mathcal{H}} \in \mathbb{R}^{(p+1)rn\times(p+1)rqr}$ of the observability matrix writes as

$$\mathcal{J}_{\mathcal{O},\mathcal{H}} \overset{\text{def}}{=} \frac{1}{2}(I_n \otimes U_1\Sigma_1^{-1/2})F_1 \begin{bmatrix} (v_1 \otimes u_1)^T \\ \vdots \\ (v_n \otimes u_n)^T \end{bmatrix} + (\Sigma_1^{-1/2} \otimes \begin{bmatrix} I_{(p+1)r} & 0_{(p+1)r,qr} \end{bmatrix}) \begin{bmatrix} B_1^\dagger C_1 \\ \vdots \\ B_n^\dagger C_n \end{bmatrix}, \tag{2.53}$$

where

$$B_i \stackrel{\text{def}}{=} \begin{bmatrix} I_{(p+1)r} & -\frac{1}{\sigma_i}\mathcal{H}_{p+1,q} \\ -\frac{1}{\sigma_i}\mathcal{H}^{0\ T} & I_{qr} \end{bmatrix} \ , \ C_i \stackrel{\text{def}}{=} \frac{1}{\sigma_i}\begin{bmatrix} v_i^T \otimes (I_{(p+1)r} - u_i u_i^T) \\ (u_i^T \otimes (I_{qr} - v_i v_i^T))\mathcal{P}_{(p+1)r,qr} \end{bmatrix}. \tag{2.54}$$

σ_i, u_i, and v_i are the i-th singular values, left and right singular vectors of the Hankel matrix. The selection matrix S_1 is

$$F_1 \stackrel{\text{def}}{=} \sum_{k=1}^{n} E^{n^2,n}_{(k-1)n+k,k}. \tag{2.55}$$

The sensitivities of system matrices A and C with respect to the observability matrix $\mathcal{J}_{A,\mathcal{O}} \in \mathbb{R}^{n^2\times(p+1)rn}$ and $\mathcal{J}_{C,\mathcal{O}} \in \mathbb{R}^{rn\times(p+1)rn}$ are derived to

$$\mathcal{J}_{A,\mathcal{O}} \stackrel{\text{def}}{=} (I_n \otimes \mathcal{O}^{\uparrow\dagger} F_2) - (A^T \otimes \mathcal{O}^{\uparrow\dagger} F_3) + ((\mathcal{O}^{\downarrow T} F_2 - A^T \mathcal{O}^{\uparrow T} F_2) \otimes (\mathcal{O}^{\uparrow T}\mathcal{O}^{\uparrow})^{-1})\mathcal{P}_{(p+1)r,n}, \tag{2.56}$$

with $\mathcal{O} = \mathcal{O}_{p+1}$, the selection matrices

$$F_2 \stackrel{\text{def}}{=} \begin{bmatrix} 0_{pr,r} & I_{pr} \end{bmatrix} \ , \ F_3 \stackrel{\text{def}}{=} \begin{bmatrix} I_{pr} & 0_{pr,r} \end{bmatrix}, \tag{2.57}$$

and

$$\mathcal{J}_{C,\mathcal{O}} \stackrel{\text{def}}{=} I_n \otimes \begin{bmatrix} I_r & 0_{r,pr} \end{bmatrix}. \tag{2.58}$$

For the sensitivities of the eigenvalues and mode shapes $\mathcal{J}_{\lambda_i,A} \in \mathbb{C}^{1\times n^2}$ and $\mathcal{J}_{\varphi_i,A/C} \in \mathbb{C}^{r\times(n^2+rn)}$ we have

$$\mathcal{J}_{\lambda_i,A} \stackrel{\text{def}}{=} \frac{1}{\chi_i^* \phi_i}(\phi_i^T \otimes \chi_i^*) \tag{2.59}$$

$$\mathcal{J}_{\varphi_i,A/C} \stackrel{\text{def}}{=} \frac{1}{(C\phi_i)_k}(I_r - [0_{r,k-1}\ \phi_i\ 0_{r,r-k}])[C\mathcal{J}_{\phi_i,A}\ \phi_i^T \otimes I_r], \tag{2.60}$$

where λ_i, ϕ_i, χ_i and φ_i are the i-th eigenvalue, right eigenvector, left eigenvector of A and the i-th mode shape respectively. * denotes the complex conjugate transpose, and $\mathcal{J}_{\phi_i,A}$ is defined as

$$\mathcal{J}_{\phi_i,A} \stackrel{\text{def}}{=} (\lambda_i I_n - A)^{\dagger}\left(\phi_i^T \otimes (I_n - \frac{\phi_i \chi_i^*}{\chi_i^* \phi_i})\right). \tag{2.61}$$

Perturbation propagation to parametric observability matrix In [DMH14] the sensitivity of the parametric observability matrix in the modal basis $\mathcal{O}_{p+1}(\theta^*)$ with respect to the modal parameters in θ^* is derived. It is computed as the derivative of the real-valued parametric observability matrix $\mathcal{O}'_{p+1}(\theta^*)$.

The system parameter θ^* is separated into its conjugate complex pairs θ_c^* and $\theta_{\bar{c}}^*$. Corresponding to this ϕ_c and Δ_c are computed such that $\phi = \begin{bmatrix}\phi_c & \phi_{\bar{c}}\end{bmatrix}$ and $\Lambda = \begin{bmatrix}\Lambda_c^T & \Lambda_{\bar{c}}^T\end{bmatrix}$ and $\Delta_c = \mathrm{diag}(\Lambda_c)$.

The real-valued parametric observability matrix writes as

$$\mathcal{O}_{p+1}(\theta^*) \stackrel{\text{def}}{=} \begin{bmatrix} \Re(\phi_c) & \Im(\phi_c) \\ \Re(\phi_c\Delta_c) & \Im(\phi_c\Delta_c) \\ \vdots & \vdots \\ \Re(\phi_c\Delta_c^p) & \Im(\phi_c\Delta_c^p) \end{bmatrix}, \tag{2.62}$$

leading to the derivative

$$\mathcal{J}_{\mathcal{O},\theta^*} \stackrel{\text{def}}{=} \begin{bmatrix} \Re(\mathcal{O}'_{p+1}(\theta_c)) & -\Im(\mathcal{O}'_{p+1}(\theta_c)) \\ \Im(\mathcal{O}'_{p+1}(\theta_c)) & \Re(\mathcal{O}'_{p+1}(\theta_c)) \end{bmatrix}. \tag{2.63}$$

$\mathcal{O}'_{p+1}(\theta_c)$ is the complex-valued derivative of the vectorized observability matrix

$$\mathcal{O}'_{p+1}(\theta_c) \stackrel{\text{def}}{=} \begin{bmatrix} \Lambda_1'^{(p)} \otimes \varphi_1 & & 0 & \Lambda_1^{(p)} \otimes I_r & & 0 \\ & \ddots & & & \ddots & \\ 0 & & \Lambda_m'^{(p)} \otimes \varphi_m & 0 & & \Lambda_m^{(p)} \otimes I_r \end{bmatrix}, \tag{2.64}$$

where

$$\Lambda_i^{(p)} \stackrel{\text{def}}{=} \begin{bmatrix} 1 & \lambda_i & \lambda_i^2 & \dots & \lambda_i^p \end{bmatrix}^T, \quad \Lambda_i'^{(p)} \stackrel{\text{def}}{=} \begin{bmatrix} 0 & 1 & 2\lambda_i & \dots & p\lambda_i^{p-1} \end{bmatrix}^T \tag{2.65}$$

for $1 \leq i \leq m$.

2.6 Model interpolation of linear parameter varying systems

In this thesis a damage detection method is developed that is robust to environmental changes. The method relies on the stochastic subspace-based damage detection and uses

a direct model interpolation method from [Zha18] for linear parameter varying (LPV) systems that is recalled in this section.

2.6.1 Concept

LPV systems are systems whose dynamical behavior depends on an over the time varying scheduling parameter P. They can be approximated by LTI systems at fixed parameter working points. Assume a LPV system from which output data is available at several working points P_j with $j = 1, 2, ..., u$. A model of the system at a particular parameter point P, where P is in general different from the previous P_j, can be obtained by the direct model interpolation from [Zha18]. In this approach local state-space models are interpolated to a large global model, which is subsequently reduced and from which data $\mathcal{Y}(P)$ at parameter P can be characterized. This data is shown to be equivalent to interpolated data from coherent local models.

2.6.2 Model interpolation

The LTI system at the j-th working point is represented by a local version of (2.3) with

$$\begin{cases} x_{j,k+1} = A_j x_{j,k} + w_{j,k} \\ y_{j,k} = C_j x_{j,k} + v_{j,k}. \end{cases} \tag{2.66}$$

Assume data sets in the undamaged state are available at parameter working points P_j with $j = 1, ..., u$. For any parameter P a global model can be derived as

$$\begin{aligned} \underline{x}_{k+1} &= \underline{A}\, \underline{x}_k + \underline{w}_k \\ y_k &= \underline{C}(P)\, \underline{x}_k + \underline{v}_k(P)\,, \end{aligned} \tag{2.67}$$

at time step k and with

$$\underline{A} = \begin{bmatrix} A_1 & & \\ & \ddots & \\ & & A_u \end{bmatrix},\ \underline{x}_k = \begin{bmatrix} x_{1,k} \\ \vdots \\ x_{u,k} \end{bmatrix},\ \underline{w}_k = \begin{bmatrix} w_{1,k} \\ \vdots \\ w_{u,k} \end{bmatrix},$$

$$\underline{C}(P) = \begin{bmatrix} \rho_1(P)C_1 & \cdots & \rho_l(P)C_u \end{bmatrix},$$

$$\underline{v}_k(P) = \textstyle\sum_{j=1}^{u} \rho_j(P)\, v_{j,k}(t)\,.$$

The state transition matrix and the state vector are not interpolated but are concatenated from all working points j.

Weighting functions $\rho(P)$ are chosen such that

$$\sum_{j=1}^{u} \rho_j(P) = 1 \quad \text{for all} \quad P \in \mathbb{P} \quad \text{and} \quad \rho_j(P) : \mathbb{P} \Rightarrow [0,1] \tag{2.68}$$

centered at P.

The global model (2.67) is of order mn and subsequently reduced by means of the well-known balanced reduction method. In the linearly transformed state vector $\underline{x}_k$ the smallest Hankel singular values are removed. This leads to a state space model of order n, same as for the local models.

2.7 Summary

In this chapter the theories and methods that are used in the context of this thesis were recalled. In particular, the background of the stochastic subspace-based damage detection was described in detail, since this method forms the basis of the presented developments.

Part II

Contribution to theory

In this part the methodological contribution of the thesis to the research field of automated vibration-based damage detection for civil structures is presented. The developments are based on the covariance-driven stochastic subspace based damage detection (SSDD). The first chapter is related to distribution properties of the SSDD residual when the reference model is estimated from data and thus afflicted with uncertainties. The second chapter provides a SSDD method that is robust do changes in the environment. Each chapter contains a theory section together with a proof of concept, as well as a discussion section.

Chapter 3

Stochastic subspace-based damage detection with uncertain reference null space

3.1 Introduction

The stochastic subspace-based damage detection (SSDD) method (section 2.4) first presented in [BAB00] works on a residual function, in which a reference null space is confronted to a data covariance Hankel estimate. The residual is evaluated statistically by means of hypothesis testing in a generalized likelihood ratio test, where the residual's covariance is an important part of the test. The covariance is derived from the uncertainty of the Hankel matrix, while the reference null space is assumed to be perfectly known without any impact on the residual uncertainty.

The assumption of a deterministic reference null space is true in ideal cases. However, in real world applications, the reference $S(\theta^*)$ usually is estimated from data. Hence, the residual is a function of two random variables, namely the Hankel matrix estimate in the testing state and the estimate of the reference null space. This has a significant impact on the residual covariance for the damage detection test (2.29), (2.33). Neglecting the uncertainties of the reference null space herein leads to test statistics that deviate from the theoretical values of the expected χ^2-distribution.

This is not only a theoretical problem, but also affects the application in practice when it comes to the determination of a threshold for decision making. Often empirical thresholds are computed from data in the reference state by Monte Carlo studies and the discrepancy between the computed and the theoretical test values is discarded. It is assumed that enough data in the reference state is available. However, especially in cases when monitoring systems are applied retroactively due to indication of initial damage usually only few data of the reference system is available. Thresholds that are derived

from theory can confirm results from empirical studies with few realizations and thus improve the reliability of the test.

In this chapter the gap of the SSDD method for real-world applications with estimated reference is closed. A test that considers the uncertainties related to the reference matrix and the testing data is derived. The residual is formulated as a function of the two random variables $\widehat{S}(\theta^*)$ and $\widehat{\mathcal{H}}$ to which the central limit theorem applies. The statistical delta method is used to derive the statistical properties of the residual and its asymptotic covariance. The associated hypothesis test is presented allowing for theoretical based threshold and predictable test behavior for damage detection.

In section 3.2 the theory for the two random variable dependent residual is derived, and the corresponding hypothesis test is presented. Subsequently, in section 3.3, the new test is evaluated on numerical data. The statistical behavior of the new test is verified towards theoretical expectations, and the test performance is discussed in detail. The impact of considering the uncertainty related to the reference null space is emphasized, and effects of data lengths, system parametrization, or reference null space computation procedure are analyzed.

3.2 Damage detection with uncertain reference

In this section the theory for a residual with an uncertain reference is derived. The developments are based on the SSDD explained in section 2.4. After putting the problem into a formalized context for SSDD, the distribution properties of a residual with uncertain reference are derived. An algorithm for computing the residual covariance is presented using perturbation theory introduced in section 2.5.

3.2.1 Formalized problem statement

The subspace-based residual of the conventional SSDD in section 2.4 is defined as a function of one random variable (cf. (2.24)) with

$$\zeta(\theta^*, \mathcal{Y}_N) = \sqrt{N}\,\mathrm{vec}(S(\theta^*)^T\,\widehat{\mathcal{H}}_{p+1,q}). \tag{3.1}$$

$S(\theta^*)$ denotes the reference matrix of a system with system parameter θ^* and is assumed to be perfectly known. $\widehat{\mathcal{H}}_{p+1,q}$ is the covariance Hankel matrix estimated from a data set of length N in the monitoring state. p and q are parameters for the block row and block

column size of the Hankel matrix and will be dropped in the following for simplicity. The statistical properties of the residual are described in (2.27) with zero mean in the reference state due to property $S(\theta^*)^T\mathcal{H} = 0$. The covariance of the residual is denoted by $\Sigma_\zeta(\theta^*)$ (2.37) and is derived from the uncertainties of the Hankel matrix estimate in the monitoring state.

Now assume that in real-world applications the reference matrix is computed in the reference state from a Hankel matrix $\widehat{\mathcal{H}}^*$ that is estimated from a reference data set $\mathcal{Y}_M$ of length M. Then the reference matrix itself is a random variable afflicted with uncertainties. The fully data-driven residual must be defined as a two random variable function with

$$\tilde{\zeta}(\theta^*, \mathcal{Y}_N) = \sqrt{N}\,\mathrm{vec}(\widehat{S}(\theta^*)^T\,\widehat{\mathcal{H}}), \tag{3.2}$$

and it follows that $\widehat{S}(\theta^*)^T\mathcal{H}$ only approximates zero. Consequently, the distribution properties in (2.27) do not hold for a residual with an estimated reference null space.

The distribution properties of the conventional residual are derived from the distribution of the underlying Hankel estimate $\widehat{\mathcal{H}}$ that is not exactly known. It is shown to be asymptotically Gaussian [Han70] and under the close hypotheses (2.26) it writes as

$$\sqrt{N}\mathrm{vec}(\widehat{\mathcal{H}} - \mathcal{H}^*) \xrightarrow{d} \begin{cases} \mathcal{N}(0, \Sigma_{\mathcal{H}}(\theta^*)) & \text{under } \mathbf{H}_0 \\ \mathcal{N}(\mathcal{J}_{\mathcal{H}}(\theta^*)\,\delta, \Sigma_{\mathcal{H}}(\theta^*)) & \text{under } \mathbf{H}_1 \end{cases} \tag{3.3}$$

δ is the change of the system parameters, $\mathcal{J}_{\mathcal{H}}(\theta^*)$ is the sensitivity of $\mathrm{vec}(\mathcal{H})$ with respect to θ evaluated at θ^*, and $\Sigma_{\mathcal{H}}(\theta^*)$ is the Hankel matrix covariance that is the same as in the reference state under the assumption of unchanged noise properties [BBM87; DMH14] and follows from (2.35).

Now remark that the central limit theorem recalled from (2.27) with

$$\zeta(\theta^*, \mathcal{Y}_N) \xrightarrow{d} \begin{cases} \mathcal{N}(0, \Sigma_\zeta(\theta^*)) & \text{under } \mathbf{H}_0 \\ \mathcal{N}(\mathcal{J}_\zeta(\theta^*)\,\delta, \Sigma_\zeta(\theta^*)) & \text{under } \mathbf{H}_1, \end{cases} \tag{3.4}$$

is a consequence of (3.3), since multiplication of (3.3) with deterministic matrix $S(\theta^*)^T$ yields $\sqrt{N}\mathrm{vec}(S(\theta^*)^T(\widehat{\mathcal{H}}-\mathcal{H}^*))$ on the left. This is equal to residual ζ due to $S(\theta^*)^T\mathcal{H}^* = 0$, which still is an asymptotically Gaussian vector (with different mean and covariance). This allows to state the residual distribution (2.27) without any knowledge on the theoretical limit value of $\mathcal{H}^*$ that is unknown in practice.

However, when replacing $S(\theta^*)$ by its estimate $\widehat{S}(\theta^*)$, this does not hold anymore

since $\widehat{S}(\theta^*)^T\mathcal{H}^* \neq 0$, and the central limit theorem in (2.27) would become incorrect. Since $\widehat{S}(\theta^*)$ is a consistent estimate of $S(\theta^*)$, the asymptotic mean of the residual is not affected, but the fact that $\widehat{S}(\theta^*)^T\mathcal{H}^*$ is only approximately but not exactly zero leads to a modification of the residual covariance. This computational inaccuracy has often been discarded in previous works [Döh+14], and empirical thresholds had to be used for the hypothesis test. For a correct computation of the corresponding damage detection test the distribution properties of $\tilde{\zeta}$ need to be derived including the exact expression for its covariance.

3.2.2 Asymptotic distribution of the residual

The asymptotic distribution of the residual is derived from the joint distribution of the testing Hankel matrix $\mathcal{H}$ and the reference null space Hankel matrix $\mathcal{H}^*$, considering the effect of the data lengths M and N. N is the length of the test data set in the monitoring state to which the residual is normalized. The distribution properties of the conventional residual in (2.27) are derived with respect to this length from the Hankel matrix distribution (3.3). However, the reference null space estimate $\widehat{S}(\theta^*)$ is computed on a data set of length M. Consequently, the error that is induced in the residual by the uncertainty afflicted reference null space depends on this M. The distribution of the Hankel matrix in the reference state $\widehat{\mathcal{H}^*}$ is asymptotically Gaussian with

$$\sqrt{M}\,\mathrm{vec}(\widehat{\mathcal{H}^*} - \mathcal{H}^*) \xrightarrow{d} \mathcal{N}(0, \Sigma_{\mathcal{H}}(\theta^*)) \tag{3.5}$$

for $M \to \infty$, similar as in (3.3). $\Sigma_{\mathcal{H}}(\theta^*)$ is the asymptotic covariance of the data Hankel matrix (2.35) and is the same in the reference and the damaged state under the assumption of unchanged noise properties [BBM87; DMH14]. When the data-driven residual is analyzed as a two random variable function depending on $\widehat{S}(\theta^*)$ and $\widehat{\mathcal{H}}$ both random variables contribute to the distribution properties of the residual and the joint asymptotic distribution of them is needed.

Denote the two random variable function with

$$g(\hat{h}) = \mathrm{vec}(\widehat{S}(\theta^*)^T\widehat{\mathcal{H}}) \tag{3.6}$$

where

$$\hat{h} = \begin{bmatrix}\mathrm{vec}(\widehat{\mathcal{H}^*})\\ \mathrm{vec}(\widehat{\mathcal{H}})\end{bmatrix}, \text{ and } h = \begin{bmatrix}\mathrm{vec}(\mathcal{H}^*)\\ \mathrm{vec}(\mathcal{H}^*)\end{bmatrix},$$

and $g(h) = 0$. With the statistical delta method [CB02] from section 2.5 the asymptotically Gaussian distribution properties of $\hat{h}$ are propagated to $g(\hat{h})$, i.e. to the residual written as $\tilde{\zeta} = \sqrt{N}(g(\hat{h}) - g(h))$. Since $\widehat{\mathcal{H}}^*$ is computed on a data set of length M but the residual is normalized with data length N of the test state, the ratio $c = \frac{N}{M}$ is introduced. Multiplication of $\sqrt{c}$ to the asymptotic distribution properties of $\widehat{\mathcal{H}}^*$ in (3.3) leads to

$$\sqrt{M}\,\sqrt{\tfrac{N}{M}}\mathrm{vec}(\widehat{\mathcal{H}}^* - \mathcal{H}^*) \xrightarrow{d} \mathcal{N}(0, c\Sigma_{\mathcal{H}}(\theta^*)). \tag{3.7}$$

It can be stated that $\widehat{\mathcal{H}}$ and $\widehat{\mathcal{H}}^*$ are independent, as they are computed from different data sets. Consequently, the cross-covariances between the two Hankel matrices will be zero. With the distribution properties of the Hankel matrix under the close hypotheses (3.3) and from (3.7) the joint distribution yields for $\sqrt{N}(\hat{h} - h)$ as

$$\sqrt{N}\left(\begin{bmatrix}\mathrm{vec}(\widehat{\mathcal{H}}^*)\\ \mathrm{vec}(\widehat{\mathcal{H}})\end{bmatrix} - \begin{bmatrix}\mathrm{vec}(\mathcal{H}^*)\\ \mathrm{vec}(\mathcal{H}^*)\end{bmatrix}\right) \xrightarrow{d} \begin{cases} \mathcal{N}\left(\begin{bmatrix}0\\0\end{bmatrix}, \begin{bmatrix}c\Sigma_{\mathcal{H}}(\theta^*) & 0\\ 0 & \Sigma_{\mathcal{H}}(\theta^*)\end{bmatrix}\right) & \text{under } \mathbf{H}_0 \\ \mathcal{N}\left(\begin{bmatrix}0\\ \mathcal{J}_{\mathcal{H}}(\theta^*)\delta\end{bmatrix}, \begin{bmatrix}c\Sigma_{\mathcal{H}}(\theta^*) & 0\\ 0 & \Sigma_{\mathcal{H}}(\theta^*)\end{bmatrix}\right) & \text{under } \mathbf{H}_1 \end{cases} \tag{3.8}$$

From the joint distribution and the first order Taylor expansion of $g(\hat{h})$

$$g(\hat{h}) = g(h) + \mathcal{J}_g(\hat{h} - h)\,, \;\; \mathcal{J}_g = \frac{\partial g(h)}{\partial h}, \tag{3.9}$$

it can be concluded according to (2.48) based on the delta method that $\tilde{\zeta} = \sqrt{N}(g(\hat{h}) - g(h))$ is asymptotically Gaussian with

$$\tilde{\zeta}(\theta^*, \mathcal{Y}_N) \xrightarrow{d} \begin{cases} \mathcal{N}(0, \tilde{\Sigma}_\zeta(\theta^*)) & \text{under } \mathbf{H}_0 \\ \mathcal{N}(\tilde{\mathcal{J}}_\zeta(\theta^*)\,\delta, \tilde{\Sigma}_\zeta(\theta^*)) & \text{under } \mathbf{H}_1. \end{cases} \tag{3.10}$$

δ and $\tilde{\mathcal{J}}_\zeta(\theta^*) = \mathcal{J}_\zeta(\theta^*)$ have not changed with respect to (2.27). The close hypotheses definition (2.26) yields that the asymptotic residual covariance is the same under both hypotheses writing as

$$\tilde{\Sigma}_\zeta(\theta^*) = \mathcal{J}_g \begin{bmatrix} c\,\Sigma_{\mathcal{H}}(\theta^*) & 0 \\ 0 & \Sigma_{\mathcal{H}}(\theta^*) \end{bmatrix} \mathcal{J}_g^T. \tag{3.11}$$

The sensitivity $\mathcal{J}_g$ is obviously of form $\mathcal{J}_g = \begin{bmatrix}\mathcal{J}_1 & \mathcal{J}_2\end{bmatrix}$, where $\mathcal{J}_1$ is related to the uncer-

tainties of the reference null space and $\mathcal{J}_2$ considers the perturbation propagated from the Hankel matrix in the tesing state. The sensitivity is derived in the following section, leading to the asymptotic residual covariance.

In the non-parametric case the residual distribution is analogous to (2.32)

$$\tilde{\zeta}(\theta^*, \mathcal{Y}_N) \xrightarrow{d} \begin{cases} \mathcal{N}(0, \tilde{\Sigma}_\zeta(\theta^*)) & \text{under } \mathbf{H}_0 \\ \mathcal{N}(\tilde{\gamma}, \tilde{\Sigma}_\zeta(\theta^*)) & \text{under } \mathbf{H}_1, \end{cases} \tag{3.12}$$

where $\tilde{\gamma}$ is a change in the residual mean due to damage and has not changed with respect to (2.32).

3.2.3 Asymptotic covariance of the residual

The asymptotic residual covariance $\tilde{\Sigma}_\zeta(\theta^*)$ follows from the Hankel matrix covariance (2.36) with sensitivity $\mathcal{J}_g$. Perturbation theory (section 2.5) is used to propagate the uncertainties from the Hankel matrices $\mathcal{H}^*$ and $\mathcal{H}$ to the residual.

Considering the definition of $g(\hat{h})$ (3.6), the sensitivity $\mathcal{J}_g$ can be computed as the derivative of $\text{vec}(S(\theta^*)^T\mathcal{H})$ with respect to $\text{vec}(\mathcal{H}^*)$, since $S(\theta^*)$ depends on $\mathcal{H}^*$, and to $\text{vec}(\mathcal{H})$. It is obtained through first-order perturbation of the asymptotically Gaussian variables. From the first-order Taylor approximation (3.9) the perturbation in g follows as $\Delta g = \mathcal{J}_g \Delta h$. With (3.6) this writes as

$$\text{vec}(\Delta(S(\theta^*)^T\mathcal{H})) = \mathcal{J}_g \begin{bmatrix} \text{vec}(\Delta\mathcal{H}^*) \\ \text{vec}(\Delta\mathcal{H}) \end{bmatrix}. \tag{3.13}$$

In (3.13) the perturbation of the residual (left side) is related to the reference matrix $S(\theta^*)$ and the tested Hankel matrix $\mathcal{H}$. Being a sum of both perturbations it writes as

$$\text{vec}(\Delta(S(\theta^*)^T\mathcal{H})) = \text{vec}(\Delta S(\theta^*)^T\mathcal{H}) + \text{vec}(S(\theta^*)^T\Delta\mathcal{H}). \tag{3.14}$$

With matrix operations in (2.40) and (2.41) and perturbation matrix $\mathcal{P}$ from (2.42) it can be transformed to

$$\text{vec}(\Delta(S(\theta^*)^T\mathcal{H})) = (\mathcal{H}^T \otimes I_s)\mathcal{P}_{t,s}\,\text{vec}(\Delta S(\theta^*)) + I_{qr} \otimes S(\theta^*)^T\,\text{vec}(\Delta\mathcal{H}), \tag{3.15}$$

which yields the partial sensitivities of the residual with respect to the reference null space

and with respect to the tested Hankel matrix

$$\begin{aligned} \mathcal{J}_{\tilde{\zeta},S} &= (\mathcal{H}^T \otimes I_s)\mathcal{P}_{t,s} \\ \mathcal{J}_{\tilde{\zeta},\mathcal{H}} &= I_{qr} \otimes S(\theta^*)^T. \end{aligned} \tag{3.16}$$

t and s are the number of rows and columns of $S(\theta^*)$, and $\mathcal{J}_{\tilde{\zeta},\mathcal{H}}$ is the sensitivity that was used for the covariance of the conventional residual in (2.37).

The sensitivity $\mathcal{J}_g$ in (3.13) is related to the Hankel matrices $\mathcal{H}^*$ and $\mathcal{H}$. Thus, with (3.16) the link between the reference matrix $S(\theta^*)$ and the Hankel matrix in the reference state $\mathcal{H}^*$ is still missing. It is denoted by the sensitivity $\mathcal{J}_{S,\mathcal{H}^*}$ and $\mathcal{J}_g$ becomes

$$\mathcal{J}_g = \begin{bmatrix} \mathcal{J}_{\tilde{\zeta},S} & \mathcal{J}_{S,\mathcal{H}^*} & \mathcal{J}_{\tilde{\zeta},\mathcal{H}} \end{bmatrix}. \tag{3.17}$$

$\mathcal{J}_{S,\mathcal{H}^*}$ depends on the computation procedure of the reference matrix. The reference null space is computed with a SVD either from the Hankel matrix or from the observability matrix in the modal basis, where the identification of the modal parameters is required in the reference state (see section 2.4.1). The respective derivatives are derived in the following two paragraphs, and finally the computation of the residual covariance estimate is presented.

Sensitivity of a reference null space computed from Hankel matrix When the reference matrix is computed from the Hankel matrix directly, the relation between them is defined through the SVD of $\mathcal{H}^*$ in accordance to (2.10). The reference matrix is the left null space U_2 of the Hankel matrix. This relation is used to derive the corresponding sensitivity $\mathcal{J}_{S,\mathcal{H}^*}$.

In a first step, the perturbation $\Delta\mathcal{H}^*$ is propagated to its column space U_1 in the SVD. This was published in [LLM08] and writes as

$$\Delta U_1 = U_1 R + U_2 U_2^T \Delta\mathcal{H}^* \; V_1 D_1^{-1}. \tag{3.18}$$

Matrices U_1, U_2, and V_1 are the column space, the left null space, and the row space, respectively. D_1 is the matrix with singular values, which expected values are nonzero. Matrix R will be eliminated later. Applying matrix operation (2.40) it follows a vectorized

form with

$$\text{vec}(\Delta U_1) = (I_n \otimes U_1)\ \text{vec}(R) + (D_1^{-1}V_1^T \otimes\ U_2U_2^T)\ \text{vec}(\Delta\mathcal{H}^*). \tag{3.19}$$

This vectorized perturbation of the column space is propagated to the left null space U_2 as follows. First it is considered that $U_1^TU_2 = 0$ holds. Introduce a perturbation $\Delta(\cdot)$ to this yields $\Delta U_1^TU_2 + U_1^T\Delta U_2 = 0$. With identity matrices I as defined in section 2.5.1, permutation matrix $\mathcal{P}$ (2.42), and (2.40) to (2.43) this can be vectorized and converted to

$$(I_s \otimes U_1^T)\ \text{vec}(\Delta U_2) = -(U_2^T \otimes I_n)\ \mathcal{P}_{t,n}\ \text{vec}(\Delta U_1). \tag{3.20}$$

Then, with $U_2^TU_2 = I$ and thus $\Delta(U_2^TU_2) = 0$, it holds $\Delta U_2^TU_2 + U_2^T\Delta U_2 = 0$ leading with the permuation matrix $\mathcal{P}$ (2.42) and (2.40) to (2.43) to

$$\mathcal{P}_{s,s}(I_s \otimes U_2^T)\,\text{vec}(\Delta U_2) + (I_s \otimes U_2^T)\,\text{vec}(\Delta U_2) = 0. \tag{3.21}$$

A particular solution for $\text{vec}(\Delta U_2)$ follows from (3.20) and (3.21) to

$$\begin{aligned}\text{vec}(\Delta U_2) &= -(I_s \otimes U_1)(U_2^T \otimes I_n)\ \mathcal{P}_{t,n}\ \text{vec}(\Delta U_1)\\ &= -\mathcal{P}_{s,t}(U_1 \otimes U_2^T)\ \text{vec}(\Delta U_1),\end{aligned} \tag{3.22}$$

using properties of the permutation matrix $\mathcal{P}$ in (2.42).

The sensitivity of the left null space to its source matrix is derived by substituting (3.19) into (3.22). This leads to

$$\text{vec}(\Delta U_2) = -\mathcal{P}_{s,t}(U_1D_1^{-1}V_1^T \otimes I_s)(I_{qr} \otimes U_2^T)\ \text{vec}(\Delta\mathcal{H}^*). \tag{3.23}$$

And with (2.43) it is

$$\mathcal{J}_{U_2,\mathcal{H}^*} = -\mathcal{P}_{s,t}(U_1D_1^{-1}V_1^T \otimes U_1^T). \tag{3.24}$$

Now coming back to the reference null space as left null space of the Hankel matrix $U_2 = S(\theta^*)$. Since the asymptotic covariance can be derived at $\mathcal{H} = \mathcal{H}^*$ in the reference

state, with (3.24) and (3.16) it is

$$\begin{aligned}\mathcal{J}_{\tilde{\zeta},\mathcal{H}^*} &= \mathcal{J}_{\tilde{\zeta},S}\mathcal{J}_{S,\mathcal{H}^*} \\ &= (\mathcal{H}^T \otimes I_s)\ \mathcal{P}_{t,s}(-\mathcal{P}_{s,t})(U_1 D_1^{-1} V_1^T \otimes S(\theta^*)^T) \\ &= -\mathcal{H}^T U_1 D_1^{-1} V_1^T \otimes S(\theta^*)^T \\ &= -V_1 V_1^T \otimes S(\theta^*)^T. \end{aligned} \tag{3.25}$$

When the reference null space is computed from the Hankel matrix, sensitivity $\mathcal{J}_g$ in (3.17) writes as

$$\mathcal{J}_g = \begin{bmatrix}\mathcal{J}_{\tilde{\zeta},\mathcal{H}^*} & \mathcal{J}_{\tilde{\zeta},\mathcal{H}}\end{bmatrix} = \begin{bmatrix}-V_1 V_1^T \otimes S(\theta^*)^T & I_{qr} \otimes S(\theta^*)^T\end{bmatrix}\ . \tag{3.26}$$

Sensitivity of a reference null space computed from observability matrix Deriving the reference null space from the observability matrix in modal basis includes several steps: First the modal parameters are identified from the Hankel matrix $\mathcal{H}^*$. Let them be collected in parameter vector θ^*. From this the parametric observability matrix $\mathcal{O}(\theta^*)$ is built. In a third step, the left null space of $\mathcal{O}(\theta^*)$ is computed with SVD. The sensitivity of the reference matrix to the Hankel matrix $\mathcal{J}_{S,\mathcal{H}^*}$ is derived by propagate the perturbation of the Hankel matrix, respectively. It is defined as $\mathcal{J}_{S,\mathcal{H}^*} = \mathcal{J}_{S,\mathcal{O}}\,\mathcal{J}_{\mathcal{O},\theta^*}\,\mathcal{J}_{\theta^*,\mathcal{H}^*}$, where all derivatives are already known from the sections before.

$\mathcal{J}_{S,\mathcal{O}}$ is the sensitivity of a left null space $U_2 = S(\theta^*)$ with respect to its source matrix, as in (3.24). Here the source matrix is the parametric observability matrix, and U_1, D_1, and V_1 are the respective matrices from the SVD of $\mathcal{O}(\theta^*)$. The derivative $\mathcal{J}_{\mathcal{O},\theta^*}$, denoting the sensitivity of the parametric observability matrix with respect to these modal parameters, is defined in (2.63). The uncertainties in the modal parameters that are induced by the SSI are propagated by $\mathcal{J}_{\theta^*,\mathcal{H}^*}$, composed from (2.53), (2.56), and (2.58) to (2.60).

When the reference null space is computed from the parametric observability matrix, sensitivity $\mathcal{J}_g$ in (3.17) writes with $\mathcal{J}_{\tilde{\zeta},S}$ and $\mathcal{J}_{\tilde{\zeta},\mathcal{H}}$ from (3.16) as

$$\mathcal{J}_g = \begin{bmatrix}\mathcal{J}_{\tilde{\zeta},\mathcal{H}^*} & \mathcal{J}_{\tilde{\zeta},\mathcal{H}}\end{bmatrix} = \begin{bmatrix}\mathcal{J}_{\tilde{\zeta},S}\,\mathcal{J}_{S,\mathcal{O}}\,\mathcal{J}_{\mathcal{O},\theta^*}\,\mathcal{J}_{\theta^*,\mathcal{H}^*} & \mathcal{J}_{\tilde{\zeta},\mathcal{H}}\end{bmatrix}. \tag{3.27}$$

Residual covariance estimate From the formulations of the derivative $\mathcal{J}_g$ in (3.26) or (3.27) the residual covariance $\tilde{\Sigma}_\zeta$ can be computed as

$$\tilde{\Sigma}_\zeta = c\Sigma_1 + \Sigma_2, \tag{3.28}$$

with the two partial covariances

$$\begin{aligned}\Sigma_1 &= \mathcal{J}_{\tilde{\zeta},\mathcal{H}^*}\,\Sigma_{\mathcal{H}}\,\mathcal{J}_{\tilde{\zeta},\mathcal{H}^*}^T \\ \Sigma_2 &= \mathcal{J}_{\tilde{\zeta},\mathcal{H}}\,\Sigma_{\mathcal{H}}\,\mathcal{J}_{\tilde{\zeta},\mathcal{H}}^T\,.\end{aligned} \tag{3.29}$$

Σ_1 is related to the uncertainty in $\widehat{S}(\theta^*)$, and Σ_2 to the uncertainty of $\widehat{\mathcal{H}}$ in the test state. $\Sigma_{\mathcal{H}}$ is the Hankel matrix covariance, computed in the reference state.

An estimate of the resiudal covariance can be obtained, when instead of the theoretical Hankel matrix covariance $\Sigma_{\mathcal{H}}$ a consistent estimate $\widehat{\Sigma}_{\mathcal{H}}$ (2.36) is used for the partial covariances in (3.29). With data sets of length M for the reference setup and length N in the testing state, the estimated residual covariance is

$$\widehat{\tilde{\Sigma}}_\zeta = \tfrac{N}{M}\widehat{\Sigma}_1 + \widehat{\Sigma}_2\,. \tag{3.30}$$

It follows that for long data sets in the reference state in relation to the data length N in the testing state, the effect of the uncertainty of the testing Hankel matrix in $\widehat{\Sigma}_2$ to the complete residual covariance is much stronger, than the contribution of the uncertainties related to the reference null space in $\widehat{\Sigma}_1$. This is reflected in a small ratio $c = \frac{N}{M}$. In this case the testing Hankel matrix is the more uncertain part of the residual. On the other hand, when for the reference setup very few data is used compared to the amount of data in the testing state, c becomes large and the uncertain reference has a high impact to the residual covariance.

3.2.4 Test statistic

Analogous to (2.29) the damage detection test for the new residual writes in the parametric case as

$$\tilde{t} = \tilde{\zeta}(\theta^*,\mathcal{Y}_N)^T\tilde{\Sigma}_\zeta(\theta^*)^{-1}\mathcal{J}_\zeta(\theta^*)\left(\mathcal{J}_\zeta(\theta^*)^T\tilde{\Sigma}_\zeta(\theta^*)^{-1}\mathcal{J}_\zeta(\theta^*)\right)^{-1}\mathcal{J}_\zeta(\theta^*)^T\tilde{\Sigma}_\zeta(\theta^*)^{-1}\tilde{\zeta}(\theta^*,\mathcal{Y}_N), \tag{3.31}$$

with non-centrality parameter $\tilde{\lambda}$ in the damaged case defined as

$$\tilde{\lambda} = \delta^T(\mathcal{J}_\zeta(\theta^*)^T\tilde{\Sigma}_\zeta(\theta^*)^{-1}\mathcal{J}_\zeta(\theta^*))\,\delta\,. \tag{3.32}$$

The non-parametric version of the test becomes equivalent to (2.33)

$$\tilde{t} = \tilde{\zeta}(\theta^*, \mathcal{Y}_N)^T \tilde{\Sigma}_\zeta(\theta^*)^{-1} \tilde{\zeta}(\theta^*, \mathcal{Y}_N)\,, \tag{3.33}$$

and non-centrality parameter $\tilde{\lambda}$ is

$$\tilde{\lambda} = \gamma^T \tilde{\Sigma}_\zeta(\theta^*)^{-1}\,\gamma\,. \tag{3.34}$$

The test statistic is consistently computed when $\mathcal{J}_\zeta(\theta^*)$ and $\tilde{\Sigma}_\zeta(\theta^*)$ are replaced by their respective estimates.

3.3 Proof of concept and discussion

In this section the previous developments on theory are validated on numerical simulation data and the results are discussed. The statistical distribution properties of the new residual are evaluated by drawing conclusions from the distribution properties of $\tilde{t}$ (3.31). Since $\tilde{t}$ is a scalar quantity, it can be evaluated easily, e.g. with histograms from a Monte Carlo study. The performance of the new test is represented by the probability of detection (POD) and the receiver operating characteristic (ROC) curves that deliver information on the ratio between POD and PFA for thresholds computed for different PFA limits.

With the main goal to emphasize the impact of the uncertainty in the reference null space $\widehat{S}(\theta^*)$, results from the new test (3.31) are compared to those from the conventional test (2.29), which neglects these uncertainties, i.e. $\Sigma_1 = 0$. In this context, the effect of different data lengths is analyzed, since they have an impact on the accuracy of the estimated matrices and consequently the residual covariance matrix (3.30). However, the estimation of the asymptotic Hankel matrix covariance $\widehat{\Sigma}_\mathcal{H}(\theta^*)$ is not in the focus of this thesis and is assumed to be consistently estimated from (2.36). Other effects are examined, such as the choice of system parametrization, which is interesting when the system is parametrized with respect to its structural parameters for damage localization with SSDD or when a fully automated damage detection procedure uses the simpler unparametrized test version (3.33).

In the following, the setup of the numerical Monte Carlo study is introduced first. Then, the statistical properties and test performance is evaluated. This is followed by four subsections on the effects of data length M, data length N, system parametrization,

and null space computation procedure.

3.3.1 Study setup

Previously, the theory of the stochastic subspace-based damage detection was derived when the reference null space is estimated from data and thus afflicted with uncertainties. The findings are applied in the following on numerical simulation data. A simple system is chosen, which allows for a clear definition of the correct theoretical values to which the results from the numerical study are compared.

Simulation data of the mass-spring-damper system in Fig. 3.1 is used. The system is defined by eight masses of $\mathbf{m}_1 = \mathbf{m}_3 = \mathbf{m}_5 = \mathbf{m}_7 = 1$ and $\mathbf{m}_2 = \mathbf{m}_4 = \mathbf{m}_6 = \mathbf{m}_8 = 2$. The stiffnesses are set to $\mathbf{k}_1 = \mathbf{k}_3 = \mathbf{k}_5 = \mathbf{k}_7 = 200$ and $\mathbf{k}_2 = \mathbf{k}_4 = \mathbf{k}_6 = \mathbf{k}_8 = 100$. In the damaged case the stiffness at element 3 is decreased. Classical damping with a damping ratio of 2% is considered for all modes. The system is excited with random white noise at elements 1, 3, 5, and 7. At the same positions the velocities are recorded sampled at 20 Hz. White measurement noise having 5% standard deviation of the signal is added.

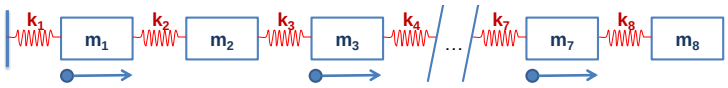

Figure 3.1 – Mass-spring chain with four sensors.

For the evaluation of the residual behavior a Monte Carlo study with 1,000 repetitions is performed. The test data and also the data for the reference null space is generated anew in each repetition. The reference null space is computed directly from the Hankel matrix estimate in the reference state.

Let the system be parametrized with respect to its modal parameters. Then the parameter vector is $\theta = [\Lambda^T \mathrm{vec}(\Phi)^T]^T$. In this case, the asymptotic residual sensitivity $\mathcal{J}_\zeta(\theta^*)$ is computed in accordance to (2.28). Assuming the sensitivity is of full rank, it holds $\mathrm{rank}(\mathcal{J}_\zeta(\theta^*)) = 2mr = 64$, with $m = 8$ degrees of freedom of the mechanical system and $r = 4$ sensors. Thus, theoretically the test statistics follows a χ^2-distribution with 64 DOF (2.31) and the expected test value mean in the reference state is 64. It should be noted that the test values in the damaged state depend on the non-centrality parameter (3.32), that contains the asymptotic covariance matrix estimate. Consequently, no theoretically expected value can be derived for the test statistics of the damaged system.

3.3.2 Statistical properties and test performance

The test values in the reference state and the corresponding theoretical χ^2-distribution are presented in Fig. 3.2. The null space is estimated from data with length $M = 50{,}000$ and the data set for the test Hankel matrix is of length $N = 100{,}000$. Obviously, considerable uncertainties related to the reference null space are neglected in the conventional test (2.29) with $\Sigma_1 = 0$. The conventional test statistics differs clearly from the theoretical value. The central limit theorem in (2.27) does not apply, since it is formulated for a residual with perfectly known reference null space. A bias is introduced in the residual leading to a non-zero mean value $b \neq 0$ in the reference state and consequently to a non-centrality of the test distribution already in the reference state. The resulting test values are significantly higher than the theoretical value. This implies also a larger spread due to the χ^2-distribution properties (Fig. 2.1, right) reflecting the uncertainty in the reference null space. When the uncertainty in the reference null space is considered correctly with the new test (3.31) the values are well centered around the expected value and the spread follows the theoretical χ^2-distribution with 64 DOF.

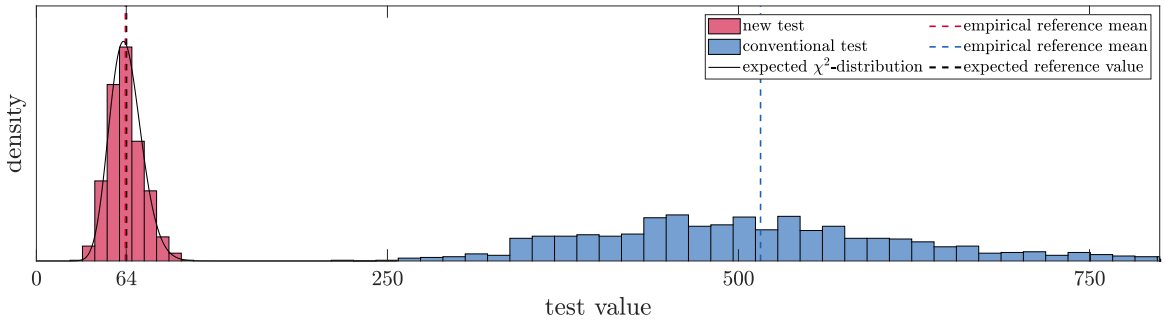

Figure 3.2 – Theoretical χ^2-distribution and histograms of the new test statistics and the conventional test with $\Sigma_1 = 0$, $M = 50{,}000$, $N = 100{,}000$.

In the damaged state, the distributions in both tests are shifted from the reference values as demonstrated in Fig. 3.3. The damage is simulated by decreasing the third element stiffness by 2%. The shift reflects the non-centrality parameter λ in the conventional test or $\tilde{\lambda}$ (3.32) in the new test. Notice, that due to neglecting the uncertainty of the reference null space the non-centrality parameter λ of the conventional test is affected by the former described bias, too. It cannot be predicted by equation (2.31) in presence of this bias. With the conventional test (left) the values have wide spread in both states resulting in a significant overlap. In contrary, the new test (right) leads to narrow distributions of the test statistics and a clear separation of both states.

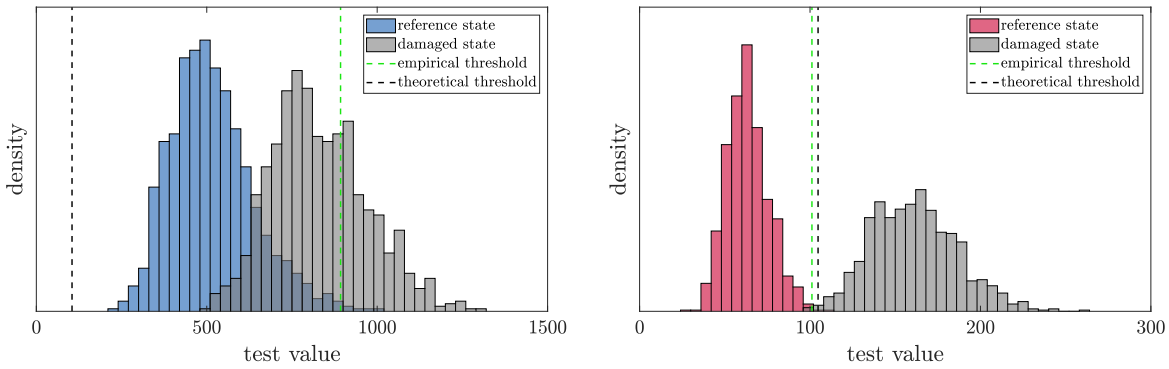

Figure 3.3 – Histogram in the reference and the damaged state of the conventional (left) and the new test (right), $M = 50{,}000$, $N = 100{,}000$, damage = 2%.

Two thresholds for damage detection are shown in Fig. 3.3, derived as explained in Fig. 2.1 (left). An empirical threshold that is based on the distribution of the test values in the undamaged state received by Monte Carlo simulations. The other threshold is derived from the theoretical χ^2-distribution in the reference state. The thresholds are chosen, allowing for a maximum probability of false alarms (PFA) of 0.1%. In cases where the test value exceeds this threshold, damage is assumed. For the conventional test in the left plot, the empirical threshold is much larger than the theoretical one, similar to the reference test values. Using the theoretical threshold will lead to 100% PFA, since all reference values are above the threshold. When the uncertainties of the reference null space are considered correctly in the new test (right), the empirical threshold coincides with the theoretical one. This allows for threshold computation a priori that is purely based on theory.

From the distributions in the reference and the damaged state, the probability of detection (POD) and the receiver operating characteristic (ROC) curves are drived in Fig. 3.4 demonstrating the impact of the new test computation on the test performance. The left plot shows the POD of both tests computed with the empirical thresholds and data length $M = 50{,}000$. The conventional test is not very sensitive towards small damages. This is due to the overlap between the two states that is apparent in Fig. 3.3 (left). Bigger damages, i.e. big change vectors δ and thus big non-centrality parameters, lead to a better separation of the states and consequently to a better POD. The new test performs well even with very small changes in the stiffness, due to the well comprised uncertainties of the reference null space and thus good separation of the system states (Fig. 3.3, right).

Regarding the relation between PFA and POD, the ROC curves in Fig. 3.4 (right)

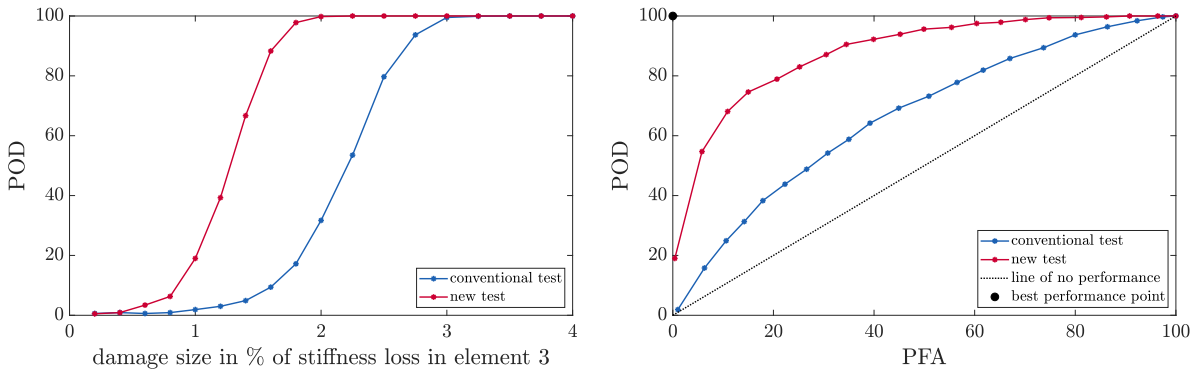

Figure 3.4 – POD (left) and ROC diagram with damage of 2% (right) of the conventional and the new test, $M = 50{,}000$, $N = 100{,}000$.

for the conventional and the new test can be derived. To computed them, the maximum allowed number of false alarms is varied leading to a corresponding POD and PFA. The ROC curve of the conventional test is much closer to the line of no performance, while the new test approaches the best performance point. In the latter the POD is less depending on the allowed PFA.

It has to be emphasized that the conventional test may show unpredictable test performance due to the former described bias in the residual. In the reference state a non-centrality exists due to the residual mean b, and in the damaged state the non-centrality parameter is a combination of terms with b and change vector δ, including mixed terms. Since this mixed terms are not necessarily positive, this may lead to a bigger or a smaller non-centrality parameter in one or the other case.

In the above evaluation it could be shown that the new test with correct consideration of the uncertainties related to $\widehat{S}(\theta^*)$ is in accordance to the theoretically expected behavior. For this test, a threshold for damage detection can be computed on a theoretical basis. The test is sensitive towards small damages and show a very good POD-PFA relation. In the following, several effects are analyzed regarding their impact on the test behavior.

3.3.3 Data length in the reference state

It can be assume that the bias and the uncertainties of the reference null space decrease when better estimates of $\widehat{S}(\theta^*)$ are achieved from longer data sets approaching the theoretical value $\widehat{S}(\theta^*) \to S(\theta^*)$. This is illustrated by the empirical mean values of both tests, plotted with respect to the reference data length M in Fig. 3.5. The conventional test that neglects the uncertainty related to the reference null space approaches the values

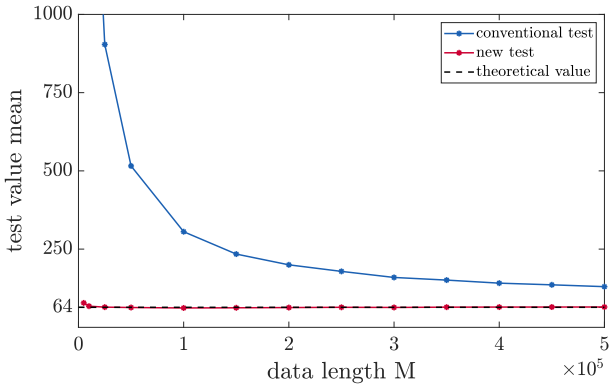

Figure 3.5 – Empirical mean of conventional and new tests for different data lengths M, $N = 100{,}000$.

of the new test and thus the theoretical value for longer data sets, i.e. when the reference null space is well estimated. The test statistics of the new test is mostly independent from the data length and is in accordance to the theoretical value, since the uncertainties are considered correctly in any case.

The distributions of both tests in the reference state for three different data lenths M in Fig. 3.6 correspond to these findings. The reference test values of the conventional test (left) approach the theoretical value with less spread for larger M, since the bias in the residual mean decreases for longer data sets due to less uncertainty in the reference null space. When the correct distribution properties are considered in the new test (right), the results in the reference state are nearly independent from the reference data length and coincide with the theoretical values for any M. This is in particular interesting for the threshold computation: While for the conventional test the threshold depends on the data length M in the reference state, the new test has one fix (theoretically based) threshold.

However, in the damaged state the test values depend on M for both tests. In the conventional test (left) the damaged test values decrease for bigger M and have less spread. This is due to less uncertainty in $\widehat{S}(\theta^*)$ and consequently smaller bias, similar as for the test values in the reference state. The shift between the mean of both states is similar for any M. As discussed before, this shift does not correspond to the non-centrality parameter in (2.31) for small M due to the bias in the residual mean, and is unpredictable. The test values of the new test in the damaged state increase with larger M. Less uncertainty on the reference null space is reflected in the decreasing covariance contribution $\frac{N}{M}\Sigma_1$ for larger M. This leads qualitatively to a smaller residual covariance $\tilde{\Sigma}_\zeta$ in (3.30), a larger inverse $\tilde{\Sigma}_\zeta^{-1}$, and thus a larger non-centrality parameter $\tilde{\lambda}$ in (3.32).

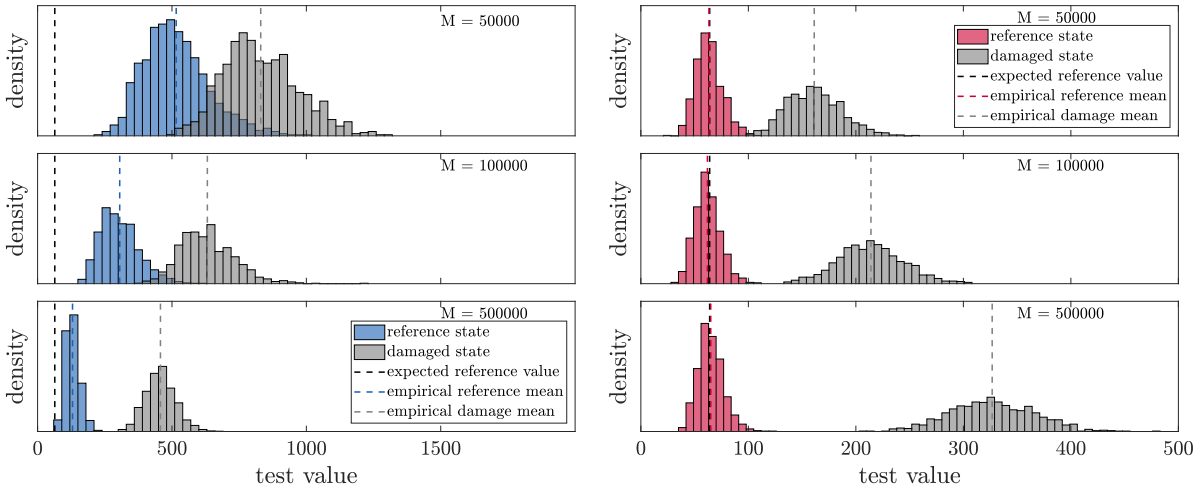

Figure 3.6 – Histogram in the reference and the damaged state of the conventional (left) and the new test (right) for different M, $N = 100{,}000$, damage = 2%.

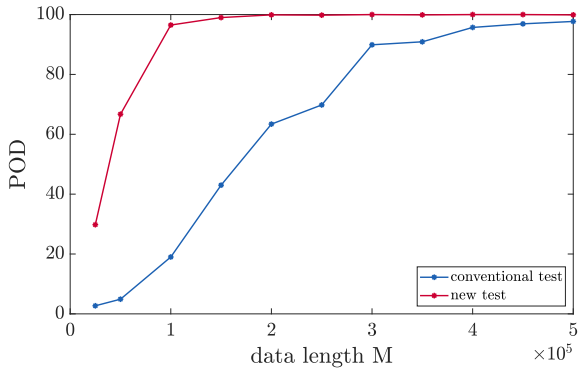

Figure 3.7 – POD of conventional and new test for different M, $N = 100{,}000$, damage = 1.4%.

The resulting test values in the damaged state become larger.

In both tests, the effect of length M leads to a better separation of the damaged from the reference state. Hence, the POD of both tests improves for larger reference data length M as shown in Fig. 3.7 for a damage of 1.4%.

When the reference null space is well estimated from a long data set with $M = 500{,}000$, the conventional and the new test perform more similar, due to small uncertainty related to the null space. This is demonstrated in Fig. 3.8.

It can be concluded that for a well estimated reference null space, the conventional test leads to results similar to the new test. Both tests have a better test performance for long reference data sets. The new test, however, does not rely on M in the reference

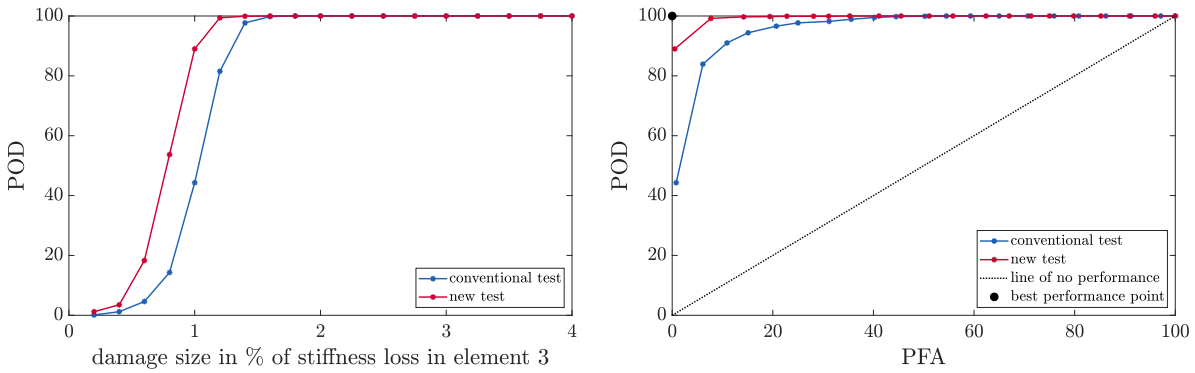

Figure 3.8 – POD (left) and ROC diagram with damage of 2% (right) of the conventional and the new test, $M = 500{,}000$, $N = 100{,}000$.

state allowing for a theory-based threshold for damage detection and a predictable test performance.

3.3.4 Data length of the testing data set

So far, the effect of the data length M in the reference state was analyzed, affecting the accuracy of $\widehat{S}(\theta^*)$ directly. In the following the impact of the testing data length N will be evaluated.

Fig. 3.9 presents the histograms of both tests for a fix damage of 2% and data length $M = 100{,}000$ for three different testing data lengths N. The reference values of the conventional test (left) increase with larger N. As in the context of the investigations to data length M, this is due to the bias that is introduced to the conventional residual by neglecting the uncertainties in $\widehat{S}(\theta^*)$ and the resulting mean b of the residual in the reference state. Since the residual is normalized to testing data length N, b depends on N and so the resulting non-centrality parameter in the reference state does. This leads to larger reference test values for longer testing data sets. A damage detection threshold for the conventional test must be computed on empirical distribution properties. Moreover, the testing data length N cannot be changed at any time, since the reference test values depend on it. The new test (right) yields reference test values that are in good accordance to the theoretical values and independent from N allowing for the definition of a fixed threshold based on theory.

In the damaged case, both tests are affected by the testing data length N. For longer test data sets but under the same physical parameter change $(\theta - \theta^*)$, the change vector δ increases as defined in the hypotheses in (2.26). This leads to larger non-centrality pa-

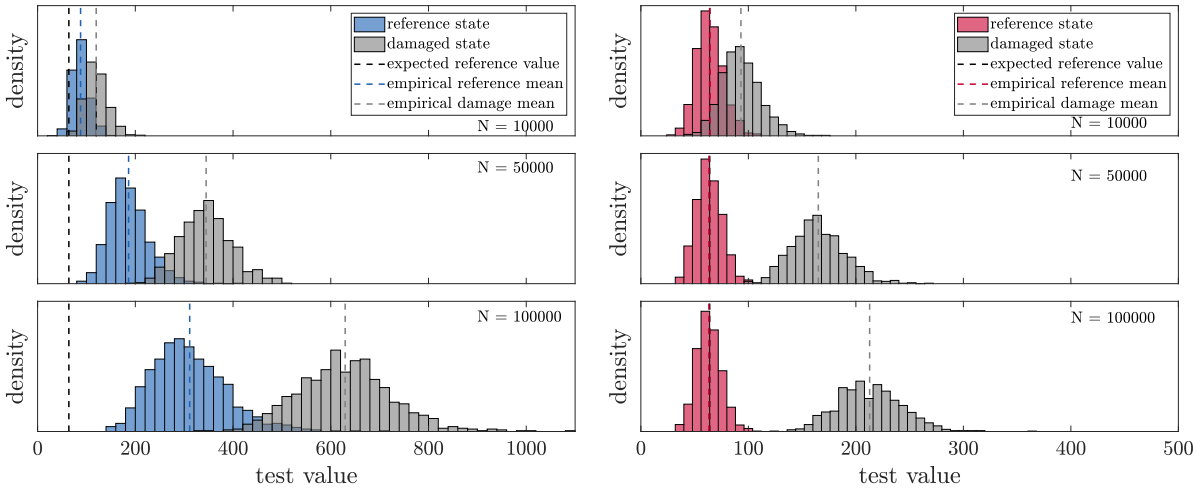

Figure 3.9 – Histogram in the reference and the damaged state of the conventional (left) and the new test (right) for different N, $M = 100{,}000$, damage $= 2\%$.

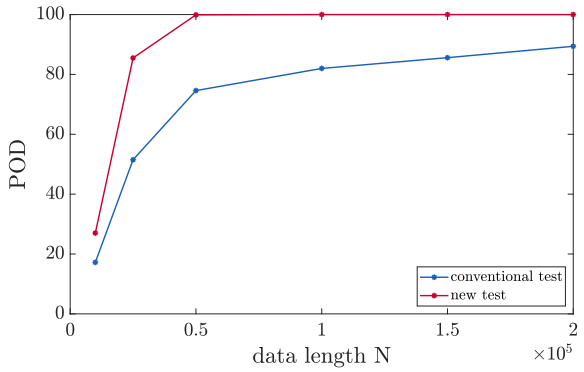

Figure 3.10 – POD of conventional and new test for different N, $M = 100{,}000$, damage $= 2\%$.

rameter λ or $\tilde{\lambda}$ (3.32). As a consequence, smaller damages can be detected with increasing data length N, which is a well known property of the SSDD. This is reflected in Fig. 3.10, where the POD for 2% damage is plotted for different data length N.

These results show that the testing data length N affects the values of the conventional test in the reference and the damaged state, and changes in data length N perturb the setup of even an empirical threshold. In the new test the effect of data length N is in accordance to theory, where longer testing data sets increase the non-centrality parameter and thus improve the POD, while N has no impact on the reference values and thus on the computation of a damage detection threshold.

3.3.5 System parametrization

It has been shown that for a system parametrized with respect to its modal parameters the new test statistics follows the theoretical expected distributions and that the test performance is reliable. However, different system parametrizations may be used. This is the case, when e.g. the SSDD is applied to damage localization or quantification [DMZ16] and a system parametrized with respect to its structural parameters is required. Or the damage detection tests are applied without focusing on a particular system parametrization θ, which corresponds to a direct detection of changes in the residual and $\mathcal{J} = I$ [DMH14; MDV21]. These non-parametric tests are attractive due to their simplicity and may be preferred e.g. when the identification of the modal parameters in the reference state of the system is inconvenient. In the following the consistency of the new residual for different system parametrizations is examined.

Assume the system in Fig. 3.1 is parametrized with respect to its structural parameters, namely to its eight stiffnesses such that $\theta = [\mathbf{k}_1\, \mathbf{k}_2 \ldots \mathbf{k}_8]^T$. Than the theoretical test value is 8. In Fig. 3.11 the corresponding test values from the conventional test with $\Sigma_1 = 0$ and the new test are presented for different data lengths M. The reference test values of the new test are nearly independent from M, while the conventional test approaches the theoretical value only for long reference data sets yielding low uncertainty of the reference null space. This is comparable to the modal parametrized system in Fig. 3.5.

The POD of both tests is presented in Fig. 3.12 computed with an empirical threshold, data lengths N = 100,000, M = 50,000 (left), and M = 500,000 (right). The POD is affected by data length M similarly to the modal parametrized system: The performance of the new test is better than of the conventional test for small M (left) and the POD of both tests is the same when $\widehat{S}(\theta^*)$ is well estimated from long data sets (right). Both tests are more sensitive when less uncertainties are related to the reference null space in case of large M due to the effect explained in the context of Fig. 3.6.

In the non-parametric case, the evaluation of the mean value towards a theoretical value is omitted in the context of the numerical study, since the theoretical value cannot be determined. It is the theoretical rank of the residual, which cannot be derived clearly from an estimate of the covariance. Only an upper bound for the number of degrees of freedom of the χ^2-distribution can be found from the covariance matrix size. Similarly to the parametric cases, the POD in Fig. 3.13 computed with the same data settings as before is better for the new test compared to the conventional test. Both tests show a better and closer performance for large M.

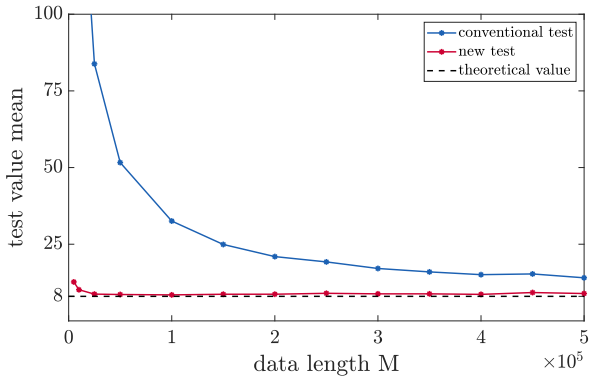

Figure 3.11 – Empirical mean of conventional and new tests for different data lengths M for a system parametrized with respect to structural parameters, $N = 100{,}000$.

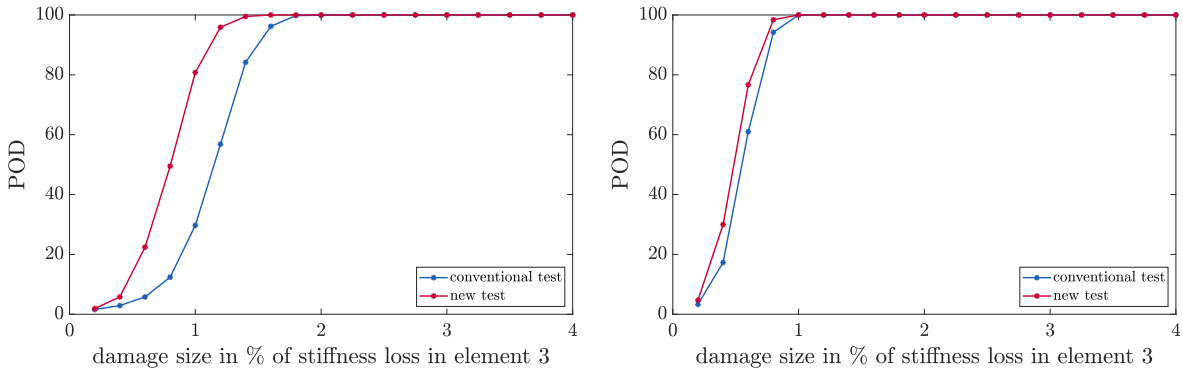

Figure 3.12 – POD of conventional and new test for a system parametrized with respect to structural parameters for $M = 50{,}000$ (left) and $M = 500{,}000$ (right), $N = 100{,}000$.

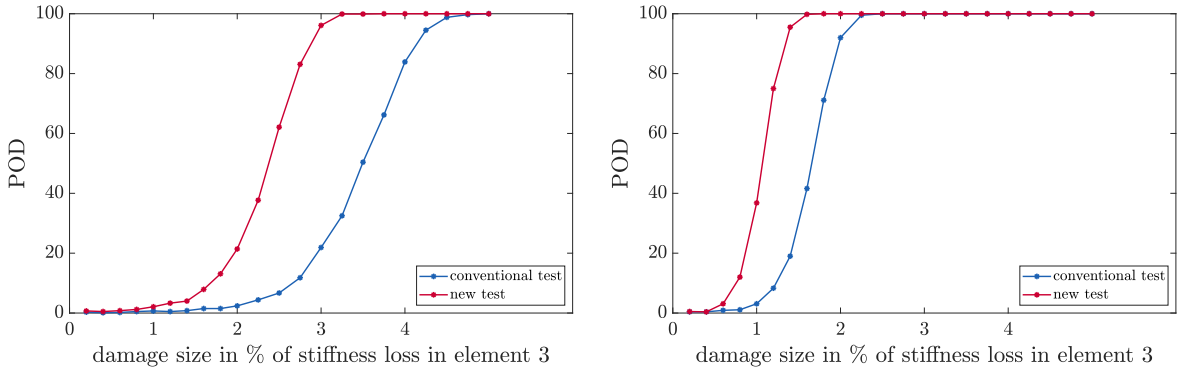

Figure 3.13 – POD of conventional and new test with non parametric test for $M = 50{,}000$ (left) and $M = 500{,}000$ (right), $N = 100{,}000$.

When comparing the test performance of the tests with different parametization, the POD in Figs. 3.4, 3.8, 3.12, and 3.13 decreases with higher DOF of the theoretical χ^2-distribution. This is coherent with the findings in [MDV21] and is due to the wider spread

of the corresponding distribution. It is not an impact of the new residual.

Independently from the parametrization, the behavior of the new test is in accordance to theory. For any parametrization, the new test yields a better POD than the conventional test in presence of considerable uncertainty in the reference null space.

3.3.6 Reference null space computed from observability matrix

The previous evaluations are based on test values that are computed with a reference null space derived from the covariance Hankel matrix in the reference state. It is possible to compute the reference matrix with a SVD from the parametric observablity matrix $\mathcal{O}(\theta^*)$, analogous to (2.10). $\mathcal{O}(\theta^*)$ is built from the m conjugate complex pairs of the system modes (2.21). Thus, the model order $n = 2m$ is known, leading to a left null space that is correctly separated from the column space.

The test value means of the conventional and the new test with a reference null space computed from the parametric observability matrix are presented in Fig. 3.14. The test values show good accordance to Fig. 3.5, where the new test matches the theoretical value even for short data and is independent from the data length. The conventional test depends on the data length and approaches the theoretical value only for longer data sets when less uncertainty is related to the reference null space. However, the test values approach the theoretical values faster than in the former cases. It is concluded that a reference null space, which is computed from the parametric observability matrix, is less afflicted with uncertainties, leading to a smaller bias in the conventional residual.

The test performance of the conventional and the new test with a reference null space computed from $\mathcal{O}(\theta^*)$ is shown in Fig. 3.15 for $M = 50{,}000$ (left) and $M = 500{,}000$

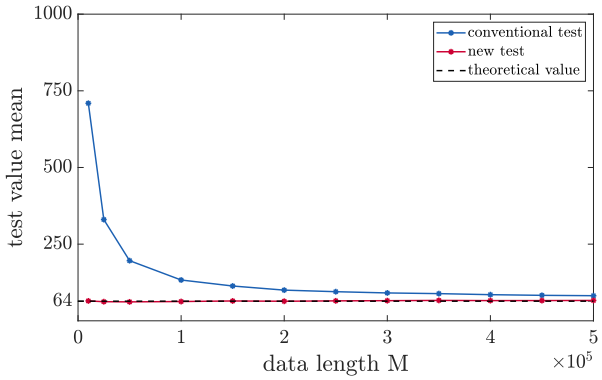

Figure 3.14 – Empirical mean of conventional and new tests for different data lengths M when the reference null space is computed from observability matrix, $N = 100{,}000$.

(right), and $N = 100{,}000$. While the null space computation procedure has no impact on the POD of the new test (cf. Figs. 3.4 and 3.8), the conventional test performs better than before when the reference null space was computed from the covariance Hankel matrix directly. In fact, the POD of the conventional test coincides with the results of the new test for any data length. This corresponds to the conclusion from above, that a null space computed from the observability matrix leads to smaller bias, which is here reflected in a similar POD. And it confirms the remarks that are made in the context of Fig. 3.4 regarding the unpredictable non-centrality and POD of the conventional test.

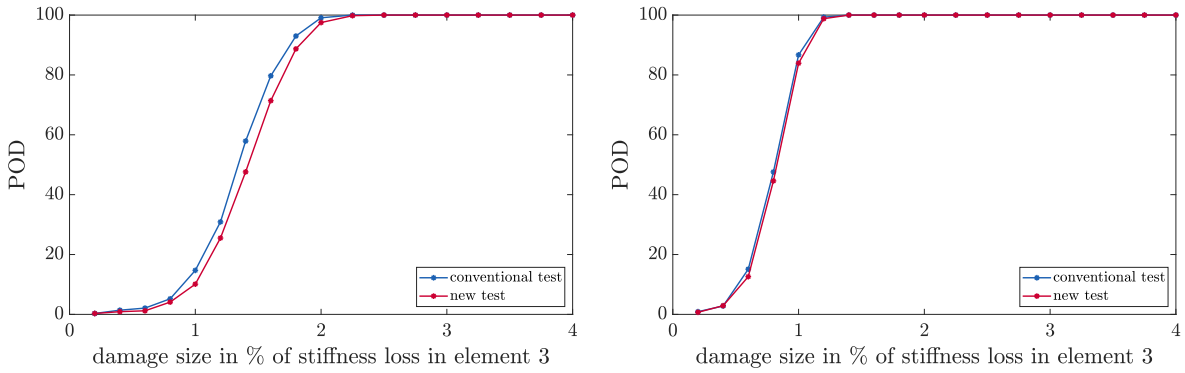

Figure 3.15 – POD of conventional and new test when the reference null space is computed from observability matrix for $M = 50{,}000$ (left) and $M = 500{,}000$ (right), $N = 100{,}000$.

It could be shown that the results of the new test are in good accordance to the theoretical expectations and that the new test performs reliably, for any null space computation procedure. The conventional test, however, performs unpredictable for different null space computations.

3.4 Summary

In this section the theory for a covariance-driven subspace-based residual with an uncertain reference has been derived. Previously, only statistical uncertainties related to test data have been considered in the formulation of the residual, and the reference matrix was assumed to be perfectly known. However, this is not true in real world applications when the reference is estimated from data. In this case the estimation uncertainties stemming from reference data must be taken into account for the residual and the associated statistical test. Now, the residual has been designed as a function of the uncertain reference and the testing data. The central limit theorem has been applied to the two random

variable residual and the statistical distribution properties have been derived. With the statistical delta method the perturbations from both variables were propagated to the residual, leading to its asymptotic residual covariance. The corresponding statistical test has been formulated.

Correct and predictable statistical behavior of the residual and the new test could be shown by means of application to numerical data. It has been demonstrated that the estimation uncertainties related to the reference data are non-negligible especially when the reference data is of short length.

Neglecting these uncertainties can lead to a considerable deviation from the theoretically expected test behavior. As a consequence, the conventional damage detection relies on empirical evaluated distribution properties, and the test behavior is not predictable as long as considerable uncertainty is related to the reference null space. It depends e.g. on the choice of null space computation. Stable results can only be achieved from sufficient long reference data sets leading to well estimated null spaces. Parameters such as the testing length N cannot be changed during the monitoring phase, since it affects the reference values. All this can lead to false alarms and makes it impossible to set thresholds between healthy and damaged states based on the expected statistical distribution of the test.

In contrary, the new test considering the uncertainties of the reference null space correctly makes the damaged detection procedure predictable and shows good accordance with the theoretically expected statistical behavior. The results are not affected by the choice of system parametrization nor by the null space computation procedure. Thresholds for damage detection can be derived from theoretical distribution properties a priori in the reference state and are not depending on any of the investigated parameters.

Results from an application of these developments to experimental data can be found in chapter 5 and 7.

3.5 Dissemination

Parts of this chapter have been published in

[Vie+17]: E. Viefhues, M. Döhler, F. Hille, and L. Mevel. « Stochastic subspace-based damage detection with uncertainty in the reference null space ». In: *IWSHM - 11th International Workshop on Structural Health Monitoring*. Stanford, United States, 2017

[Vie+18]: E. Viefhues, M. Döhler, F. Hille, and L. Mevel. « Asymptotic analysis of subspace-based data-driven residual for fault detection with uncertain reference ». In: *IFAC-PapersOnLine* 51.24 (2018). 10th IFAC Symposium on Fault Detection, Supervision and Safety for Technical Processes SAFEPROCESS 2018, pp. 414–419

[Vie+22]: E. Viefhues, M. Döhler, F. Hille, and L. Mevel. « Statistical subspace-based damage detection with estimated reference ». In: *Mechanical Systems and Signal Processing* 164 (2022)

Chapter 4

Stochastic subspace-based damaged detection under changing environmental conditions

4.1 Introduction

The application of automated vibration-based damage diagnosis to structural health monitoring (SHM) of civil engineering structures often fails due to changing environmental conditions, since the dynamical behavior of the structures is affected [Soh07] leading to high false alarm rates. The subspace-based damage detection (SSDD) method (section 2.4 and chapter 3) is based on a residual that is sensitive to changes in the dynamical system. So far it is difficult to classify if these changes are due to damages or result from environmental effects. In this chapter a SSDD approach robust to such changes in the environmental conditions and suitable for automated methods is derived.

The developments are motivated by the model interpolation approach for linear parameter varying (LPV) systems from [Zha18] introduced in section 2.6. A mechanical system that is affected by e.g. temperature, can be interpreted as a LPV system depending on an external, measurable parameter. To derive an appropriate reference null space for the residual in (3.2) that is valid at a certain (testing) parameter, a global state-space model is computed. It is based on local reference models, which are obtained from data at some parameter points in the reference state. The global model describes the system with its dynamical properties at the parameter point of interest, i.e. the testing temperature.

The new damage detection approach is appropriate for automated vibration based SHM with high robustness to the effects of a varying measurable environmental parameter. The method reduces the probability of false alarms and is sensitive to small damages. The notation in this chapter refers to the residual from chapter 3 that takes the uncertainties of an interpolated reference null space into account, but the developments hold for the

conventional residual from section 2.4 as well.

In the following, the theory for SSDD with a reference null space that is adapted to the current testing temperature is derived pursuing three different strategies in section 4.2 and the associated testing procedure is presented including the covariance computation for a residual with interpolated reference null space. In a numerical study in section 4.3 the concept is evaluated regarding its performance. The results are compared to the performance of an existing approach from [Bal+08a] that defines a global reference model built from a merged data set smoothing out the temperature effect by the averaging operation.

4.2 Damage detection robust to temperature effects

In this section the theory for the subspace-based damage detection method robust to changes in the environmental conditions is derived. First, the formalized problem statement is given. The theory for a parameter adapted reference null space for a covariance driven subspace-based residual follows considering three different computation strategies: computation of a null space from an interpolated output covariance Hankel matrix, computation from an observability matrix built from an interpolated eigenstructure, and a null space computed from an observability matrix that is based on modal parameters derived by means of regression analysis. Afterwards, the residual function with the interpolated reference null space and the associated statistical test procedure are presented and the appropriate residual covariance is derived. The section closes with comparing the principles of the new approach with previous temperature rejection approaches for SSDD.

4.2.1 Formalized problem statement

When a mechanical system, such as a civil engineering structure, is affected by an external scalar parameter P, such as the temperature, it is represented for any parameter working point $P = P_j$ by a local version of the equation of motion from 2.1 writing as

$$\mathbf{M}_j \ddot{q}_j(t) + \mathbf{C}_j \dot{q}_j(t) + \mathbf{K}_j q_j(t) = \nu_j(t). \tag{4.1}$$

Matrices $\mathbf{M}_j$, $\mathbf{C}_j$, and $\mathbf{K}_j \in \mathbb{R}^{m \times m}$ contain the masses, dampings, and stiffnesses at the m degrees of freedom arising at the working point $P = P_j$. In accordance to (2.1) t denotes the continuous time, vector $q_j \in \mathbb{R}^m$ contains the displacements at the degrees of

freedom of the structure, and the excitation force $\nu_j \in \mathbb{R}^m$ is considered to be unknown. Consequently, the state-space representation at time instance k in (2.3) derived from the mechanical system matrices is similarly affected by the external parameter. This results in an individual state-space model for any parameter working point $P = P_j$ with state transition matrix A_j and observation matrix C_j writing as

$$\begin{cases} x_{j,k+1} = A_j x_{j,k} + w_{j,k} \\ y_{j,k} = C_j x_{j,k} + v_{j,k}. \end{cases} \tag{4.2}$$

As defined for (2.3) $x_{j,k} \in \mathbb{R}^n$ is the state vector of the system at time instance k, $n = 2m$ is the model order, and $y_{j,k} \in \mathbb{R}^r$ contains the measured outputs. The noise terms $w_{j,k}$ and $v_{j,k}$ are related to the unknown excitation and the measurement noise, and are considered to be stationary and white. This is what is called the *local model* in the model interpolation approach introduced in section 2.6.

To each local model a parameter vector θ_j with a nominal value θ_j^* in the reference state is associated. The considered damage detection method described in section 2.4 and further developed in chapter 3 is based on a subspace-based feature vector that evaluates changes in the monitored system with respect to an undamaged reference state statistically on the basis of the parameter vector θ_j [BAB00]. A local version of the covariance-driven subspace-based damage detection method can be derived for a fixed working point as follows.

The block Hankel matrix in (2.12) is built from theoretical output covariances at $P = P_j$, which are defined as

$$R_{j,i} = \mathbf{E}(y_{j,k+i}\, y_{j,k}^T) = C_j A_j^{i-1} G_j, \tag{4.3}$$

with $G_j = \mathbf{E}(x_{j,k+1}\, y_{j,k}^T)$. The local Hankel matrix $\mathcal{H}_j \in \mathbb{R}^{(p+1)r \times qr}$ writes as

$$\mathcal{H}_j \overset{\text{def}}{=} \begin{bmatrix} R_{j,1} & R_{j,2} & \dots & R_{j,q} \\ R_{j,2} & R_{j,3} & \dots & R_{j,q+1} \\ \vdots & \vdots & \ddots & \vdots \\ R_{j,p+1} & R_{j,p+2} & \dots & R_{j,p+q} \end{bmatrix}. \tag{4.4}$$

With the factorization property of the Hankel matrix into the observability matrix $\mathcal{O}_j$

and the controllability matrix $\mathcal{C}_j$ (cf. (2.13))

$$\mathcal{H}_j = \mathcal{O}_j \mathcal{C}_j, \quad \text{where} \quad \mathcal{O}_j = \begin{bmatrix} C_j \\ C_j A_j \\ \vdots \\ C_j A_j^p \end{bmatrix}, \quad \mathcal{C}_j = \begin{bmatrix} G_j & A_j G_j & \dots & A_j^{q-1} G_j \end{bmatrix}, \tag{4.5}$$

the underlying property in the reference state for the residual formulation in (2.23) and (2.22) becomes

$$S_j^T \mathcal{H}_j = 0 \quad \text{and} \quad S_j^T \mathcal{O}_j = 0. \tag{4.6}$$

S_j denotes the reference null space for parameter point P_j computed either from the Hankel matrix or from the observability matrix $\mathcal{O}_j$, e.g. by means of the singular value decomposition.

With a data set $\mathcal{Y}_{j,N} = \{y_{j,1}, \dots, y_{j,N}\}$ of length N in the test state, for $P = P_j$ the residual in (3.2) is defined as

$$\tilde{\zeta}(\theta_j^*, \mathcal{Y}_{j,N}) \stackrel{\text{def}}{=} \sqrt{N}\, \text{vec}(\widehat{S}_j^T \widehat{\mathcal{H}}_j). \tag{4.7}$$

The close hypotheses write as

$$\begin{aligned} \mathbf{H}_0^j &: \ \theta = \theta_j^* \quad \text{(reference state)}, \\ \mathbf{H}_1^j &: \ \theta \neq \theta_j^* \quad \text{(damaged state)}, \end{aligned} \tag{4.8}$$

and the distribution properties of the residual in the non-parametric version correspond to (3.12) with

$$\tilde{\zeta}(\theta_j^*, \mathcal{Y}_{j,N}) \longrightarrow \begin{cases} \mathcal{N}(0, \tilde{\Sigma}_{\zeta,j}) & \text{under } \mathbf{H}_0^j \\ \mathcal{N}(\tilde{\gamma}, \tilde{\Sigma}_{\zeta,j}) & \text{under } \mathbf{H}_1^j, \end{cases} \tag{4.9}$$

where $\tilde{\gamma}$ is a change in the residual mean due to damage, and $\tilde{\Sigma}_{\zeta,j}$ is the asymptotic residual covariance that can be easily estimated from data in the reference state with (3.28) at parameter point $P = P_j$. The associated statistical test is (cf. (3.33))

$$\tilde{t} = \tilde{\zeta}(\theta_j^*, \mathcal{Y}_{j,N})^T \, \tilde{\Sigma}_{\zeta,j}^{-1} \, \tilde{\zeta}(\theta_j^*, \mathcal{Y}_{j,N}). \tag{4.10}$$

The described method works under the premise that the testing data $\mathcal{Y}_{j,N}$ is obtained under the same external parameter as the left reference null space S_j in the definition of

the residual in (4.7). If the Hankel matrix is computed from testing data under a different external parameter than the left reference null space, condition (4.6) of the reference state may not hold anymore, since the external parameter may change the dynamic properties of the system without the presence of damage. Thus, the residual mean is not zero anymore in the reference state under a change in the external parameter leading to false alarms of the damage detection test (4.10).

Suppose testing data is obtained under a known external parameter P that is possibly different from a set of reference parameter points $\{P_1, P_2, \ldots, P_u\}$ for which measurements in the reference state of the structure are available. To avoid false alarms, a left reference null space is required that is appropriate for the environmental conditions of the testing data, i.e. for parameter P such that condition (4.6) of the system in the reference state is actually satisfied. It is the goal to develop from the available reference measurements an appropriate reference null space $\underline{S}(P)$ and the associated damage detection test for data under parameter P.

4.2.2 Parameter adapted reference null space

The idea of computing a reference null space $\underline{S}(P)$ based on weighted references was already used in [FKB13]. In the following, an approach is developed based on system theoretic considerations, where $\underline{S}(P)$ is obtained by means of the local model interpolation approach from [Zha18] as recalled in section 2.6. With the goal to characterize data of a dynamical system at parameter P, in this approach a global reference model that is valid at external parameter P is interpolated from local models (4.2) at parameters $\{P_1, P_2, \ldots, P_u\}$. Then, the outputs of the system at parameter P can be considered as an interpolated version of the outputs at parameters $\{P_1, P_2, \ldots, P_u\}$ [Zha18]. However, no data is generated explicitly. Instead, the matrices from which the reference null space is derived (2.23) or the underlying parameters for (2.22) are interpolated yielding a temperature adapted reference null space for the subspace-based residual at parameter P.

The global model recalled from (2.67) writes as

$$\begin{aligned} \underline{x}_{k+1} &= \underline{A}\,\underline{x}_k + \underline{w}_k \\ y_k &\overset{\text{def}}{=} \underline{C}(P)\,\underline{x}_k + \underline{v}_k\,, \end{aligned} \tag{4.11}$$

with

$$\underline{A} \overset{\text{def}}{=} \begin{bmatrix} A_1 & & \\ & \ddots & \\ & & A_u \end{bmatrix}, \quad \underline{x}_k \overset{\text{def}}{=} \begin{bmatrix} x_{1,k} \\ \vdots \\ x_{u,k} \end{bmatrix}, \quad \underline{w}_k \overset{\text{def}}{=} \begin{bmatrix} w_{1,k} \\ \vdots \\ w_{u,k} \end{bmatrix},$$

$$\underline{C}(P) \overset{\text{def}}{=} \begin{bmatrix} \rho_1(P)C_1 & \cdots & \rho_u(P)C_u \end{bmatrix}, \quad \underline{v}_k \overset{\text{def}}{=} \textstyle\sum_{j=1}^{u} \rho_j(P)\, v_{j,k}(t)\,.$$

The interpolation weights $\rho_j(P)$ for each of the u reference models are determined for the current parameter P in dependence of the reference parameters $P_1, \ldots, P_u$. The weighting function can be chosen depending on prior knowledge of the qualitative behavior of the mechanical structure under changes in the external paramete, and yields

$$\sum_{j=1}^{u} \rho_j(P) = 1 \tag{4.12}$$

for any P with $0 \leq \rho_j(P) \leq 1$. For example, a bell-shaped (Gaussian) function centered at P can be chosen, and the weights $\rho_j(P)$, $j = 1, \ldots, u$, are the values of this function at P_j after normalization by (4.12). Fig. 4.1 shows how the weights for the local models are obtained from a Gaussian weighting function for any P. Wile the local models near to the centered point have a high impact to the global model, the far away located models have a small weighting factor.

In the following three null space computation strategies are presented that are based on or motivated by the local model interpolation approach from [Zha18]. It is derived how the interpolated Hankel matrix at parameter P can be obtained by means of the model

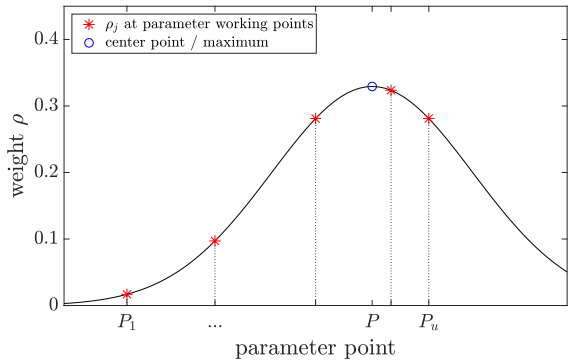

Figure 4.1 – Determination of weights at parameter working points for any P from a Gaussian function.

interpolation approach but without actually generating reference output. With this idea in mind, interpolation of the reference modal parameters is used in the second strategy to obtain the left reference null space from the respective observability matrix, and the third approach pursues this strategy with regression of the reference modal parameters.

Note that the following notation is used:

$\mathcal{H}_j$ is the Hankel matrix in the reference state under parameter P_j

$\widehat{\mathcal{H}_j}$ is the consistent estimate of $\mathcal{H}_j$

S_j is the left null space of $\mathcal{H}_j$

$\widehat{\mathcal{H}}(P)$ denotes the Hankel matrix estimate under parameter P in the testing state

Strategy 1: Hankel matrix interpolation The outputs of the interpolated state-space model in (4.11) can be used to compute the respective reference Hankel matrix under parameter P, denoted by $\underline{\mathcal{H}}(P)$, in order to obtain its left reference null space. Based on the properties of model (4.11), it is now shown that it is not necessary to compute the interpolated outputs explicitly, but that $\underline{\mathcal{H}}(P)$ follows directly as an interpolated version of the reference Hankel matrices $\mathcal{H}_j$, $j = 1, \ldots, u$, that can be estimated from measurements in the reference state at the respective reference parameters P_j.

From the output equation of model (4.11) it follows that $y_k = \sum_{j=1}^{u} \rho_j(P) y_{j,k}$. Hence, with (4.3) $\mathbf{E}(x_{j,k+1} y_k^T) = \rho_j(P)\mathbf{E}(x_{j,k+1} y_{j,k}^T) = \rho_j(P) G_j$ since the cross terms from measurements under different parameters and thus at different times are uncorrelated, and the cross-correlation between states and outputs of the interpolated model follows as $\underline{G}(P) = \mathbf{E}(\underline{x}_{k+1} y_k^T) = \begin{bmatrix}\rho_1(P)G_1^T & \ldots & \rho_u(P)G_u^T\end{bmatrix}^T$. The output covariances of the interpolated model follow from (4.3) and (4.11) as

$$\begin{aligned}\underline{R}_i(P) = \mathbf{E}(y_{k+i} y_k^T) &= \underline{C}(P)\underline{A}^{i-1}\underline{G}(P) \\ &= \sum_{j=1}^{u} \rho_j^2(P) C_j A_j^{i-1} G_j = \sum_{j=1}^{u} \rho_j^2(P) R_{j,i} \ ,\end{aligned}$$

The respective "interpolated" Hankel matrix is filled similarly as in (4.4) with these output covariances to

$$\underline{\mathcal{H}}(P) = \sum_{j=1}^{u} \rho_j^2(P) \mathcal{H}_j. \tag{4.13}$$

The desired left reference null space $\underline{S}(P)$ can finally be computed as the left null space of the interpolated Hankel matrix $\underline{\mathcal{H}}(P)$.

Strategy 2: Observability matrix interpolation Suppose the reference data is recorded over a longer time period to obtain systems at different reference temperatures, changes in the excitation covariance must be suspected at the different reference points. In the context of civil structures such changes may result from different wind conditions or changes in the traffic loads affecting the output covariances from which the reference null space is derived. Due to general unknown excitation within the output-only framework those unmeasured changes are not covered in the system matrices of the state-space model and thus perturb the interpolation from strategy 1.

This motivates for computing the reference null space from the observability matrix in (2.62) exploiting the property $S_j^T \mathcal{O}_j = 0$ (cf. (4.6)). A parametric version of the observability matrix uses the system matrices in (4.5) in the modal basis [DMH14] and can be obtained from the modal parameters of the system, which are not affected by the excitation covariance. A set of modal parameters under P can be obtained by interpolating the eigenstructure under the different P_j, $j = 1, \ldots, u$. Subsequently, the observability matrix $\underline{\mathcal{O}}(P)$ and its left reference null space $\underline{S}(P)$ can be computed.

The local modal parameters are identified from the reference measurements at each of the parameters P_j, using e.g. subspace-based system identification as recalled in section 2.3. The eigenvalues $\lambda_{j,l}$, eigenvectors $\phi_{j,l}$ and mode shapes $\varphi_{j,l}$ of (4.2) yield in accordance to (2.15)

$$A_j \, \phi_{j,l} = \lambda_{j,l} \, \phi_{j,l} \, , \quad \varphi_{j,l} = C_j \, \phi_{j,l} \, , \quad l = 1, 2, \ldots, n. \tag{4.14}$$

The parameter vector θ_j^* can be defined as the collection of the modal parameters, or equivalently the eigenvalues and mode shapes of the system

$$\theta_j^* \stackrel{\text{def}}{=} \begin{bmatrix} \Lambda_j \\ \text{vec}(\Phi_j) \end{bmatrix} \tag{4.15}$$

with $\Lambda_j = [\lambda_{j,1} \ \lambda_{j,2} \ \ldots \ \lambda_{j,n}]^T$, $\Phi_j = [\varphi_{j,1} \ \varphi_{j,2} \ \ldots \ \varphi_{j,n}]$. Notice that the mode shapes are only obtained up to a constant factor. Their comparability is required for the different reference parameters P_j for interpolation. It is therefore supposed that the mode shapes are normalized such that one component is always one and that the chosen component is the same for the same mode under the different j.

The modal parameters at parameter P can then be interpolated as

$$\underline{\theta}^*(P) = \sum_{j=1}^{u} \rho_j(P)\, \theta_j^* \tag{4.16}$$

and used for the computation of the observability matrix $\underline{\mathcal{O}}(P)$. The desired left reference null space $\underline{S}(P)$ can finally be computed as the left null space of $\underline{\mathcal{O}}(P)$.

Strategy 3: Observability matrix with regression Instead of interpolating the whole modal parameter vector (4.16) to obtain the modal parameters at P, they can also be analyzed individually in a regression, which allows a functional description of each modal parameter (eigenvalues and all mode shape components) in dependence of the external parameter. Let $\mathcal{G}$ denote the collection of functions generated by the regression analysis. The modal parameters at parameter P can then be obtained as

$$\underline{\theta}^*(P) = \mathcal{G}(P) \tag{4.17}$$

and used for the computation of the observability matrix $\underline{\mathcal{O}}(P)$, whose left reference null space is computed as $\underline{S}(P)$.

4.2.3 Residual function and statistical evaluation

In the testing state at parameter P the Hankel matrix estimate $\widehat{\mathcal{H}}(P)$ is computed from a data set $\mathcal{Y}_N(P)$ of length N. The Hankel matrix is confronted to the reference null space $\underline{S}(P)$ derived from either of the three presented strategies. Replacing $\underline{S}(P)$ by its consistent estimate $\underline{\widehat{S}}(P)$, the subspace-based residual at parameter P in the testing state writes in accordance to (4.7) as

$$\tilde{\zeta}(\underline{\theta}^*(P), \mathcal{Y}_N(P)) = \sqrt{N}\, \mathrm{vec}(\underline{\widehat{S}}(P)^T \widehat{\mathcal{H}}(P)). \tag{4.18}$$

The test statistic analogous to (4.10) becomes

$$\tilde{t} = \tilde{\zeta}(\underline{\theta}^*(P), \mathcal{Y}_N(P))^T\, \underline{\tilde{\Sigma}}_\zeta(P)^{-1}\, \tilde{\zeta}(\underline{\theta}^*(P), \mathcal{Y}_N(P)), \tag{4.19}$$

where $\underline{\tilde{\Sigma}}_\zeta(P)$ is the covariance of the residual, which is detailed in section 4.2.4.

4.2.4 Residual covariance

It is assumed that the testing data under parameter P can be described by the interpolated state-space model (4.11). To evaluate changes in the corresponding residual (4.18) at parameter P with the statistical test in (4.19) the residual covariance at external parameter P is required. This is derived in accordance to (3.30) from the covariance of the underlying Hankel matrix $\Sigma_{\mathcal{H}(P)}$ at parameter P. It is either re-computed from the current data set $\mathcal{Y}_N(P)$ in the testing state, or it is related to the covariances of the reference data under parameters $\{P_1, P_2, \ldots, P_u\}$ as follows.

Suppose that under each reference parameter P_j a data set $\mathcal{Y}_{j,M}$ of length M is available in the reference state of the structure. The Hankel matrix estimate $\widehat{\mathcal{H}}_j$ obtained from $\mathcal{Y}_{j,M}$ is asymptotically Gaussian distributed with (cf. (3.5))

$$\sqrt{M}\,\mathrm{vec}(\widehat{\mathcal{H}}_j - \mathcal{H}_j) \longrightarrow \mathcal{N}(0, \Sigma_{\mathcal{H}_j}), \tag{4.20}$$

where $\Sigma_{\mathcal{H}_j}$ is the asymptotic Hankel matrix covariance that can be easily estimated by means of the sample covariance as in (2.36). Using (4.13) the covariance of the Hankel matrix under P can be approximated as a weighted mean of the Hankel matrix covariances under P_j, $j = 1, \ldots, u$, as

$$\underline{\Sigma}_{\mathcal{H}(P)} = \left(\sum_{j=1}^{u} \rho_j^4(P)\right)^{-1} \sum_{j=1}^{u} \rho_j^4(P)\Sigma_{\mathcal{H}_j}, \tag{4.21}$$

where the factor in front of the sum ensures that the sum of the weights is one.

With this result, the asymptotic covariance of residual (4.18) can be developed. With an uncertainty afflicted reference null space, the covariance related to the null space estimate as well as the covariance related to the testing Hankel matrix estimate contribute to the residual covariance, denoted by $\underline{\Sigma}_1(P)$ and $\underline{\Sigma}_2(P)$, respectively. Following (3.30), the residual covariance yields

$$\tilde{\underline{\Sigma}}_\zeta(P) = \tfrac{N}{M}\underline{\Sigma}_1(P) + \underline{\Sigma}_2(P), \tag{4.22}$$

where

$$\begin{aligned}
\underline{\Sigma}_1(P) &= (\underline{\mathcal{H}}(P)^T \otimes I_s)\,\mathcal{P}_{t,s}\,\underline{\Sigma}_{S(P)}\,\mathcal{P}_{t,s}^T\,(\underline{\mathcal{H}}(P) \otimes I_s),\\
\underline{\Sigma}_2(P) &= (I_{qr} \otimes \underline{S}(P)^T)\,\underline{\Sigma}_{\mathcal{H}(P)}\,(I_{qr} \otimes \underline{S}(P)).
\end{aligned}$$

$\mathcal{P}_{t,s}$ is the permutation matrix in (2.42), t and s are the number of rows and columns of $\underline{S}(P)$. The asymptotic covariance matrix $\underline{\Sigma}_{S(P)}$ of the estimated reference null space is derived from the covariance of the underlying Hankel matrix and depends on the strategy that is adopted for the left reference null space computation in section 4.2.2.

Residual covariance for strategy 1 When the left reference null space is obtained from the interpolated Hankel matrix $\underline{\mathcal{H}}(P)$, $\underline{\Sigma}_{S(P)}$ is directly related to $\underline{\Sigma}_{\mathcal{H}(P)}$ with the sensitivity in (3.24). It writes as

$$\underline{\Sigma}_{S(P)} = \mathcal{J}_{\underline{S}(P),\underline{\mathcal{H}}(P)} \underline{\Sigma}_{\mathcal{H}(P)} \mathcal{J}^T_{\underline{S}(P),\underline{\mathcal{H}}(P)}, \tag{4.23}$$

with $\mathcal{J}_{\underline{S}(P),\underline{\mathcal{H}}(P)} = -\mathcal{P}_{s,t}(U_1 D_1^{-1} V_1^T \otimes U_1^T)$, where U_1, D_1, and V_1 are the column space, the matrix with the non-zero singular values, and the row space that are computed from $\underline{\mathcal{H}}(P)$ in the reference state.

Residual covariance for strategy 2 When the left reference null space is obtained from an observability matrix $\underline{\mathcal{O}}(P)$ computed from interpolated modal parameters, the covariance of the estimates of the modal parameter vectors θ_j^*, $j = 1, \ldots, u$ is first related to their interpolation $\theta^*(P)$, then to the observability matrix $\underline{\mathcal{O}}(P)$, and finally to its left null space to obtain $\underline{\Sigma}_{S(P)}$ as follows: In the first step, the covariance $\Sigma_{\theta_j^*}$ of the modal parameter vectors under each reference parameter P_j is obtained with respect to the used system identification method, e.g. for stochastic system identification (SSI) with the sensititvities from (2.53), (2.56), and (2.58) to (2.60) leading to

$$\Sigma_{\theta_j^*} = \mathcal{J}_{\theta_j^*,\mathcal{H}_j} \Sigma_{\mathcal{H}_j} \mathcal{J}^T_{\theta_j^*,\mathcal{H}_j}. \tag{4.24}$$

Then, the covariance of the interpolated modal parameters follows similarly to (4.21) as

$$\underline{\Sigma}_{\theta^*(P)} = \left(\sum_{j=1}^{m} \rho_j^2(P) \right)^{-1} \sum_{j=1}^{m} \rho_j^2(P) \Sigma_{\theta_j^*}. \tag{4.25}$$

The covariance of the observability matrix follows as $\Sigma_{\underline{\mathcal{O}}(P)} = \mathcal{J}_{\underline{\mathcal{O}}(P),\underline{\theta}^*(P)} \underline{\Sigma}_{\theta^*(P)} \mathcal{J}^T_{\underline{\mathcal{O}}(P),\underline{\theta}^*(P)}$, where the sensitivity $\mathcal{J}_{\underline{\mathcal{O}}(P),\underline{\theta}^*(P)}$ of the observability matrix towards the modal parameters is detailed in (2.64). Finally, the covariance of its left null space $\underline{\Sigma}_{S(P)}$ is directly related to $\underline{\Sigma}_{\mathcal{O}(P)}$ with (3.24), where U_1, D_1, and V_1 are the column space, the matrix with the

non-zero singular values, and the row space that are computed from $\underline{\mathcal{O}}(P)$ in the reference state

Residual covariance for strategy 3 In the third strategy the left reference null space is similarly obtained from the interpolated observability matrix $\underline{\mathcal{O}}(P)$, but where $\underline{\theta}^*(P)$ is computed on a regression analysis instead of interpolation. At this point it is assumed that the covariance computation is only slightly affected by the exact modal parameter uncertainties related to the estimate of $\theta^*(P)$, and therefore in this approach the same covariance computation for $\underline{\Sigma}_{S(P)}$ is carried out as described for strategy 2. The weights are not very much different, since both consider a linear behavior between two neighbored reference temperature.

4.2.5 Discussion and comparison to previous approaches

The developed strategies account for environmental variation in subspace-based damage detection by creating an appropriate reference under the current parameter P of the testing state, based on reference measurements at values $\{P_1, P_2, \ldots, P_u\}$ that are in general different from P. Using the knowledge of the external parameter in addition to the vibration measurements (e.g., the temperature needs to be measured), these strategies have the potential to define a more precise reference for the current environmental condition than other approaches that mix data blindly from different but unknown environmental conditions for the definition of a reference. In particular, in the context of subspace-based damage detection under environmental variation, a previously developed approach is the *average approach* from [Bal+08a], where the left reference null space is computed on the mean of the Hankel matrices $\frac{1}{u}\sum_{j=1}^{u}\mathcal{H}_j$ that are obtained from measurements in the reference state under different environmental conditions. While this approach provides some robustness in practice when the external parameter is unknown, it is not optimal particularly when the current external parameter is quite far from the mean. Besides, a previous approach based on weighted reference Hankel matrices has been presented in [FKB13], which is similar to the developed *strategy 1*, whereas this work provides in addition a theoretical justification for the Hankel matrix interpolation and derives the adapted covariance computation.

Within the developed temperature rejection strategies, *strategy 1* based on the Hankel matrix interpolation in the reference state is the simplest and the most straight-forward to implement, as it is purely data-driven and modal analysis is not required. *Strategy 2*

requires in addition modal parameter estimation, but only once from the reference measurements. Modal analysis in the testing state is never required. Using their interpolation to construct an appropriate left reference null space, strategy 2 considers more directly the well-known effect of environmental variation on the modal parameters than on the related Hankel matrices in strategy 1. Moreover, with this approach a reference null space can be computed robustly even if the excitation covariance between the reference data sets changes, since the eigenstructure is independent from the excitation covariance. This is also guaranteed with *Strategy 3* that is based on individual regressions of the reference modal parameters. It is again more complex, and offers in addition an interesting possibility to extrapolate for cases where P is outside the interval of the reference parameters, thanks to the definition of the regression functions. In either case, if structure-specific behavior in dependence of the environmental parameter is known a priori, it can be taken into account in the definition of the respective interpolation or regression function.

4.3 Proof of concept and discussion

In the previous section, the theory for a SSDD approach robust to changes in external parameters such as temperature was derived. In this section these developments are validated on numerical simulation data and the results are discussed. The method is evaluated regarding its damage detection performance and compared to the existing temperature rejection approach using average reference matrices from [Bal+08a] as outlined in section 4.2.5. The test performance is measured by means of probability of detection (POD) and the receiver operating characteristic (ROC) curves, that deliver information on the ratio between POD and probability of false alarms (PFA) for thresholds computed for different PFA limits, as described in section 2.4.4. The residual is formulated such that the uncertainty of the reference null space due to its estimation from data is taken into account, accordingly to the developments in chapter 3.

After introducing the study setup used for the generation of the numerical data, in section 4.3.2 the test performance is evaluated when the reference null space is computed with the three proposed robust strategies from the previous section. The test results are compared to results when no effects from the external parameter are considered in the reference setup and when the reference null space is computed with the average method. In this context the impact of the uncertainty consideration of the reference null space is studied. In section 4.3.3 it is shown how the covariance computation affects the

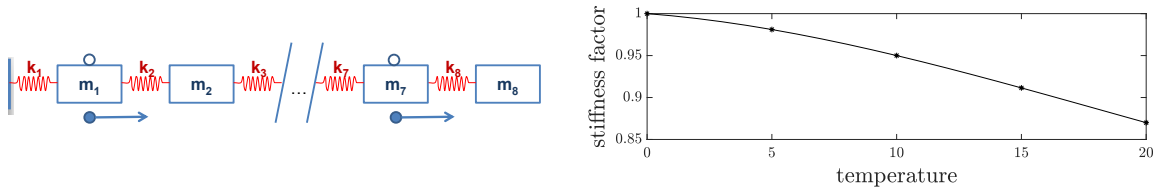

Figure 4.2 – Mass-spring chain and temperature dependent stiffness.

test procedure and its performance, i.e. if the covariance is interpolated or re-computed in the testing state. In section 4.3.4 the test performance is analyzed with respect to different reference setups, i.e. for different combinations of reference parameter states and for different choices of the interpolation function. Finally, it will be shown in section 4.3.5 that the new approach can be applied even when the excitation covariance changes between the reference states.

4.3.1 Study setup

The numerical data for validation of the theoretical developments from section 4.2 is obtained from an eight mass-spring-damper as illustrated in Fig. 4.2 (left). It is set up by masses $\mathbf{m}_1 = \mathbf{m}_3 = \mathbf{m}_5 = \mathbf{m}_7 = 1$ and $\mathbf{m}_2 = \mathbf{m}_4 = \mathbf{m}_6 = \mathbf{m}_8 = 2$ and stiffness $\mathbf{k}_1 = \mathbf{k}_3 = \mathbf{k}_5 = \mathbf{k}_7 = 200$ and $\mathbf{k}_2 = \mathbf{k}_4 = \mathbf{k}_6 = \mathbf{k}_8 = 100$. Classical damping is defined such that the damping ratio of all modes is 2%. The structure is excited by white noise at elements 1, 3, 5 and 7, and velocities are recorded at the same elements with a sampling frequency of 8 Hz. Measurement noise with 5% standard deviation of the signals is added.

The external parameter is considered to be the temperature. Its effect is simulated by changing the stiffness of all elements in accordance to a non-linear function as depicted in Fig. 4.2 (right). This stiffness-temperature relation is much stronger than in real applications such that the limits of the developed methods can be shown. Damage is simulated by reducing the temperature dependent stiffness of element 3 by 1.5%.

The test performance of the different strategies that account for the environmental variation is evaluated in a Monte Carlo simulation with vibration data generated at temperatures between 0°C and 20°C, using 10 data sets with length $N = 200{,}000$ at each temperature step. The respective damage detection methods are set up in the reference state at selected reference temperatures, as detailed in the following. At these reference temperatures, 10 additional Monte Carlo data sets are generated for the determination of the threshold for damage detection, which is set up for 0.1% probability of false alarms.

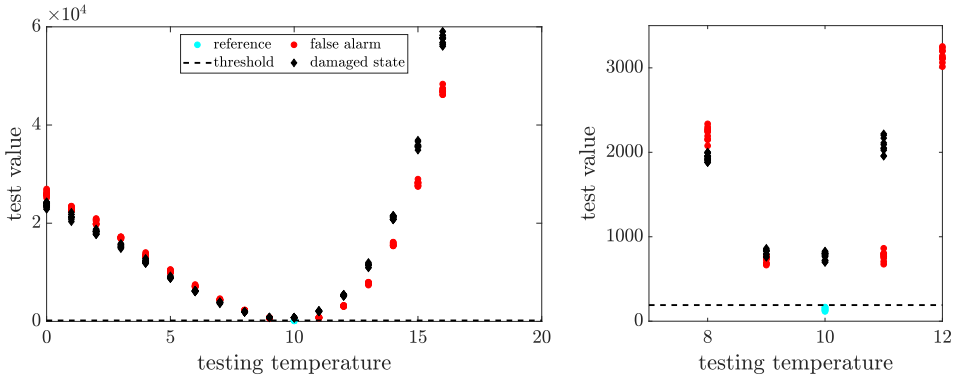

Figure 4.3 – Test values at different testing temperatures computed from a single reference data set at 10°C for the whole temperature range (left) and with zoom on the temperatures close to the reference temperature (right).

4.3.2 Damage detection under changing temperatures

When the conventional SSDD from (3.2) is applied to a dynamical system that depends on an external parameter, changes in this parameter in the testing state with respect to the reference state lead to a significant number of false alarms. Fig. 4.3 shows the test values from the Monte Carlo simulation at different testing temperatures when the reference null space and the residual covariance are computed from data at only one single reference temperature $T_1 = 10°\text{C}$, and the associated empirical threshold as described before. At the reference temperature $T_1 = 10°\text{C}$ the test performs well, as can be seen in the zoom on Fig. 4.3 (right): the test values from data of the reference state are below the threshold (cyan dots), i.e. no false alarms occur, and the test values from data of the damaged state are above the threshold (black diamonds), so damage is detected. However, for any testing temperature different from the reference temperature at 10°C, the test values computed on data from the undamaged state also react strongly leading to false alarms (red dots) at all temperatures except the reference temperature. In fact, the test is not able to distinguish between changes due to damage and changes due to temperature effects. For temperatures below 10°C, the test values in the damaged state are even lower than the values in the undamaged state, as the effects of decreasing stiffness caused by damage seem to be weaker than increasing stiffness from temperature effects. It becomes clear that a proper setup of the reference and a meaningful threshold is of vital importance for a reliable and robust damage detection method, especially to avoid false alarms.

In [Bal+08a] a more robust *average approach* for SSDD was derived that has been discussed in section 4.2.5. The approach uses the averaged Hankel matrices from different

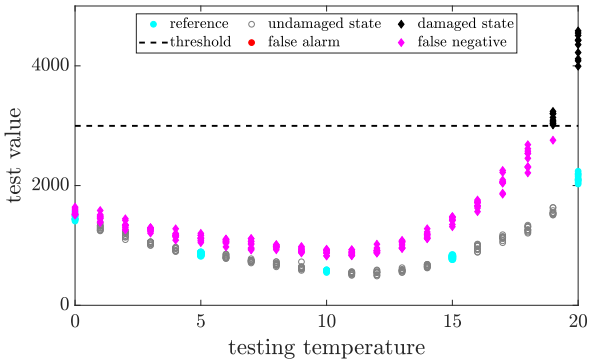

Figure 4.4 – Test values at different testing temperatures computed with the *average approach* [Bal+08a].

reference temperature states of the structure for the definition of the left reference null space and the computation of the covariance matrix for the computation of (3.2) and (3.11). In Fig. 4.4 the numerical data is evaluated by means of these averaged matrices considering reference data from the system at five reference temperatures $T_1 = 0°\text{C}$, $T_2 = 5°\text{C}$, $T_3 = 10°\text{C}$, $T_4 = 15°\text{C}$, and $T_5 = 20°\text{C}$. It shows the test values in the undamaged and the damaged state for testing temperatures between 0°C and 20°C. Compared to the conventional algorithm, the test values for the undamaged and damaged states of the system are better separated for each of the testing temperatures and false alarms can be avoided. However, it is impossible to separate the test values from the undamaged and damaged states with a common threshold for all temperatures. The threshold that is obtained based on the test values from the reference temperature states does only permit the detection of damages at temperatures above 19°C, while the damages at all other temperatures remain undetected. In this respect, the damage sensitivity of the test is poor.

The new approach derived in the previous section uses a temperature adapted reference null space $\underline{S}(P)$ in the residual (4.18) providing information on the current testing temperature linked to the temperature depending system behavior to improve the test performance. In the following the robustness of this approach to environmental variation will be evaluated considering the three strategies: *strategy 1* with the left reference null space $\underline{S}(P)$ computed on the interpolated Hankel matrix is denoted by "S(H) interpolated" in the figures, *strategy 2* based on the interpolation of modal parameters to retrieve the left reference null space from the parametric observability matrix is denoted by "S(O) interpolated", and *strategy 3* based on the regression of the modal parameters

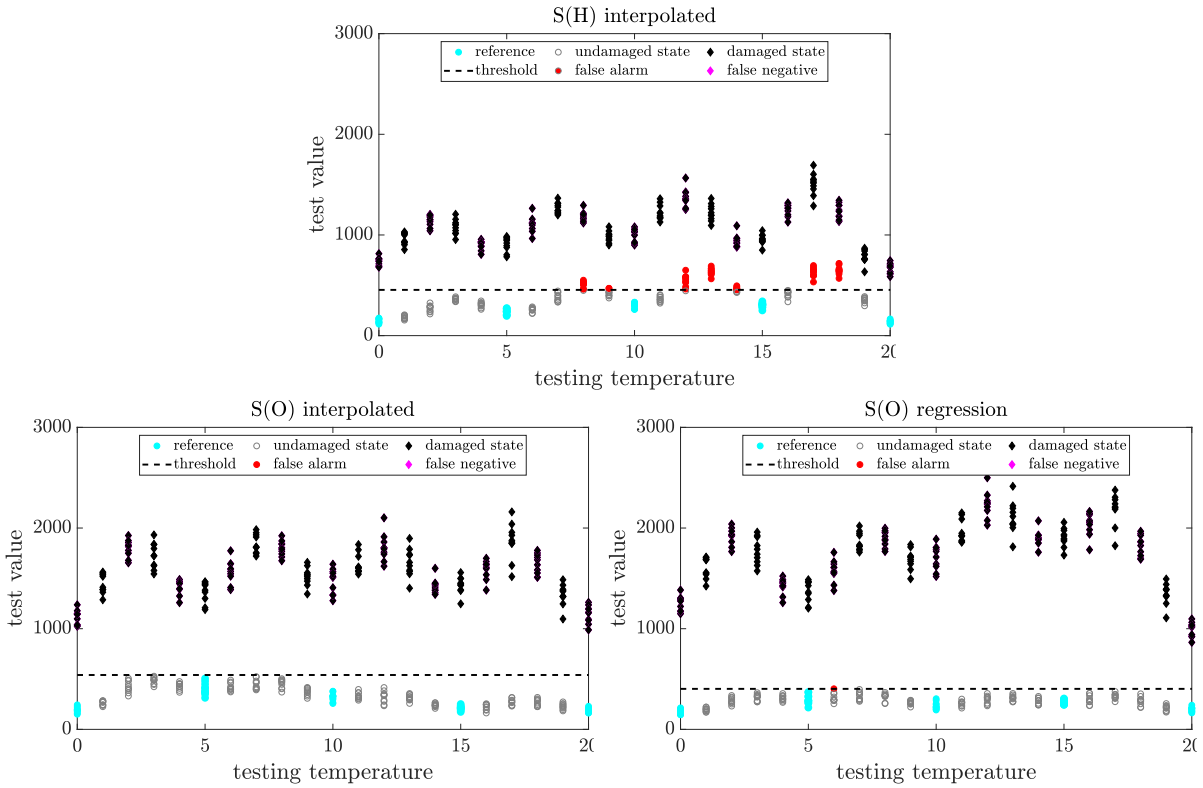

Figure 4.5 – Test values at different testing temperatures computed with the three strategies of the new method.

is denoted by "S(O) regression". The considered reference temperatures are $T_1 = 0°C$, $T_2 = 5°C$, $T_3 = 10°C$, $T_4 = 15°C$, and $T_5 = 20°C$, same as for the average approach in Fig. 4.4.

The weights for the interpolation are generated for each testing temperature, considering a Gaussian function with $\sigma^2 = 11$ centered at the testing temperature. For the interpolation close to the borders of the interval of the reference temperatures, where the interpolation function would overlap strongly outside of the interval, the weights of the reference points are re-evaluated for the interpolation assuming a (virtual) linear extrapolation outside the interval.

The statistical test in (4.19) is performed with an interpolated residual covariance from (4.22) considering the Gaussian weighting function used for the interpolation of the reference null space.

Fig. 4.5 shows the tests values with the three strategies in the undamaged and the damaged states for all testing temperatures. In the undamaged state the test values at the reference temperatures (cyan dots) are quite stable for each of the strategies. At the

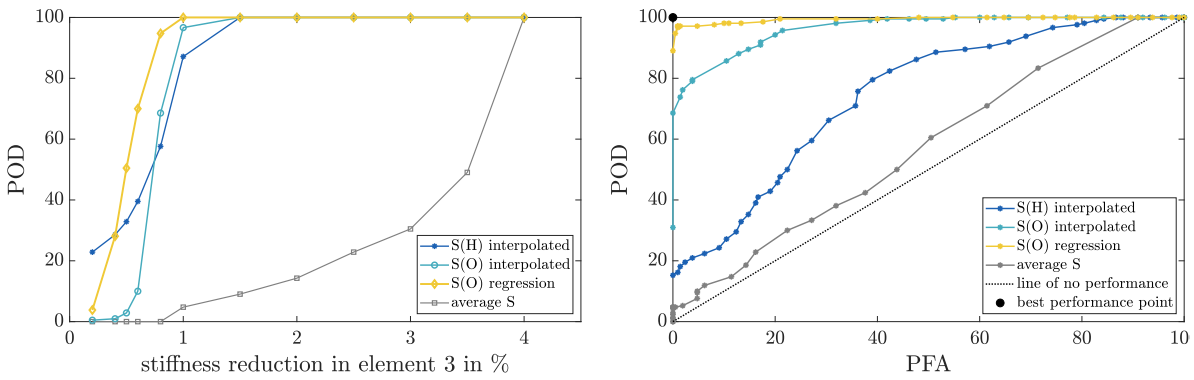

Figure 4.6 – Test performance of the average method and the three strategies of the new method. Probability of detection (left) and ROC curves for 0.8 % stiffness reduction (right).

testing temperatures in between the reference temperatures in the undamaged state the test values increase in particular for strategy 1 ("S(H) interpolated") but remain overall quite stable. This shows that the left reference null space $\underline{S}(P)$ and the covariance can be computed well for any testing temperature based on the interpolation or regression strategies. From test values at the reference temperatures empirical thresholds can be set up, which are valid globally over all temperatures. In the S(H) strategy about 25% false alarms occur, while in both S(O) strategies the rate is around 1 to 2%. It seems indeed that the temperature dependency of the modal parameters is easier to cover by an interpolation or regression rule, than it is directly for the Hankel matrix. Nevertheless, in all test versions the test values in the damaged state are separated clearly from the reference values. Damage can be detected even for the very small damage of 1.5% stiffness loss at one element.

The test performances for damages in element 3 of increasing extent are shown by the POD in Fig. 4.6 (left) for the average approach and the three developed strategies for robustness to environmental variation. All three developed strategies show good performance for small damages, with the S(O) approaches outperforming the S(H) approach, whereas the previous average approach can detect bigger damages only. This is confirmed by the ROC curves of the three strategies and the average approach in the right plot in Fig. 4.6, where the POD is plotted against the PFA. The POD and PFA values are computed for stiffness reduction of 0.8 % at element 3 varying the allowed false positive rate for the computation of the threshold. The average approach is very close to the line of no performance, that is when the POD equals the PFA. The performances of the new

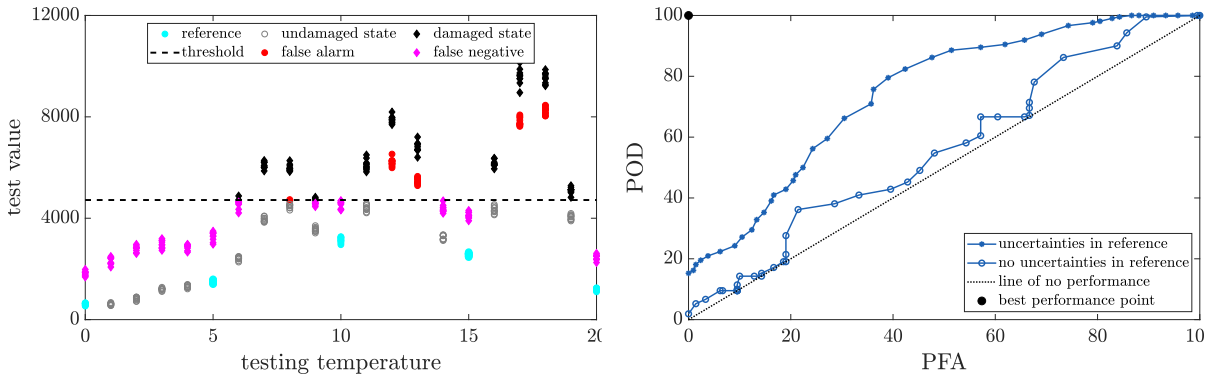

Figure 4.7 – Test values at different testing temperatures when the uncertainties of the reference null space are neglected (left) and ROC curves for 0.8 % stiffness reduction computed with S(H) strategy.

algorithms and especially the S(O) strategies approach the best performance point, which is where no false alarms occur and the damage of 0.8 % can be detected in any case.

Neglecting uncertainties in the reference null space When in the robust damage detection procedure the uncertainties of the reference null space are neglected, i.e. $\underline{\Sigma}_1 = 0$ which corresponds to the origin residual from [BAB00] recalled in (2.24), the damage detection test using the "S(H) interpolation" strategy yields the test values in Fig. 4.7 (left). Compare to Fig. 4.5 (top) the test values increase significantly at any testing temperature and show bigger variance, also regarding the reference temperatures, which leads to a bigger threshold. As a consequence, the test that takes the uncertainties into account shows a much better test performance as illustrated by the ROC curves in Fig. 4.7 (right) computed for stiffness reduction of 0.8 % at element 3, varying the allowed false positive rate for the computation of the threshold.

4.3.3 Covariance computation from test data

In statistical damage detection such as in (4.19) the residual covariance $\tilde{\underline{\Sigma}}_\zeta$ is an important part of the test, since it carries the information of the natural variance of the residual values stemming from the uncertainties in the underlying data in contrary to changes due to damage. So far interpolated residual covariances as described in section 4.2.4 have been used in the damage detection test (4.19). Another possibility is to recompute the covariance in the testing state from testing data. This leads to increasing computational effort and Fig. 4.8 shows that there is no significant benefit from this

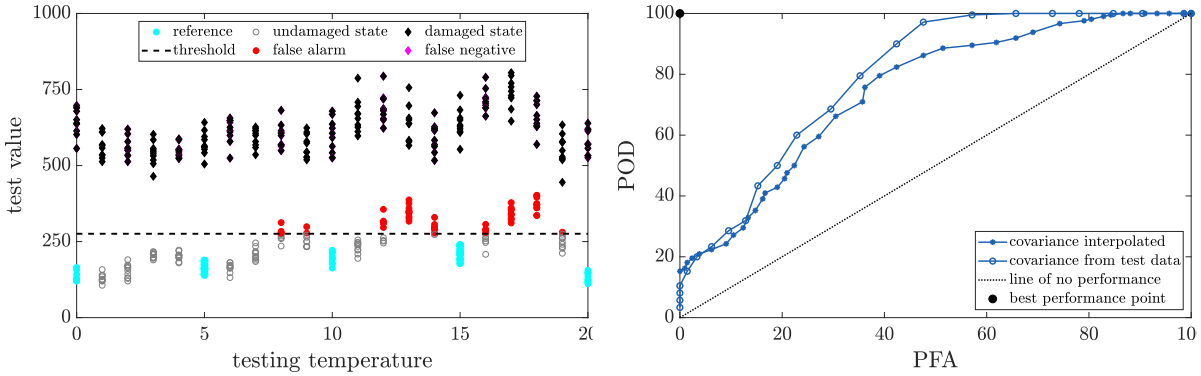

Figure 4.8 – Test values at different testing temperatures when the covariance is computed from the testing data (left) and ROC curves for 0.8 % stiffness reduction computed with S(H) strategy.

procedure. On the left side the test values of the S(H) strategy is shown for a stiffness reduction of 0.8 %, which behave similarly as in Fig. 4.5 (top). The test performance measured by the ROC curves on the right side increases only slightly, when the covariance is re-computed in the testing state. The interpolated covariance can be applied reliably also overcoming problems to estimate the covariance when only short data is available in the testing state.

4.3.4 Considerations for reference setup

In the previous a reference setup has been used considering reference data at five reference temperatures with distance of $\Delta T = 5°\text{C}$. In the following results from two more reference setups are analyzed regarding the robustness of the developed method and considerations for the design of the reference setup. Tbl. 4.1 summarizes the settings of the evaluated reference setups, with setup "A" denoting the previous reference configuration. In setup "B" the reference data at the borders is not taken into account. This provides information on the capability of the algorithms to yield an *extra*polated temperature adapted reference null space outside the reference temperature interval. In reference setup "C" the distance between the reference temperatures is bigger leading to conclusion for the choice of weighting function with respect to the available reference data. Setup "C2" considers the same reference data, but uses a wider Gaussian weighting function (W2 with $\sigma^2 = 25$ instead of W1 with $\sigma^2 = 11$) for the interpolation. These modifications are made to optimize the computation of the temperature adapted reference null space with respect to the bigger distance between the reference temperatures.

setup name	**reference T °C**	**weighting function**
A	[0 5 10 15 20]	W1
B	[5 10 15]	W1
C	[0 10 20]	W1
C2	[0 10 20]	W2

Table 4.1 – Reference setups

The respective test results at testing temperatures between 0 and 20°C are shown for the new approaches and the average method in Fig. 4.9. At the top the results form reference setup "A" are plotted. In the second line the test values of reference setup "B" are shown. This is followed by setup "C" and "C2" at the bottom.

When in the reference setup "B" no reference data is taken into account at the borders, i.e. at 0°C and 20°C, the test values for temperatures below 5°C and above 15°C are computed with extrapolated system matrices. The extrapolated system matrices lead to increasing reference test values for all methods, since the reference null spaces are less good fitting than in setup "A", where additional information was available from the reference data at the borders. In the undamaged state in all strategies the false alarm rate increases, especially the average method and the S(H) strategy are not able to distinguish the undamaged from the damaged state reliably. However, the S(O) strategies are robust for testing temperatures that are not too far from the reference temperatures. In the damaged state, all new approaches are able to detect damage reliably, while the average method fails to distinguish between damage and undamaged case.

When the distance between the reference temperatures increases as in setup "C" the test values computed with the temperature adapted reference matrices are much smaller at the reference temperatures than at the testing temperatures in between. Computing the threshold from these test values leads to a significant number of false alarms. This is due to the weighting function that was optimized for the temperature model in Fig. 4.2 combined with the reference setup "A" with temperature distance of 5°C. In the present setup the distance is 10°C and the used weighting function is too sharp, i.e. when the testing temperature is one of the reference temperatures this reference point has a strong effect, while the other reference points are neglected. When the testing temperature is different from the reference temperatures, all reference points gets the same weight.

With these findings the interpolation function is modified in setup "C2", i.e. a wider weighting function is chosen. For the S(H) strategy the effect is small, but in the S(O) strategies the false alarm rate decreases. With all new approaches damages is detected

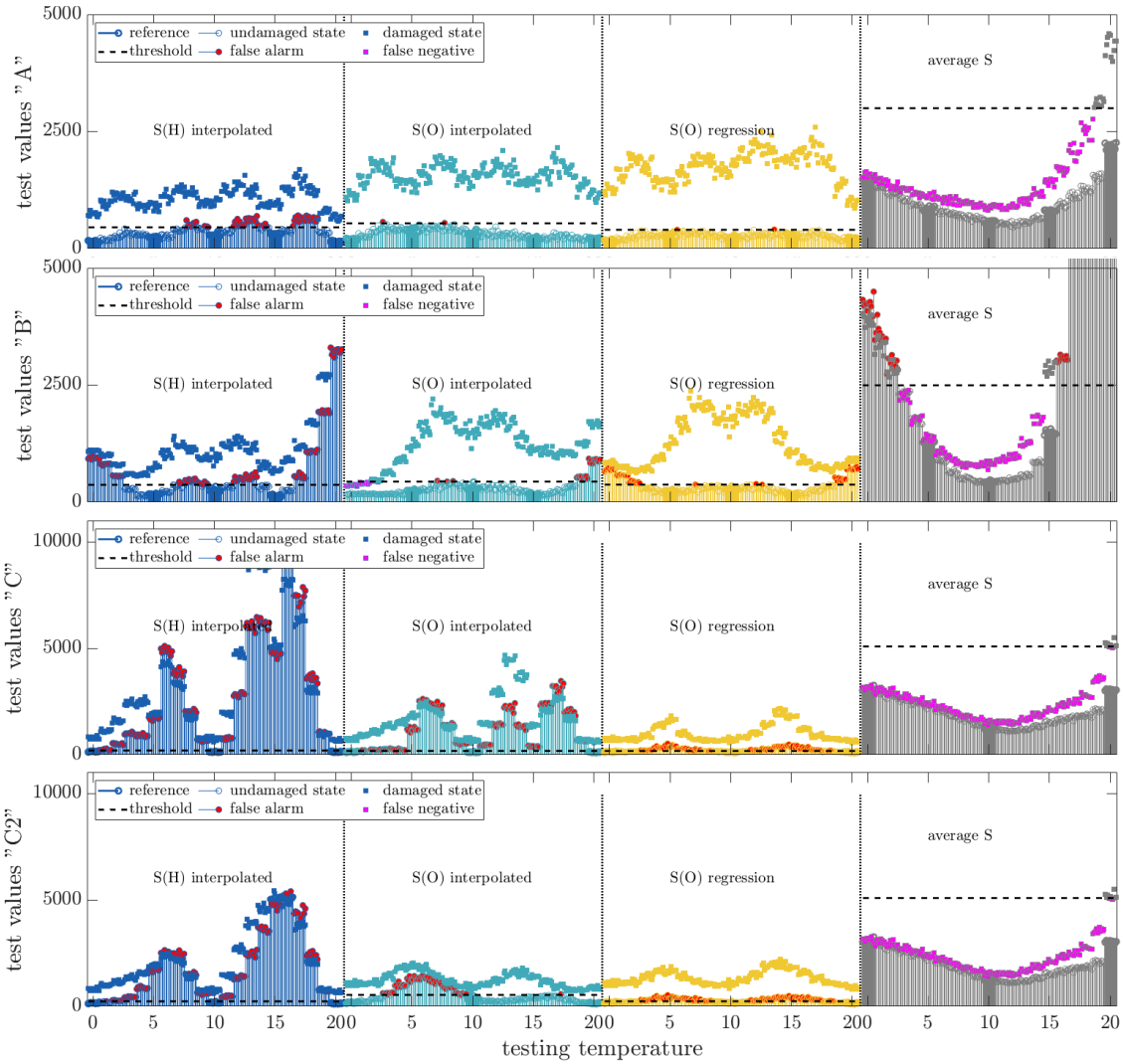

Figure 4.9 – Test values at different testing temperatures for different reference setups.

reliably, which is not the case with the average method.

4.3.5 Effects of changes in the excitation covariance

The previous results apply when the excitation covariance is constant for all reference data sets. In real applications in the structural engineering field this may not hold, and changes e.g. in the traffic or wind conditions may lead to changes in the covariance of the excitation, i.e. the variance in $w_{j,k}$ in (2.66). This perturbs the interpolation of the Hankel matrix in (4.13).

Fig. 4.10 (left) shows the test values computed with strategy S(H) in the undamaged

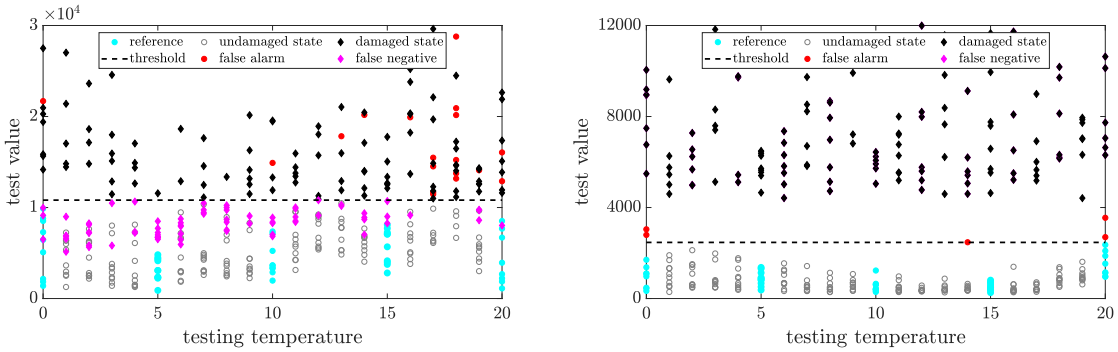

Figure 4.10 – Test values when reference and testing data sets have different excitation covariance, computed with S(H) interpolation (left) and S(O) interpolation (right) strategies.

and the damaged state when the stiffness at element 3 is decreased by 4%. The standard deviation of the excitation in the reference state is changed from 1 to 0.2 and the standard deviation of the excitation in the test state is uniformly randomly varied between 1 and 10. Many damages cannot be detected and false alarms occur.

This problem can be overcome by means of the strategies, which uses the interpolated eigenstructure of the system (4.16) to compute the observability matrix $\underline{\mathcal{O}}(P)$, since the modal parameters are independent from the excitation covariance. Fig. 4.10 (right) shows the test values computed with the "S(O) interpolation" strategy with the above defined changes in the excitation covariance. Those changes are reflected in the variance of the test values in the unchanged and in the damaged system but the different system states are separated clearly and damage detection is successful.

4.4 Summary

In this chapter the theory for a damage detection procedure has been derived that is robust to changes in the environmental conditions, and the results have been validated in a numerical study.

The robust approach is based on a model interpolation leading to a temperature adapted reference null space. Three strategies for computing the reference null space were considered. Firstly, the reference null space is computed from an interpolated Hankel matrix. This is convenient as the system identification step is avoided, but gives less good results in the interpolation step of the Hankel matrix and requires sufficient reference points. Secondly, interpolated modal parameters lead to an interpolated observablity ma-

trix, from which the reference null space can be computed. With this procedure good results could be reached also for few reference points. Both approaches need some extra effort, if the testing temperature is at the border or outside the range of the reference temperatures, e.g. higher than the highest reference point or lower than the lowest reference point, by introducing virtually extrapolated reference points. Thirdly, a null space is computed from an observability matrix based on modal parameters obtained from a regression analyis. In this method the regression function has to be optimized carefully, especially when only few reference points are available.

The strategies that are based on the interpolated observability matrix can also be applied robustly when changes in the excitation covariance between the reference data sets occur, since the modal parameters are independent from the excitation covariance, whereas the Hankel matrix interpolation fails under these circumstances.

The new approach outperforms the existing average approach from [Bal+08a], which is not able to detect damages when the temperature effect is higher than the effect due to damage, while the newly developed method is still sensitive. With a temperature adapted reference null space false alarm rate can be decreased significantly when a well designed weighting or regression function is used taking at least the two neighbored reference points into account for interpolation.

4.5 Dissemination

Parts of this chapter have been published in

[Vie+19] E. Viefhues, M. Döhler, Q. Zhang, F. Hille, and L. Mevel. « Subspace-based damage detection with rejection of the temperature effect and uncertainty in the reference ». In: *Proceedings of IOMAC 2019 - 8th International Operational Modal Analysis Conference*. Copenhagen, Denmark, 2019

[Vie+20] E. Viefhues, M. Döhler, F. Hille, and L. Mevel. « Fault detection for linear parameter varying systems under changes in the process noise covariance ». In: *IFAC-PapersOnLine* 53.2 (2020). 21th IFAC World Congress, pp. 13668–13673

[Vie+21] E. Viefhues, M. Döhler, P. Simon, R. Herrmann, F. Hille, and L. Mevel. « Stochastic subspace-based damage detection of a temperature affected beam structure ».

In: *Proceedings of SHMII-10 2021 - 10th International Conference on Structural Health Monitoring of Intelligent Infrastructure*. Porto, Portugal, 2021, pp. 1–6

A journal paper based on this chapter is in preparation for submission to “Mechanical Structures and Signal Processing“.

Part III

Applications

Chapter 5

Damage detection of a steel frame considering uncertainties in the reference matrix

5.1 Introduction

In chapter 3 the theory for a subspace-based damage detection with estimated reference null space was derived. The developed damage detection test has been validated on simulation data, where its behavior was shown to be coherent with the theoretically expected properties thanks to the consideration of the uncertainty related to the reference data. Moreover, it was shown to be robust for different data lengths with an increased performance especially for short reference data lengths compared to the conventional test. In this chapter, the tests are applied to a laboratory steel frame structure for an evaluation of the test performance on experimental data.

The experiments were performed within the scope of work from [Hil18] at the Federal Institute of Materials Research and Testing (BAM), where damage detection of off-shore wind turbine jacket structures with subspace-based methods was evaluated. A laboratory steel structure has been designed, such that reversible damage can be introduced to the structure. The eigenstructure of the down-scaled test specimen is comparable to the modes of real jacket structures in the lower frequencies within the limits of minimum material thickness.

In the following, the test setup and the dynamical properties of the laboratory tests are summarized. Then damage detection with the algorithms from chapter 3 is performed using the experimental data, and the effect of data length is discussed.

5.2 Experimental setup and dynamical properties

The laboratory steel frame structure represents a 1 : 10 scaled two-dimensional section of a jacket-type support structure of an off-shore wind turbine, as it is shown in Fig. 5.1 in the lab of BAM. The structure is of 2.36 m height, 1.92 m width at the bottom, and 1.62 m width at the top. It is made of steel pipe components with an I-sectional steel beam on the top. At the bottom the structure is bolted to the floor. At the top the structure is fixed perpendicular to the in-plane-direction.

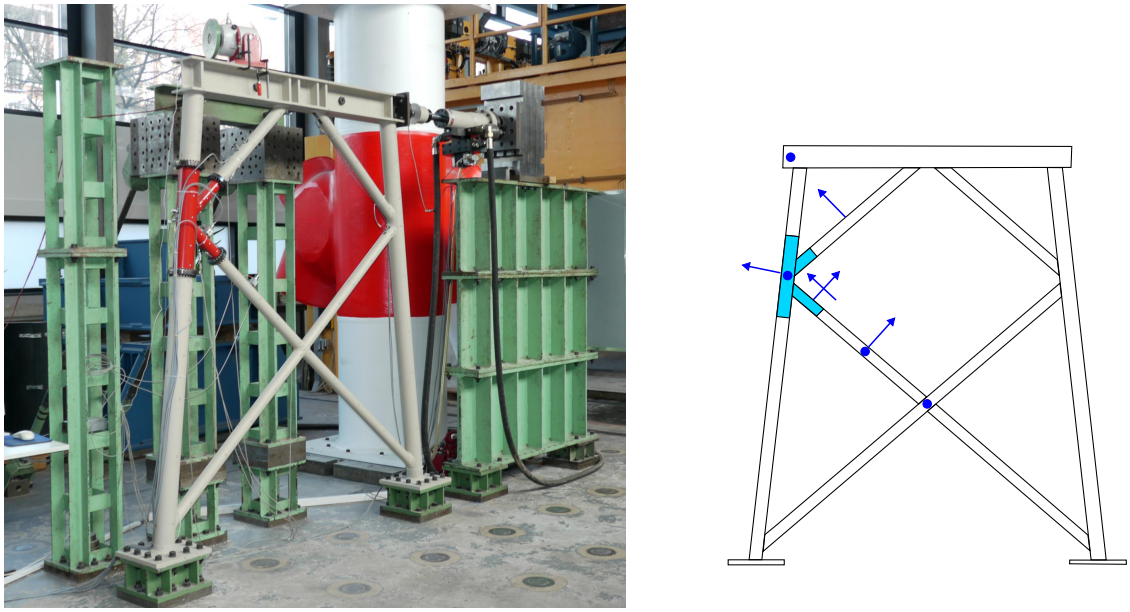

Figure 5.1 – Laboratory testing structure (left) and sensor positions (right).

The structural parts are mainly welded, except for the area where a reversible damage can be introduced. This damage area is defined by a K-node, which is fixed to the structure by means of bolted end plates as demonstrated in Fig. 5.2. The damage is designed such that the global behavior is affected. By loosening the bolts at the lower brace successively, the progress of a fatigue crack-like damage can be introduced. A high number of bolts is used to provide a high resolution of the induced stiffness loss. At the columns 26 and at the diagonals 18 M6 screws are installed, from which seven screws are used to simulate damage, while the remaining are needed for structural safety. In the reference state all bolts are screwed tight. For increasing damage, 1, 2, 3, 5, or 7 bolts are unscrewed. Loosening 1 and 2 bolts results in less than 1% reduction of the moment of inertia. When 3, 5, and 7 bolts are loosened, this represents a fatigue crack, leading to reduction of the moment of inertia of about 3%, 10%, and 30%, respectively [Hil18].

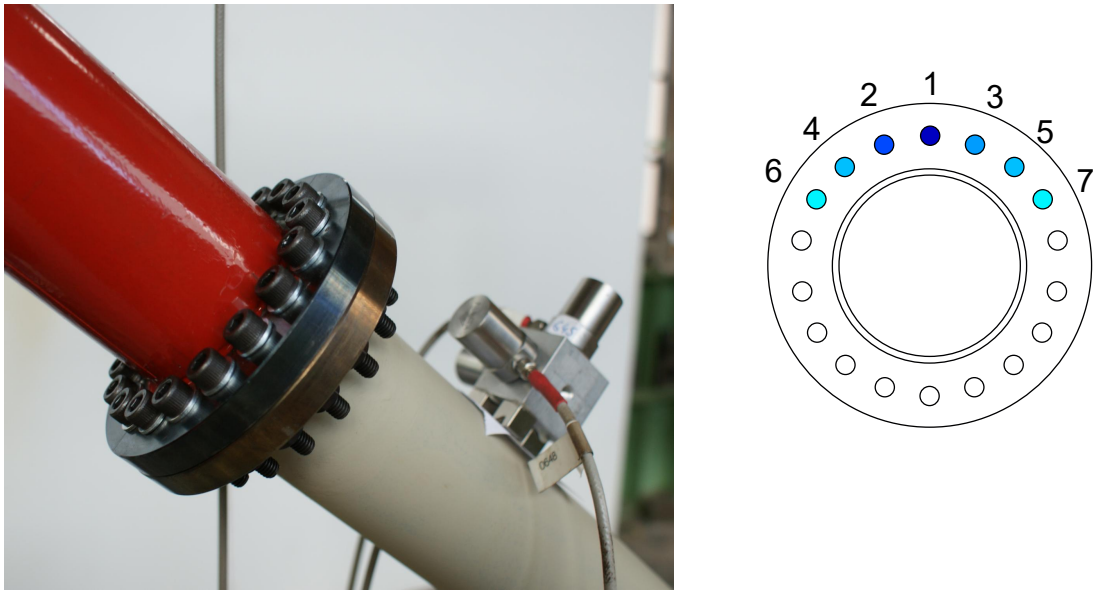

Figure 5.2 – Reversible damage detail (left) and screw configuration (right).

An electrodynamic shaker of type “LDS V406“ (Co. Brüel & Kjaer) equipped with an extra mass of 5 kg is used to excite the structure with a random white noise signal in the range of 10 to 1000 Hz. The excitation direction is approximately 30° rotated out of the in-plane-direction. Accelerations are measured with a sampling rate of 2500 Hz at nine locations in accordance to Fig. 5.1 (right). The sensors have a resonance frequency of more than 10 Hz and were of type “KD41V“ (Co. MMF Radebeul, 8 pieces) and of type “7251A“ (Co. Endevko, 1 piece).

The dynamical properties of the steel frame are evaluated in [Hil18] with the covariance driven SSI. 50 robust modes can be identified under different test scenarios. Also the higher modes are identified, since it is assumed that they are affected by damage. The table 5.1 recalls the frequencies in the undamaged case.

Further details of the test setup and dynamical properties can be found in [Hil18]. In the following application, data is used from tests without changes in the environmental and excitation conditions.

f1	f2	f3	f4	f5	f6	f7	f8	f9	f10
31.4	48.2	65.1	78.7	81.1	93.9	108.0	149.6	150.4	164.5
f11	f12	f13	f14	f15	f16	f17	f18	f19	f20
168.9	179.5	182.5	192.9	201.7	208.2	211.4	232.9	238.6	280.4
f21	f22	f23	f24	f25	f26	f27	f28	f29	f30
283.1	292.8	304.5	311.4	337.1	360.1	393.2	415.1	431.1	441.7
f31	f32	f33	f34	f35	f36	f37	f38	f39	f40
452.9	486.9	500.8	520.2	524.2	535.3	544.2	562.8	574.0	587.6
f41	f42	f43	f44	f45	f46	f47	f48	f49	f50
595.6	603.4	623.7	633.7	685.5	717.7	750.5	785.6	812.3	856.8

Table 5.1 – Frequencies of the steel frame in Hz from [Hil18]

5.3 Damage detection with uncertain reference null space

For damage detection, the reference system is defined when all bolts are tightened, and five damaged states are considered with 1, 2, 3, 5, and 7 loosened bolts. For each system state, eight data sets are prepared. One data set in the undamaged state is used to compute the reference matrix $\widehat{S}$, as well as the residual covariance $\widehat{\Sigma}$ and $\widehat{\tilde{\Sigma}}$ for the conventional and the new test, respectively.

Since in the system identification more than 50 modes are found, parametrization with respect to the damage sensitive modal parameters is not an easy task. This motivates for the application of the non-parametric test (3.33), which is the most convenient test setup with a high practicability, since the system identification step is also avoided in the reference state. It corresponds to a direct detection of changes in the residual. The number of degrees of freedom of the test is related to the rank of the converged covariance matrices Σ or $\tilde{\Sigma}$ of the tests, which however cannot be evaluated with limited data. Nevertheless, an upper bound is given by their size, which is limited by the number of data blocks in their estimation [DMH14]. In this application, $n_b = 500$ data blocks have been used for the computation of $\widehat{\Sigma}$ and $\widehat{\tilde{\Sigma}}$, hence the degrees of freedom of the χ^2 test distributions are limited by 500, where the threshold allowing for 0.1% false positive alarms is at 603.

Fig. 5.3 shows the test values in the undamaged reference state of the conventional test (left) and when the uncertainty of the reference is considered in the new test procedure (right) for different reference data lengths M. The testing data length is about 8 seconds with $N = 20{,}480$. In accordance with the numerical evaluation in section 3.3

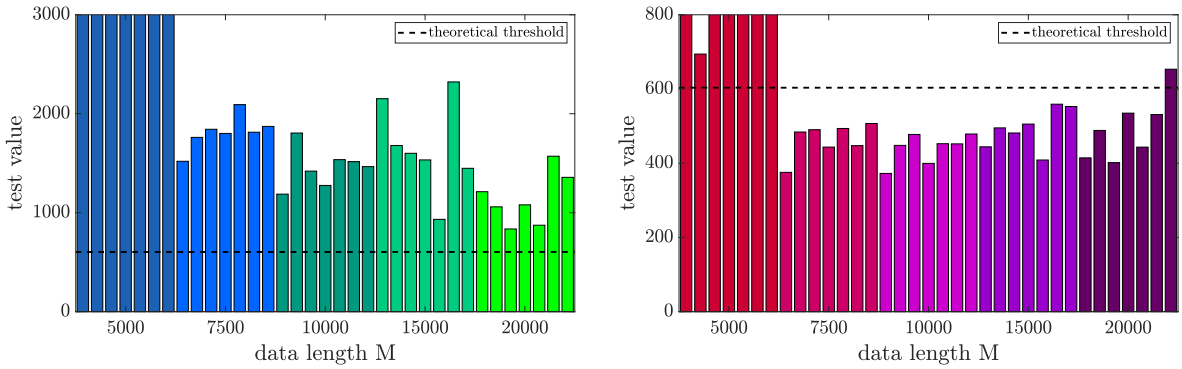

Figure 5.3 – Test values of the conventional (left) and the new test (right) in the undamaged reference state computed with different reference data lengths M.

the conventional test leads to test values clearly above the threshold in Fig. 5.3 (left). Moreover, the test values depend on the reference data length M used for the computation of the reference null space and the covariance matrix. They tend to decrease with increasing M as it could similarly be seen in the numerical simulation in Fig. 3.5. With the new testing method only the test values for the very short data length $M = 5{,}000$ are above the threshold in Fig. 5.3 (right), and indeed it can also be observed in Fig. 3.5 that the test value mean has not converged yet for very small M. For the other used data lengths, the test values are consistently below the theoretical threshold and do not show any dependence on M.

The test values in different system states are presented in Fig. 5.4 for both tests, where the reference data length $M = 15{,}000$ was chosen and $N = 20{,}480$. Both tests are able to indicate changes in the system by an increase in the test values, even for damages below

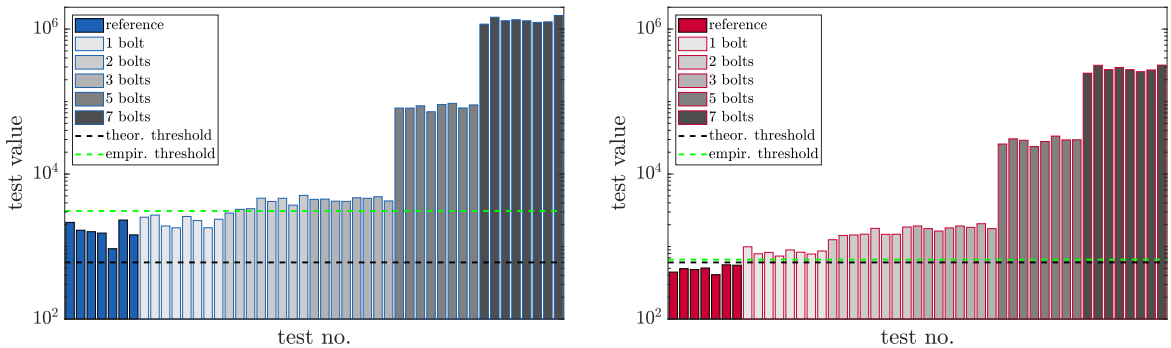

Figure 5.4 – Test values of the conventional (left) and the new test (right) in the reference and at different damaged states.

1% stiffness reduction. Two different thresholds are marked: the theoretical threshold from above and an empirical threshold, that is computed from the values in the reference state allowing for 0.1% false alarms. Notice that a threshold computed from such a small sample size is not very reliable. Still, with the new test the empirical threshold coincides with the theoretical one, thanks to very stable test values. The undamaged and the damaged state can be distinguished reliably. With the conventional test method, however, the theoretical and the empirical threshold are significantly different. The method fails to recognize the healthy state when using the theoretical threshold, while with the empirical threshold the test sensitivity is small. In particular, the smallest damage of one loose bolt cannot be detected with the conventional test, even when using the empirical threshold, while this damage can already be detected with the new test.

The effect of testing data length N is evaluated in Fig. 5.5. Test values, which are computed with three different testing lengths N, and the empirical and the theoretical threshold are shown. The reference matrices are estimated from a data set of length $M = 15{,}000$, the thresholds are defined such that the maximum number of false alarms is 0.1%. When the uncertainties of the reference null space are taken into account with the new test (right), the reference values are mostly independent from N and the theoretical and empirical threshold are similar. The damaged state is better separated from the reference state, when the testing data length N increases. Thus, damage can be detected even with very small damages, which is in accordance to the formulation of the

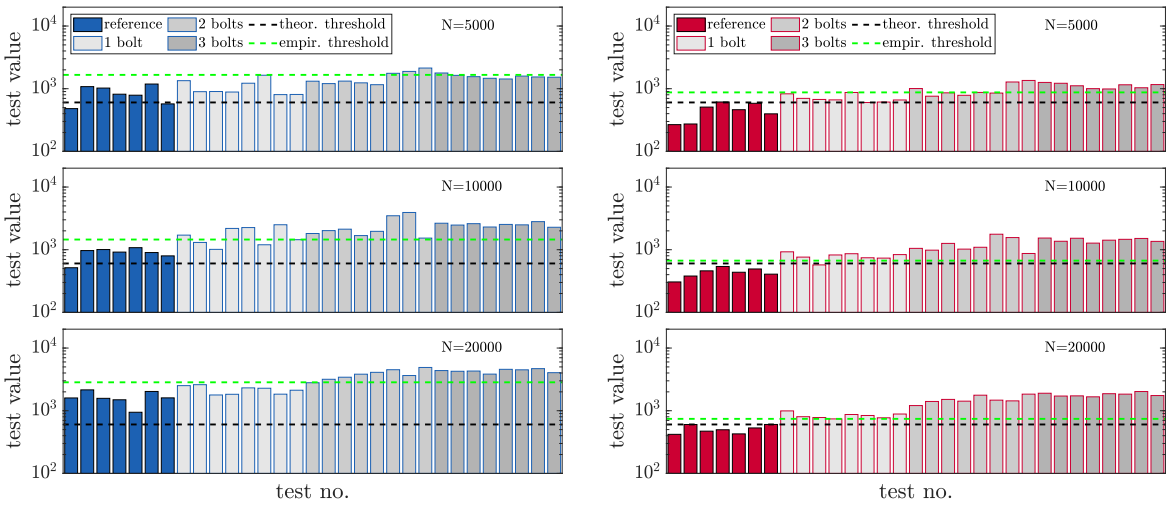

Figure 5.5 – Test values of the conventional (left) and the new test (right) in the reference and at different damaged states for different N.

close hypothesis (2.26). In contrary, the conventional test method shows an unpredictable damage detection behavior, when the data length N increases, leading to larger test values in all states. This was pointed out in the context of Fig. 3.4. Since both tests show some variance of the test values in the reference state, the small sample size perturbs the setup of a reliable empirical threshold, making the big advantage of a theoretical based threshold obvious. Furthermore, the new test shows a better damage sensitivity, where smaller damages can already be detected compared to the conventional test.

5.4 Summary

In this chapter the damage detection method for a residual with uncertain reference (chapter 3) has been applied to experimental data from a laboratory steel structure. Since over 50 modes were found for the structure, a non-parametric test procedure was used, which avoids the identification of the damage sensitive modes.

The results correspond to the findings in the numerical study. The new test shows good accordance to theoretically expected values, while the conventional test leads to higher test values due to the bias that is introduced by neglecting the uncertainties in the reference state. It was confirmed that the new test is very robust to changes in data lengths M and N and thus allows for computing the threshold on a theoretical basis. Such theory-based a priori thresholds offer important benefits, especially when only few reference data is available and bad reference estimate or small sample size perturb the setup of an empirical threshold. Moreover, the new test had a better damage sensitivity than the conventional test in this case study. When the uncertainty of the reference null space is neglected in the conventional test method, the test values and the test performance are not predictable and consequently require comprehensive study of the reference state based on data to e.g. derive reliable thresholds.

5.5 Dissemination

Parts of this chapter have been published in

[**Vie+22**] E. Viefhues, M. Döhler, F. Hille, and L. Mevel. « Statistical subspace-based damage detection with estimated reference ». In: *Mechanical Systems and Signal Processing* 164 (2022)

Chapter 6

Damage detection of a temperature affected laboratory beam structure

6.1 Introduction

Three strategies for a stochastic subspace-based damage detection (SSDD) approach that is robust to changes in the environmental conditions such as temperature have been presented in chapter 4 and validated on numerical data. The approaches are based on or motivated by the model interpolation approach for linear parameter varying (LPV) systems from [Zha18] leading to a reference null space that is adapted for the current parameter state, e.g. for the temperature conditions in the testing state.

Up to now, the interpolation-based temperature rejection approach was validated theoretically on numerical data of a mass-spring-damper. A very simple temperature model in section 4.3 was used that simulates the effect of temperature on the dynamical behavior of the structure by decreasing stiffness of the springs with increasing temperature. In this section the simplest of the developed algorithms, namely the one based on the interpolated Hankel matrix, is applied to data from a reinforced concrete beam tested in a climate chamber in the testing facilities of the Federal Institute for Materials Research and Testing (BAM) at defined temperatures and at three different system states. The data is obtained by experiments that have been performed by Simon et al. [Sim+20]. It is shown that the new test behaves robustly towards temperature effects and still provides a reliable sensitivity towards damages.

In the following the test setup and the dynamical properties of the test specimen are presented. Then, the damage detection approach with the interpolated Hankel matrix from (4.13) is applied to the experimental data and the robustness towards temperature effects and the test sensitivity are discussed and compared to previous approaches.

6.2 Experimental setup and dynamical properties

A reinforced concrete beam is tested in a climate chamber at defined temperatures and at different system states. The test setup is shown in Fig. 6.1. The beam of 2.72 m span is supported at two points. The cross section is reinforced with two bars of 16 mm diameter at the bottom and no additional stirrups.

Three geophones measure vertical vibration velocities on the top of the beam. The structure is excited by an external shaker with a white noise signal in the range of 30 Hz to 2000 Hz, to simulate ambient excitation as it will occur similarly in e.g. bridges under operational conditions. The shaker is installed upside down (Fig. 6.2) and isolated against the changing temperature conditions. The data is recorded with 5 kHz.

Three different system states are considered: the undamaged reference state, damage level 1 after the beam was loaded in the midspan with 20 kN, and damage level 2 after the structure was loaded up to 28 kN. In the second damage level obvious cracks have been occurred in the middle of the beam. The load is removed after introducing the damage.

The experimental temperatures are chosen to be -25°C, -5°C, 5°C, 25°C, and 40°C. The temperatures are measured at several points inside the chamber and with two embedded sensors in the middle of the beam. In each system state and at all five testing temperatures the velocities are recorded, after reaching a constant temperature level in the beam. Further details on this experiment are described in [Sim+20].

With a SSI-algorithm the eigenstructure of the system is identified. Due to high noise

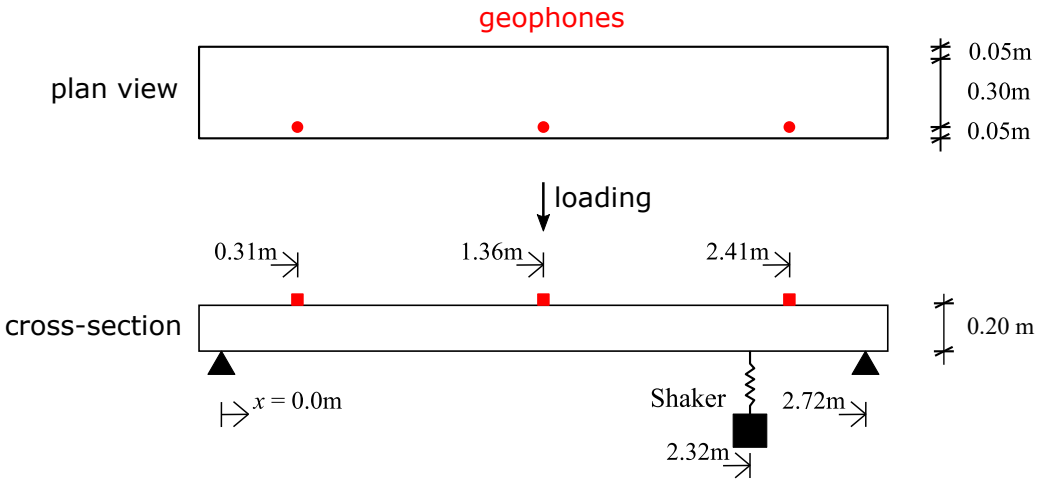

Figure 6.1 – Test setup of the concrete beam with locations of geophones, shaker, and loading for the damage introduction.

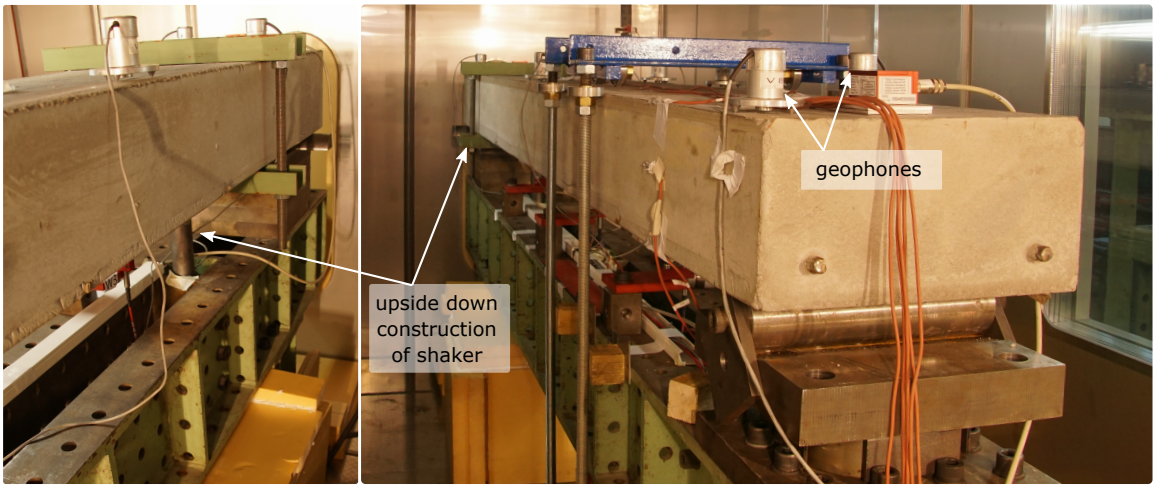

Figure 6.2 – Concrete beam in the climate chamber.

impact above 500 Hz, the data is sampled down to 400 Hz. Fig. 6.3 shows the first four eigenfrequencies in dependence of the temperature, which can be clearly identified in every system state and at every temperature. The first and the second eigenfrequency are quite close. This is due to the construction of the shaker installation, which works as a tuned mass damper to the beam structure. Simulation results from a model of the corresponding structure with a mass damper have shown a good accordance to these first four eigenfrequencies.

Each frequency is plotted within its 5%-range to give an idea of the quantity of the temperature and the damage effect. The black full line marks the frequencies in the undamaged state. Effects due to temperature become more obvious for the second and the third frequency. While the damage level 2 leads to significant decrease of the eigenfrequencies of about 5%, the effect of damage level 1 does not become obvious in the first and the second eigenfrequency. The third and fourth frequencies increase by about 3% due to damage. This was not expected and cannot be explained from the information gained from the experiments. However, this fact has no impact on the usability of the data for the application study.

6.3 Damage detection with temperature effects

For the damage detection the data is sampled down to 400 Hz, and data sets with 350,000 data points are prepared at each temperature state. For the setup of the reference matrices the first half of the respective data set is used, such that $M = 175{,}000$, which is

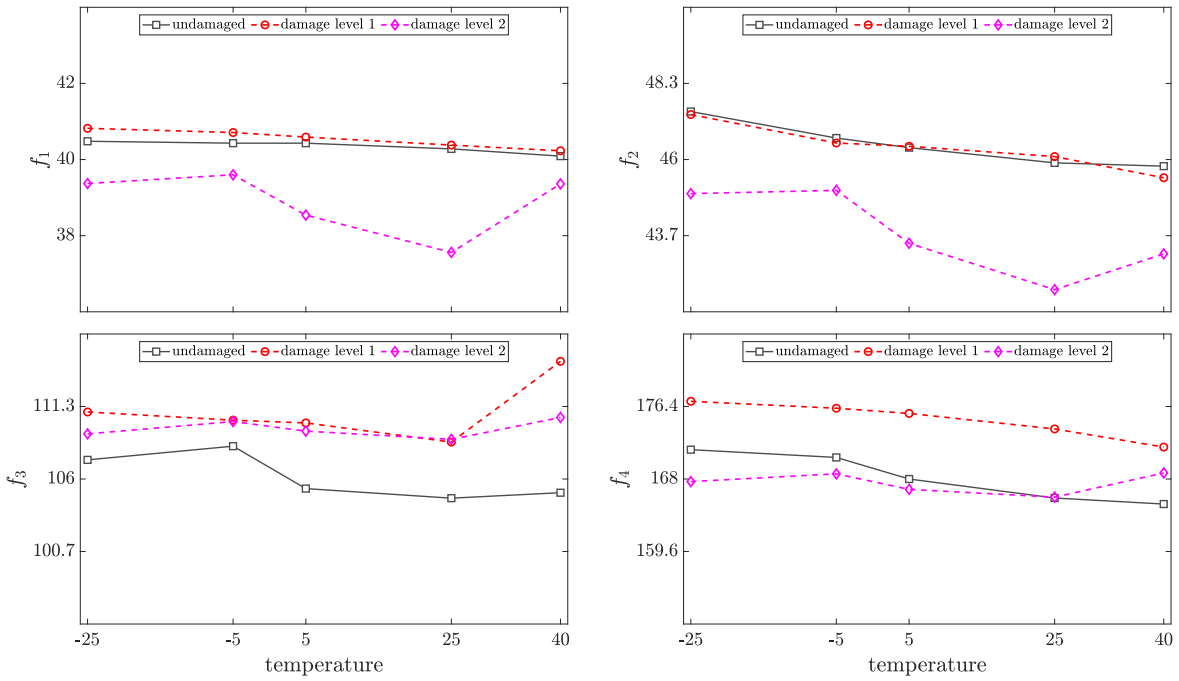

Figure 6.3 – 1st to 4th eigenfrequencies at different system states and at different temperatures. The y-axis is scaled to about 5 % of each frequency.

about seven minutes. For the damage detection test the data sets are split into eight data samples each of length $N = 40{,}000$ or 100 seconds. In this first application to real data a fully data-driven non-parametric test setup (4.19) is used where the residual is computed from an interpolated Hankel matrix (4.13). The residual covariance is derived with (4.22) from the interpolated Hankel matrix covariance (4.21) and without consideration of the uncertainty in the reference null space, i.e. $\underline{\Sigma}_1 = 0$ in accordance to the conventional test in (2.37). Other test variants are further investigated in the subsequent chapter 7.

To illustrate the effect of the changing temperature to damage detection of the concrete beam, the interpolation based method is compared to 1/ taking a fixed reference at one of the temperatures (without consideration of the temperature effect), and 2/ the averaging approach from [Bal+08a] that defines a fixed reference by mixing data from different reference temperatures.

Fixed reference The tests are done firstly for the case where only data from one fixed reference temperature is considered in the reference state. This corresponds to the conventional residual in (2.24). The null space and the residual covariance in (2.37) are computed from a data set at 5°C. Fig. 6.4 shows the test values of the hypothesis test

(2.33) at different testing temperatures in the undamaged state and at the two damage levels. For the setup of the testing Hankel matrices $\widehat{\mathcal{H}}$ data samples of 100 seconds are used. From the test values in the reference state for the undamaged structure at 5°C (grey bars) a threshold is defined, which allows for false positive alarms of 1% maximum.

It becomes obvious that changes in the temperature in the undamaged state (green bars) affect the test values in a similar way as the different damages do. This results in a high number of false alarms in the undamaged state, namely for all cases where the test temperature is different from the reference temperature. While all test values in the damaged cases also exceed the threshold, they cannot be distinguished from the test values in the reference state due to the temperature effect.

This is in accordance to the findings with the numerical simulation data, where in Fig. 4.3 all test values at temperatures different from the reference temperature are above the threshold, no matter if they classify the damaged or the undamaged case.

Averaging approach from [Bal+08a] The temperature rejection approach in [Bal+08a] that was discussed in section 4.2.5 uses data from different temperatures in the reference state together in one merged data set. From this merged data set the averaged reference Hankel matrix and its left null space are computed with, as well as the covariance of the resulting residual. In Fig. 6.5 the test values from this method are presented, where reference data samples from three reference temperatures, 25°C, 5°C, and 40°C, are merged in one reference data set. The testing Hankel matrices $\widehat{\mathcal{H}}$ are computed from a 100 second data sample. A threshold is defined from data in the reference state, thus of the undamaged structure at the three reference temperatures (grey bars), allowing for 1% false alarms.

The structure is correctly classified as undamaged if the testing temperature corresponds to one of the used reference temperatures. Information about all reference states is contained in the merged reference data set and thus considered in the reference null space and the covariance matrix.

If the temperature differs from the reference temperatures, the changes in the structure due to temperature lead to higher test values even in the healthy states exceeding the threshold. The structure is detected to be damaged. These changes due to new testing temperatures have a quantitatively similar effect to the test values as damages do. While damages can be detected at all temperature levels, they cannot be distinguished from the healthy state at testing temperatures that are not contained in the reference data.

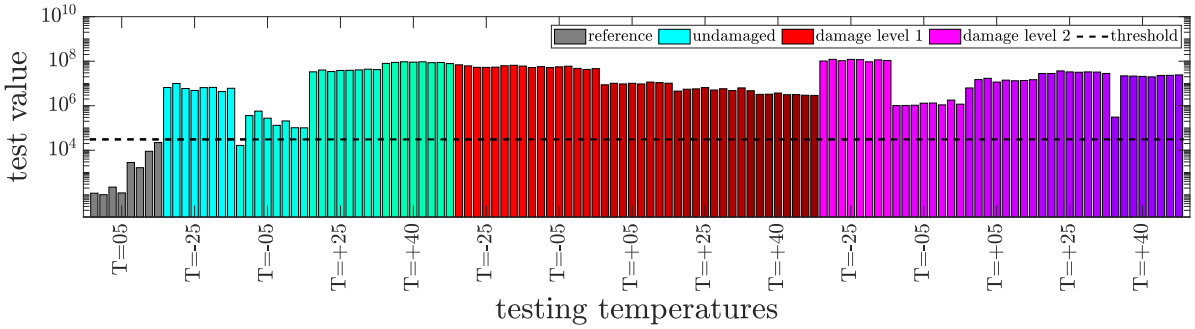

Figure 6.4 – Fixed reference null space and covariance matrix. Test values at different testing temperatures in the undamaged and damaged states. Reference data at 5°C.

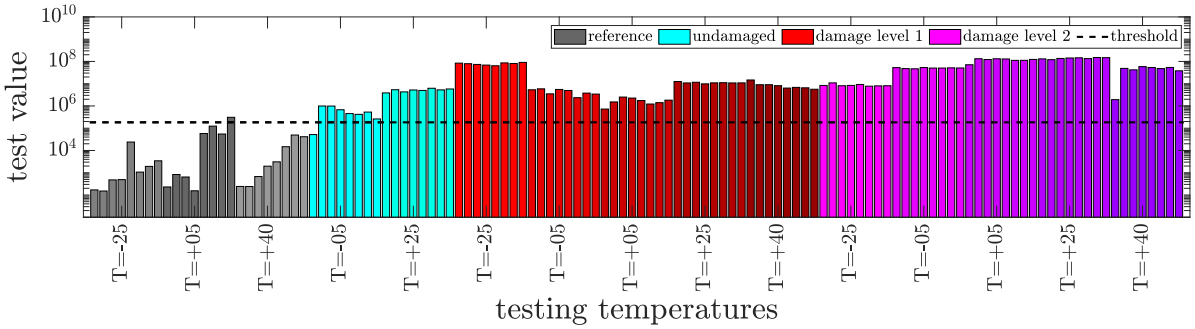

Figure 6.5 – Averaged reference null space and covariance matrix. Test values at different testing temperatures in the undamaged and damage states. Reference data at -25°C, 5°C, and 40°C.

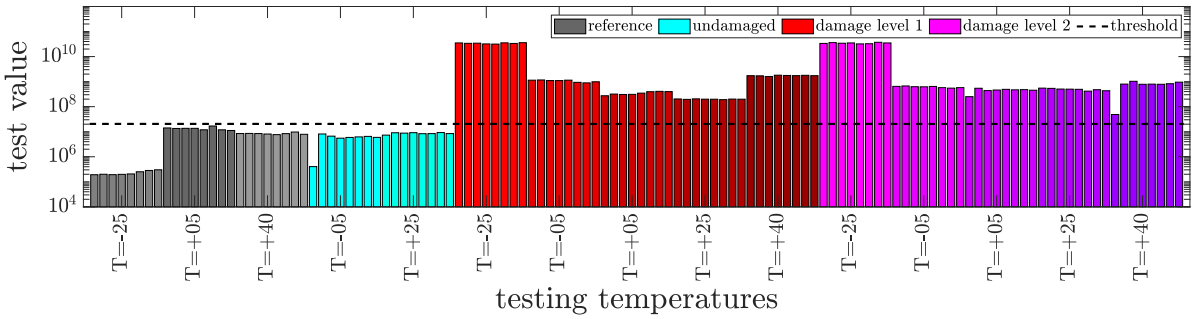

Figure 6.6 – Interpolated reference null space and covariance matrix. Test values at different testing temperatures in the undamaged and damage states. Reference data at -25°C, 5°C, and 40°C.

Approach with interpolated Hankel matrix With the robust SSDD approach from chapter 4 using the interpolated Hankel matrix the information about the temperature depending behavior of the structure at testing temperatures different from the reference temperatures can qualitatively be carried by an adequate weighting function within the interpolation step. In Fig. 6.6 test values of the experimental data are presented that are computed with null space derived from an interpolated Hankel matrix (4.13). The residual covariance is computed with (4.22) from the interpolated Hankel matrix covariance (4.21). The uncertainties in the reference null space are neglected, i.e. $\underline{\Sigma}_1 = 0$ which corresponds to the conventional test with (2.37).

In the reference state three reference temperatures are considered 25°C, 5°C, and 40°C as in the previous paragraph. For the weighting of the respective Hankel matrices $\mathcal{H}_j$ in (4.13) a Gaussian function with a variance of 30, centered at the testing temperature, is applied. A threshold is computed in the reference state of the undamaged structure at the three reference temperatures (grey bars), allowing for 1% false alarms.

With this approach the undamaged state can be distinguished clearly from the damaged state for any testing temperature. There is no difference in the test values, whether data from the testing temperature was available for the reference set up or not. An adequate null space can be found in any case, and false alarms in the undamaged state are avoided. The damages can be detected reliably.

In general, the test values of the interpolation method are higher than in the other computation methods. This can be explained from the choice of the weighting of the local reference models. For any testing temperature, the Gaussian function with variance of 30 leads to a weighted mixture between all of the used reference models. This means that even at the reference temperatures, where data for a more precise reference null space exists, an interpolated reference null space is used, which is affected by the other reference null spaces. This leads to some bias and as a result to higher test values of the hypothesis test. However, in the damaged case this effect persists, and damages still can be detected reliably.

It could be confirmed that the usage of bell-shaped functions centered at the testing temperature is adequate, if the temperature effects can be assumed to be approximately linear for each section. However, the choice of the variance of these weighting functions is quite important as Fig. 6.7 shows. If a sharp weighting function is used ($\sigma^2 = 10$) in Fig. 6.7 (top) the test values at the reference temperatures are much lower than at the temperatures in between, since in the latter case two local models are considered

for the interpolation, while at the reference temperatures only the local model from the reference temperature itself is taken into account. This holds for the test values in the undamaged as well as in the damaged case. When a wide interpolation function is chosen (bottom), this leads to results that are similar to the averaging approach in Fig. 6.5. The undamaged structure at temperatures different from the reference temperatures is falsely classified as damaged. In the damaged case the test values increase. In the present case the interpolation worked well with a function with $\sigma^2 = 30$ variance (Fig. 6.6) and it is recommended not to use weighting functions that neglect nearby local models, even if a good local model is known from existing reference data. In this case the test values for testing temperatures different from the reference ones would be higher and lead to more false alarms.

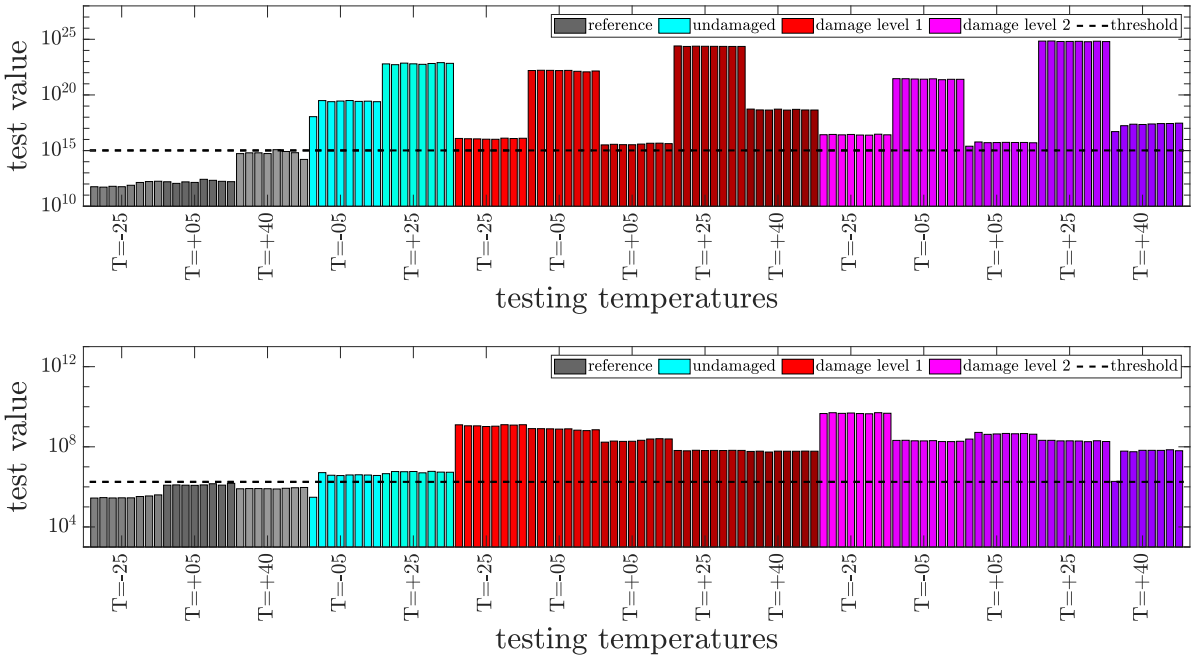

Figure 6.7 – Effect of weighting function in interpolated reference null space and covariance matrix. Sharp weighting function (top) and wide weighting function (bottom). Test values at different testing temperatures in the undamaged and damaged states. Reference data at -25°C, 5°C, and 40°C.

6.4 Summary

In this chapter a first test of the robust methods from chapter 4 on real data has been performed. Experimental data from a concrete beam tested in a climate chamber at five different temperatures and three different system states has been used. With the goal to provide a data-driven damage detection procedure strategy 1 from chapter 4 based on direct Hankel matrix interpolation (4.13) has been applied together with a non-parametric test procedure. The residual covariance was derived once in the reference state from the interpolated covariance from (4.22) with $\underline{\Sigma}_1 = 0$.

The results correspond to the findings in the numerical study in section 4.3. It could be shown that the interpolation approach is able to distinguish between damaged and undamaged states reliably, and false alarms can be avoided, while previous methods fail to classify the undamaged state correctly when the testing temperature is different from the temperatures for which reference data is available. Some suggestions were made regarding the choice of an adequate weighting function.

6.5 Dissemination

Parts of this chapter have been published in

[Vie+21] E. Viefhues, M. Döhler, P. Simon, R. Herrmann, F. Hille, and L. Mevel. « Stochastic subspace-based damage detection of a temperature affected beam structure ». In: *Proceedings of SHMII-10 2021 - 10th International Conference on Structural Health Monitoring of Intelligent Infrastructure*. Porto, Portugal, 2021, pp. 1–6

Chapter 7

Damage detection of a testing bridge exposed to ambient temperature variations

7.1 Introduction

An approach for the stochastic subspace-based damaged detection that is robust to changes in environmental conditions of a mechanical structure was derived in chapter 4. The environmental effects are considered as external parameters, e.g. temperature, affecting the dynamical behavior of the structure. In the method a reference null space is derived that is adapted for the parameter in the testing state. In a numerical study the developed damage detection tests were proven to be robust to such parameter changes and led to meaningful global thresholds allowing for sensitive damage detection.

A first application to real data is described in chapter 6, where the algorithms of strategy 1 from chapter 4 are used with data of a laboratory structure tested in a climate chamber under defined conditions. In this chapter the robust approaches are applied to data from a testing bridge located on an outdoor testing field that is exposed to real environmental conditions. All strategies from chapter 4 are used, and it will be shown that the test with a temperature adapted reference null space also performs well for data under more realistic and less controllable conditions.

In the following, the experimental setup and the dynamical properties of the testing bridge are presented. Then, the three strategies for damage detection robust to temperature variations from chapter 4 are applied to the experimental data. The test robustness is evaluated similarly to section 4.3 in several reference setups and compared to previous temperature rejection approaches.

7.2 Experimental setup and dynamical properties of the structure

Within this thesis and related to an interdisciplinary project in the Federal Institute of Materials Research and Testing Germany (BAM) a multi-sensor equipped testing bridge with variable pre-stessing is designed and constructed. The 24 m long concrete structure, displayed in Fig. 7.1, is built on an outside testing field of BAM. Its purpose is to provide data for this work and for future research on developments and applications of SHM strategies and new testing hardware [Ung+17; LMK18; ZU18; Pir+19; Lia+21]. Data can be generated under near-realistic environmental conditions, and the system state can be varied well defined and reversibly.

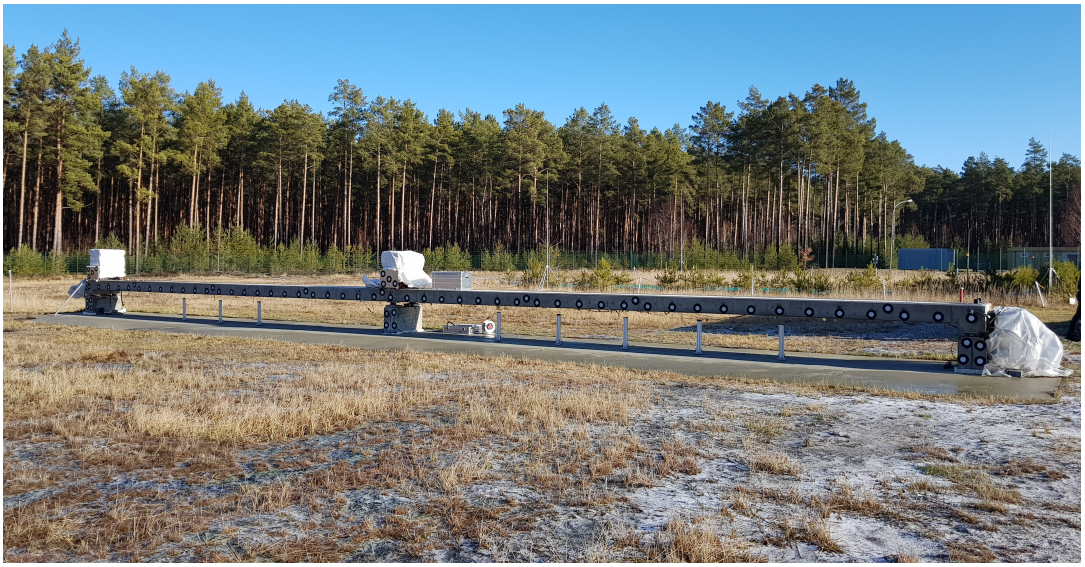

Figure 7.1 – Testing bridge.

The bridge is designed as a two-span girder with 12 m span each supported with floating bearings at two points in each of the three axis as detailed in Fig. 7.2. The U-shaped cross-section is 90 cm wide and 30 cm high with 15 cm top thickness. The ratio of static height to length is chosen such that eigenfrequencies are obtained similar to those from realistic civil engineering structures and the resulting structural mass and damping allow for artificial and environmental excitation. Two external tendons are located between the flanges of the cross-section allowing for variations of the pre-stressing between 0 and 1200 kN. The pre-stressing load is applied at the beginning and at the end of the bridge (Fig. 7.3, left).

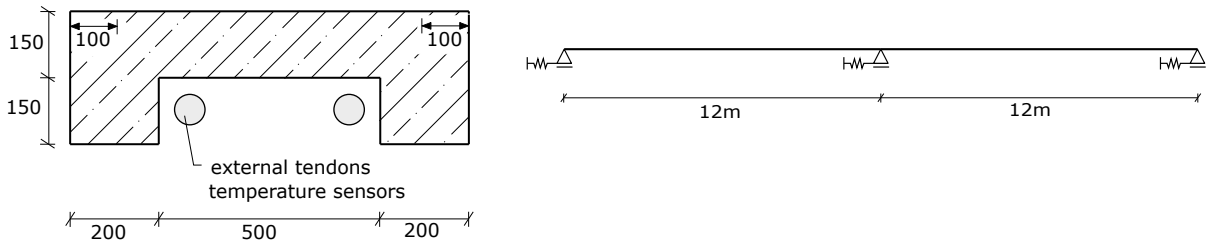

Figure 7.2 – Static system of the testing bridge.

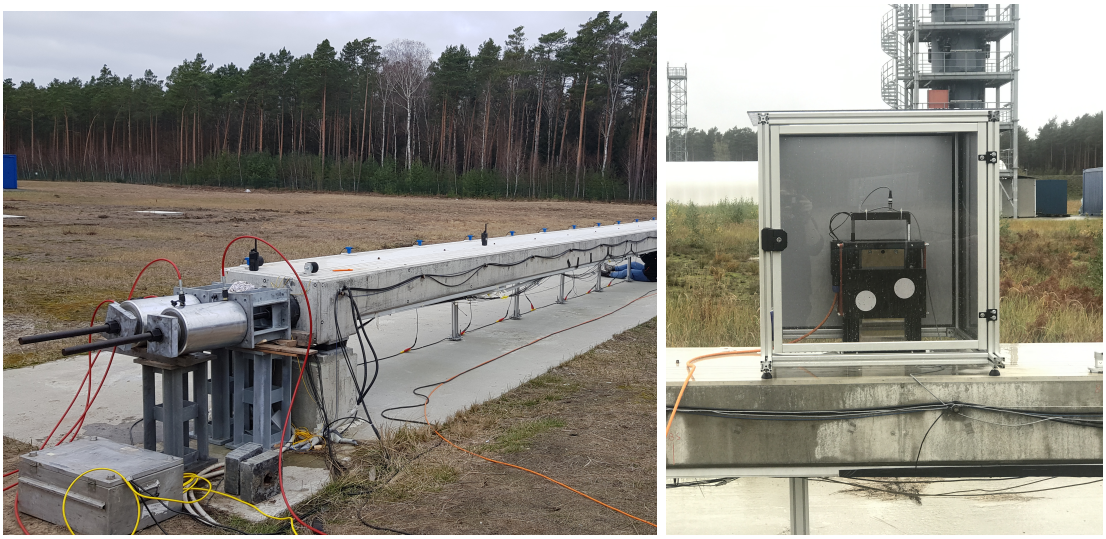

Figure 7.3 – Pre-stressing facility (left) and encased shaker (right).

For the evaluation of the temperature rejection approach vibration data is recorded for 14 days while the structure is excited by an 80 kg shaker with white noise signal between 2 and 80 Hz for 10 minutes every half hour. The shaker is encased to be protected from direct sun and water (Fig. 7.3, right). It is located at 7.8 m from the beginning of the bridge with an eccentric position as shown in Fig. 7.4. The data is recorded with 5 geophones located at an eccentric axis (y1 in Fig. 7.4) and one additional geophone at axis y2 to cover torsional effects sampled at a frequency of 1200 Hz.

Three embedded and one external temperature sensors enable the monitoring of the temperature conditions. The positions of the embedded sensors are seen in Fig. 7.4. They are located in the middle span of the bridge. A linear temperature variation over the cross section is observed. However, the structural temperature during this experiment is derived with respect to the central sensor without detailed consideration of positive or negative temperature gradients along the cross-section. Structural temperatures between 8°C and

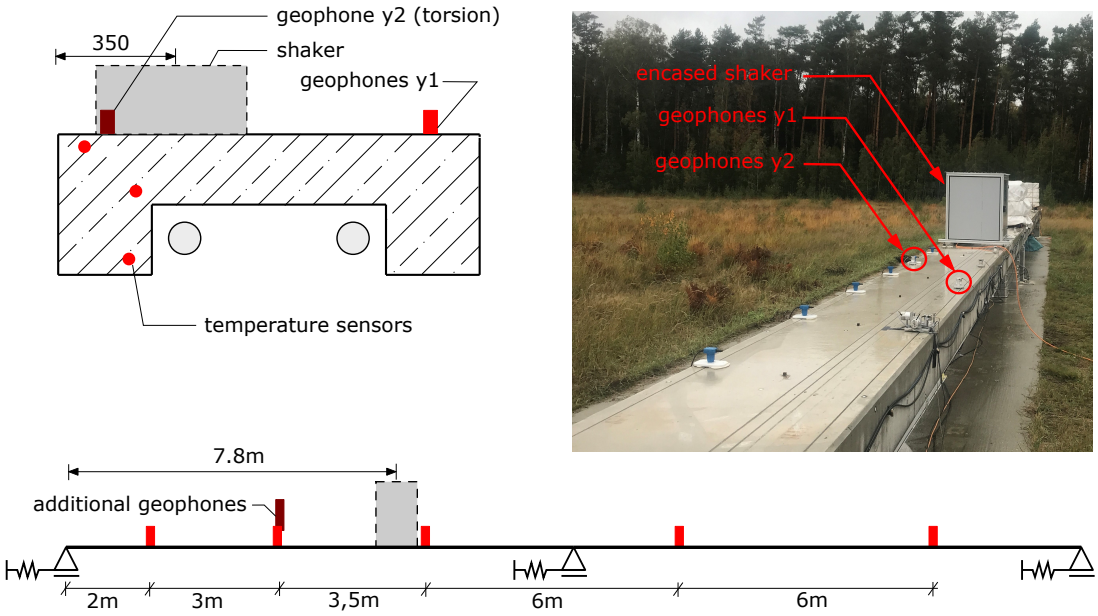

Figure 7.4 – Test setup testing bridge with geophones and shaker for excitation.

24°C are measured.

Before the experiment started, the test specimen has been pre-loaded with a four tons weighting shifted over the bridge from on side to the other, such that in the case of no pre-stressing the section is cracked significantly. During the experiment the pre-stressing was set to 450 kN from day 1 to day 7 and then lowered to 250 kN.

The dynamical properties of the bridge are identified with a covariance-driven SSI algorithm with data sampled down to 40 Hz and filtered between 1 and 20 Hz. Fig. 7.5 (left) exemplarily shows the stabilization diagram of one data set at 15°C with pre-stressing of 450 kN. The first three modes can be identified clearly from each considered data set. The identification of the fourth mode is afflicted with more uncertainties as marked by the horizontal bars at the identified modes in the stabilization diagram. The frequencies at 15°C are summarized in Tab. 7.1 together with the damping ratios. The respective modeshapes at 15°C are presented in Fig. 7.6. They are in accordance to the expected first four modeshapes of a two-span beam including some torsional effects in the first mode (blue dot).

Decreasing the pre-stressing load to 250 kN leads to changes in the frequencies of about 12%, which increases the effect of the temperature, significantly. A smaller effect due to pre-stressing release to the dynamical properties was expected from results of previous tests. Those were performed before the pre-stressing of the structure has been

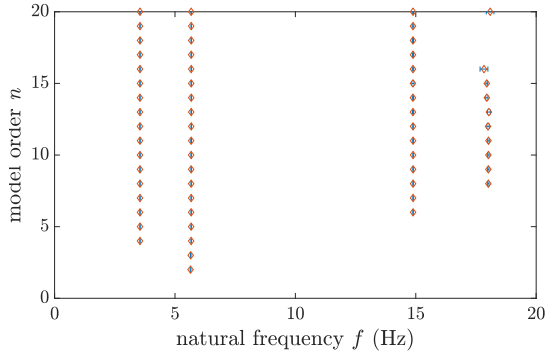

Figure 7.5 – Stabilization diagram at 15°C.

frequency	damping ratio
3.54 Hz	1.39 %
5.67 Hz	1.04 %
14.88 Hz	0.90 %
17.73 Hz	2.39 %

Table 7.1 – Frequencies and damping ratios at 15°C.

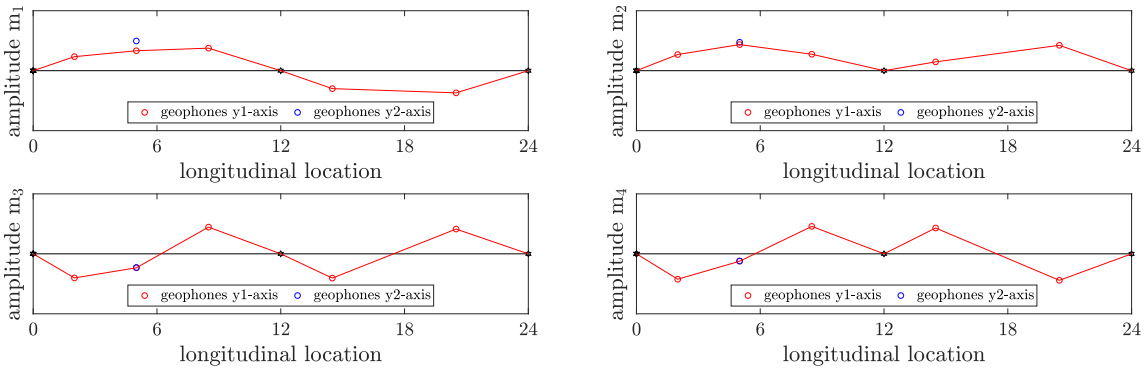

Figure 7.6 – First four modeshapes of the testing bridge.

fully released to 0 kN and the load of four tons has been applied, while the present experiments are made after this full release. This must be kept in mind when performing the damage detection and evaluating the test regarding its sensitivity.

The temperature effect to the dynamical properties of the structure can be derived from Fig. 7.7, where the fourth mode shows no clear dependence on the temperature.

7.3 Damage detection with temperature effects

7.3.1 General settings and temperature effect

The damage detection with the roust methods from chapter 4 is evaluated with the experimental data sampled down to 40 Hz and filtered between 1 Hz and 20 Hz. Only data is used that is recorded with activated shaker yielding data sets of 10 minutes length at several temperatures. The first half of these data sets is considered for the reference

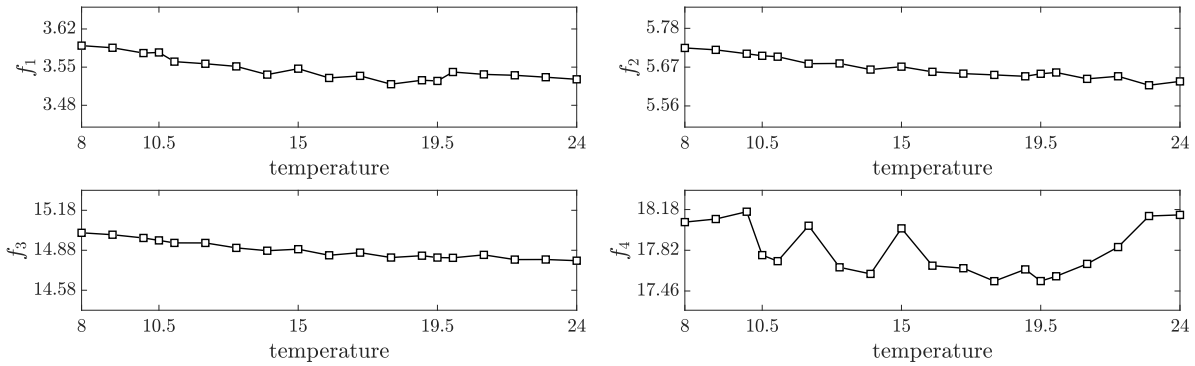

Figure 7.7 – Temperature effect to the first four eigenfrequencies of the testing bridge.

data, the second part is used for testing.

From the reference data the reference matrix S and the residual covariance from (4.22) are computed. The damage detection is processed with five data sets of 50 seconds length at $T = [8, 9, ..., 24]$°C and additionally at 10.5°C and 19.5°C.

For the interpolation method weights are computed from a Gaussian function with variance of $\sigma^2 = 64$ centered at the testing temperature. To improve the results at the borders, virtual reference points are used that are extrapolated from the two nearest reference points assuming a linear relationship. When the reference matrix S is computed from the observability matrix, the first four modes as identified in the previous section are used as system parameter θ_j^* in (4.16) or (4.17).

Two system states are considered: One system with pre-stressing load of 450 kN, referred to as undamaged and a damaged system with the pre-stressing load decreased to 250 kN. A threshold for damage detection is computed from the data in the undamaged state at the reference temperatures allowing for 0.1% false alarms.

When the standard damage detection test setup e.g. from (3.2) is applied that uses reference data from only one fix reference temperature at $T = 15$°C for the computation of the reference matrix and the covariance the test values in Fig. 7.8 are obtained at different testing temperatures. When the testing temperature is different from 15°C the test values are significantly larger than those at the reference temperature. Hence, setting up an empirical threshold with the test values at the reference temperature leads to false alarms at any other testing temperature for the undamaged structure. This is in accordance to Fig. 4.3 for the numerical simulation data. Due to the high impact of the changes in the pre-stressing on the dynamical properties the test values in the damaged state are very large and from the experimental data no conclusions can be drawn for the sensitivity

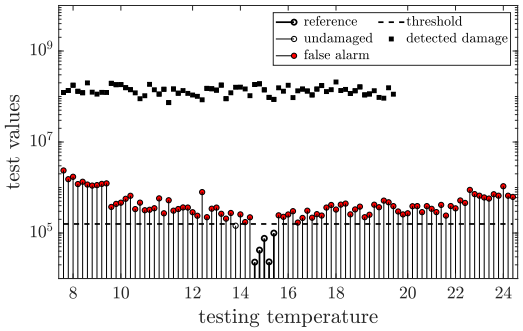

Figure 7.8 – Test values with reference data from one fixed reference temperature.

of the robust damage detection. In the following the robust damage detection test from chapter 4 is applied and compared to results from the average approach from [Bal+08a].

7.3.2 Robust damage detection

First, a reference setup denoted by "A" is designed that is based on five data sets at the reference temperatures $T_1 = 8°C$, $T_2 = 10.5°C$, $T_3 = 15°C$, $T_4 = 19.5°C$, and $T_5 = 24°C$. Fig. 7.9 presents the test values in the undamaged and the damaged state when the three strategies robust to temperature changes and an averaged reference matrix S are used. The test values at the reference temperatures in the reference state are bold plotted. The horizontal dashed line denotes the empirical threshold for damage detection leading to a red dotted false alarm if it is exceeded.

In the undamaged state at the reference temperatures, the test values of the three interpolation versions follow a flat curve. This is in accordance to the numerical results in Fig. 4.5. While again the test values of the S(H)-version show some variation due to inaccuracies in the interpolation of the Hankel matrix, the test values computed from a observability matrix based null space are very stable. The thresholds, which are based on values at the reference temperatures, are at a similar range for each testing procedure. Very few false alarms occur. Thus, compared to the numerical study, the more realistic temperature and noise effects, confirm or even increase the robustness of the interpolation approach towards false alarms in the undamaged state.

In contrary, the values computed with the average method are affected by temperature, even when testing at the reference temperatures. This effect was already observed (more clear) with the numerical data (Fig. 4.4). At testing temperatures between the reference points the test values show high variance and despite the high threshold, many false

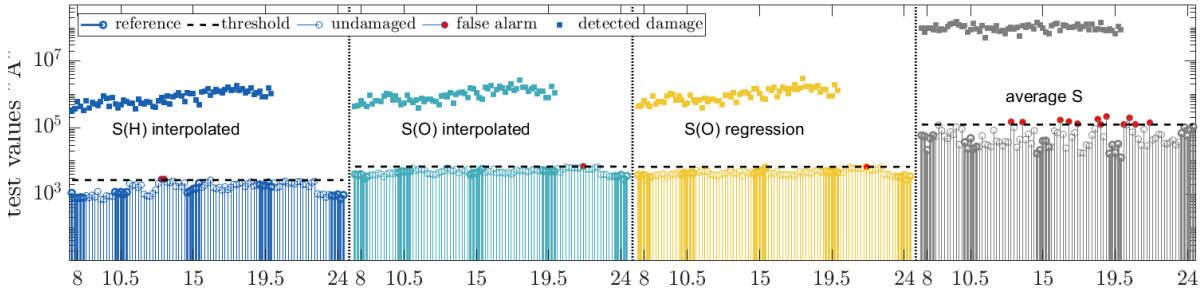

Figure 7.9 – Test values of the 4 algorithms for different testing temperatures in the undamaged and the damaged case, computed for reference setup A.

setup name	reference T
A	[8.0 10.5 15.0 19.5 24.0]
B	[10.5 15.0 19.5]
C	[8.0 15.0 24.0]
D	[10.5 19.5]
E	[8.0 24.0]

Table 7.2 – Reference setups for testing bridge

alarms occur.

With all algorithms damage can be detected clearly at any testing temperature and the ratios of threshold to test value in the damaged state are in a similar range. However, due to the high effect of the pre-stressing change to the dynamical system no more conclusion can be drawn regarding the sensitivity of the tests. In the following, the test performance is evaluated in the reference state and through the probability of false alarms (PFA).

7.3.3 Effect of reference setup

The previous results revealed the capability of the interpolation method being very robust towards false alarms, due to the computation of a very well fitting reference null space and covariance for the testing temperature. This motivates for deeper analysis of the effect of different reference setups within the temperature rejection methods.

Four additional reference setups are evaluated with the three algorithms robust to temperature changes and the average approach considering different combinations of reference temperatures as summarized in table 7.2. Fig. 7.10 shows the test values for the reference setups “B“ to “E“.

Comparing scenario “A“ and “B“, the robustness of the new temperature rejection approach is not affected obviously. In both setups the distance between the reference

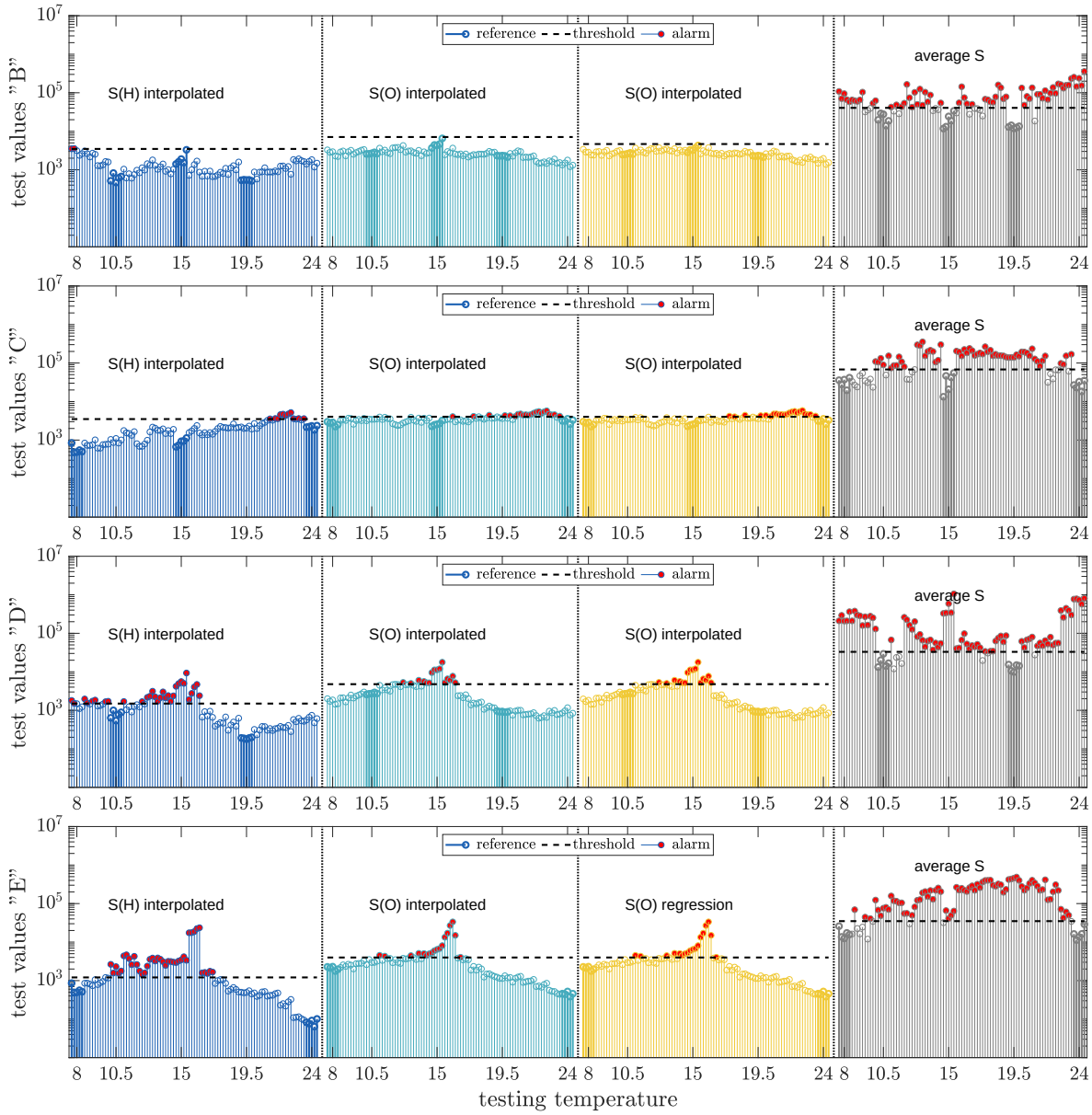

Figure 7.10 – Test values of the 4 algorithms for different testing temperatures in the undamaged case, computed for reference setup B, C, D and E from top to bottom.

temperatures is 4.5°C, but in "B" only the central reference temperatures are taken into account in the reference state although testing temperatures outside the reference temperature range occur. With the interpolation approach this is an extrapolation task, which is handled by the weightings for the considered reference points, similar to the interpolation between two reference points. Especially the algorithms using the observability matrix computed from the eigenstructure show very stable test values, due to a good interpola-

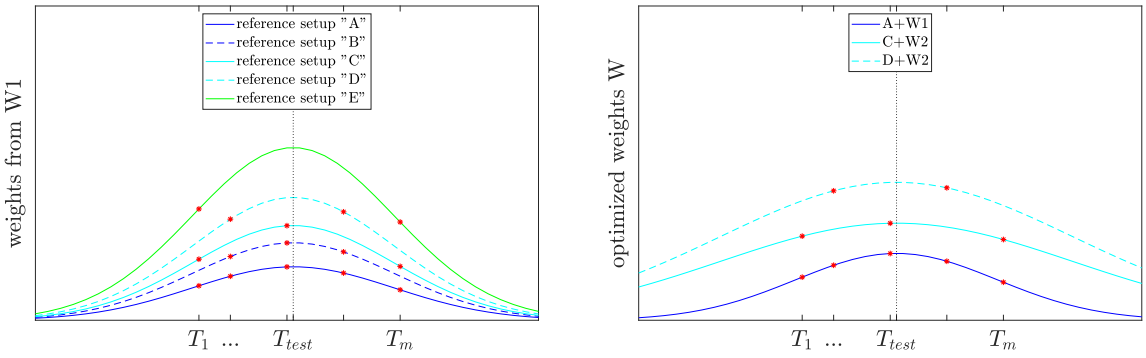

Figure 7.11 – Weights for different reference setups with weighting function W1 (left) and with optimized weighting functions (right).

tion of the reference null space. With the average method the variation in the test values increases, in particular at testing temperatures differing from the reference temperatures.

In the setups “C“, “D“ and “E“ the PFA of the new algorithms with temperature adapted reference null space increases. This is due to the change of the distance between the reference temperatures in these scenarios. In setup “A“ and “B“ the reference null space and the covariance are very well interpolated with the chosen weights. In both cases the distance between the reference temperatures is about 4.5°C. In the remaining variants the ΔT is about 9°C and 16°C, while the weighting functions are not modified with respect to this change. Consequently, the chosen weights do not cover the qualitative temperature depending behavior of the structure in these cases. However, the false alarms with the average method exceed by far the PFA of the interpolation method.

In an optimization step for the reference setups “C“ to “E“ modified weighting functions are used that are shown in Fig. 7.11. In the left plot the weights are shown that are generated with the initial weighting function. With respect to the bigger distance ΔT between the reference temperatures in these setups a wider weighting function is designed with an increased $\sigma^2 = 196$ (right). This ensures that not mainly one reference point but several points are considered for the computation of the reference matrix and the residual covariance, and that the nearby reference points are weighted similarly. Notice that if in the limit an extremely wide weighting function is used, the results with the interpolated Hankel matrix will become similar to the results from the average approach.

The effect of the optimized weights can be seen from the PFA in Fig. 7.12. For scenario “C“ the temperature adapted reference matrices can be optimized in each strategy by the choice of a proper weighting function reflecting the temperature behavior of the structure

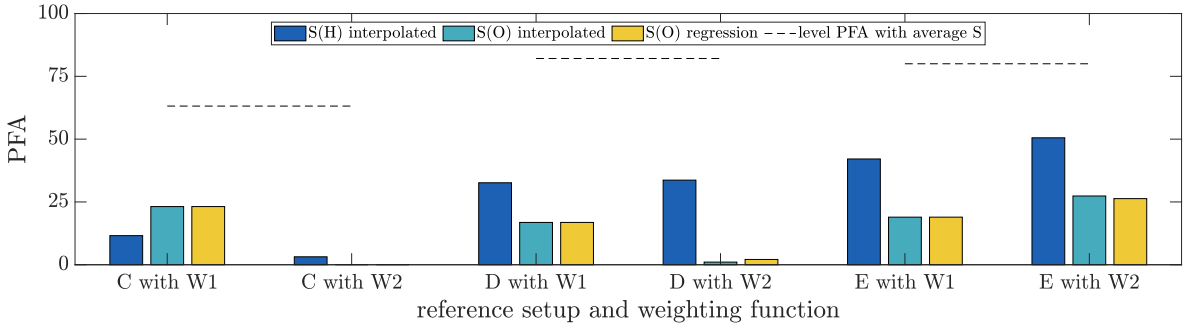

Figure 7.12 – Effect of optimized weighting function to false positives for the interpolation approach in reference setups C, D, and E.

with respect to the reference systems. Notice that the improvement of the algorithm using the observability matrix with regression analysis for the eigenstructure is due to a different weighting of the covariance matrices for the interpolated covariance. In setup “D“ significant improvement of the interpolation of the observability matrix can be reached by a wider weighting function, while for the interpolation of the Hankel matrix information from only two reference points is too low. In scenario “E“ false alarms cannot be avoided by changing the weighting function, as the distance between the reference points is very far and only two reference points are available.

7.4 Summary

In this chapter the temperature rejection approaches from chapter 4 for subspace-based damage detection were applied to experimental data from a testing bridge that is exposed to environmental conditions. Experiments have been carried out recording data for 14 days providing measurements at temperatures between 8 and 24°C.

The application showed that the new method with the temperature adapted reference matrices provide robust algorithms with significant reduced false alarm rate when compared to other approaches. In particular when reference data is available at a temperature range and the structure is tested at a temperature outside of this range this can be solved properly with the proposed method with extrapolation from the reference points.

The effect of the weighting function design has been analyzed and it could be shown that the test performance can be improved by choosing a weighting function that is adapted to the reference setup and the temperature depending behavior.

Compared to results in the numerical study in section 4.3 with the more realistic data

providing a more realistic effect of the temperatures to the dynamics of the structure the new algorithms perform better and an optimization of the weighting function for the interpolation succeeds.

7.5 Dissemination

Parts of this chapter are in preparation for submission to "Mechanical System and Signal Processing".

Conclusion

Considered aspects

In vibration-based damage detection in engineering structures automated, data-driven methods are particularly of interest. In the context of the present thesis developments were made that aim at higher robustness and sensitivity of such methods for application on engineering structures.

The developments are based on the covariance-driven stochastic subspace-based damage detection (SSDD) method. In this method the damage indicator is derived from a residual related to output data covariances. The statistical properties of the damage indicator can be described precisely for the reference and the testing system state when the statistical properties of the residual are known. Previously, uncertainties of the testing data are considered in the SSDD, but it was assumed that the reference is perfectly known without uncertainties. This is true in ideal cases but does not hold in real world applications, since the reference usually is estimated from data and thus contains considerable uncertainties. The resulting test behaves unpredictable. Furthermore, environmental variability perturbs the damage detection with SSDD, similar to many other approaches, since the residual is sensitive to those changes, too. This has motivated a robust approach for the method.

The developments within the thesis accounted for the following aspects of robust vibration-based damage detection with the SSDD method:

- consideration of all uncertainties of the residual in statistical evaluation for damage detection,
- robustness to environmental variability without explicit temperature model.

Summary, improvements and limits

(1) Damage detection with uncertain reference Damage detection methods that derive reference models of a system from data are in particular appealing for automated applications. This is the case in the SSDD, but so far the uncertainties related to those

estimated reference models have not been considered in the tests leading to inherent bias and unpredictable test behavior.

In the context of this thesis this gap was closed. The covariance evaluation of the residual was carried out considering uncertainties related to the testing data and the estimated reference. Its distribution properties were evaluated on the basis of the local approach [BBM87]. A general formulation was derived that also applies when the data length in the reference state is different from the length in the testing state. The associated hypothesis test has been formulated in a parametric and a non-parametric version and its statistical properties have been derived from the distribution properties of the residual. Considering the test statistics as damage indicator, the impact of the new developed residual is not only academic. The crucial part of defining a threshold between healthy and damaged state now can be done apriori based on theoretical considerations without extensive empirical studies on reference data.

The test behavior and thereby the distribution properties of the new residual have been validated on numerical simulation data of a simple structure. The test showed very good accordance to the theoretical predicted behavior and the results were independent from data lengths in the reference and the testing state, system parametrization, and reference computation method. It was also demonstrated that neglecting the uncertainty of the reference null space leads to an inherent bias in the residual, which is eliminated with the new formulation resulting in a damage detection test with significant higher sensitivity.

The new test has been applied to experimental data of a steel frame structure. The results correspond to those evaluated on numerical data, and it could be shown that an upper bound for the threshold can be found apriori from a theoretical value. Furthermore, the covariance computation related to the reference data is also part of the second contribution on robustness to changing external parameters with further application.

From these developments the practical applications could be improved as follows:

- The behavior of the new test is predictable and independent from data length and null space computation procedure.
- A damage detection threshold can be defined apriori.
- The approach is also suitable when only relatively few data is available in the reference state.
- The damage detection is more sensitive due to avoided bias in the residual.

Some limitations can be defined as follows:

- Careful estimation of the data covariance matrix is required, since its quality affects the uncertainty quantification of the residual.
- When the non-parametric test is applied only an upper bound for the threshold can be computed, since a theoretical rank of the (estimated) covariance matrix cannot be determined.

(2) Damage detection under changing environmental parameters Damage detection of structures exposed to environmental variability often fails, since the environmental effects lead to changes of the dynamical system similar to damage effects.

In this thesis, an approach has been derived for robustness of the SSDD to environmental changes. The procedure is inspired by a model interpolation approach formulated for a state-space representation from [Zha18] postulating an engineering structure under environmental changes as a linear parameter varying system with linear time-invariant behavior at fixed parameter points. Assuming reference data at a few reference parameter points, a parameter adapted reference null space has been derived using three different strategies: two interpolation methods for either the covariance Hankel matrix or the modal parameters and an approach using regression analysis of the modal parameters. The parameter adapted null space is computed in the testing state for the particular testing parameter value and then used in the residual definition of the SSDD. The uncertainties of the interpolated reference null space have been quantified and it was shown how to compute them directly from the interpolated covariance matrices of either the Hankel matrix or the modal parameters, depending on the chosen strategy.

The developed strategies have been validated on numerical data of a simple structure with a non-linear parameter depending behavior and compared to an existing approach from [Bal+08b] using an average procedure, where, however, the actual temperature is not needed to be known. It could be shown that the new approach is much more sensitive to damage, while false alarms due to changes in the environmental conditions could be mostly avoided. Considerations of different reference setups, i.e. different number and distances of reference parameter values, illustrated the strengths and weaknesses of the developed strategies. Robust results could be achieved even when the testing data is recorded under a parameter outside of the reference parameter interval or when changes in the excitation covariance are supposed. Again, considering the uncertainties of the reference improves the test results significantly.

The developed approaches were applied to experimental data from a concrete beam

in a climate chamber, as well as to data from a testing bridge. This testing bridge was constructed within this thesis and related to an interdisciplinary project at BAM. It is subjected to natural daily temperature variations. The bridge is equipped with several sensor types and provides the possibility to activate and deactivate two external prestressing tendons for the simulation of different structural states. The experimental results from the developed approach showed similar robustness to temperature variations as the numerical study.

From these contribution the following improvements for practical applications can be concluded:

- The robust approach is widely insensitive to changing external parameters without requiring explicit parameter model formulation.
- The approach works with reference data sets from only few parameter working points and even succeeds under parameters outside of the reference parameter interval.
- The rate of false alarms under changing external parameters is reduced compared to previous approaches.
- The approach is more sensitive to damage under changing external parameters than previous approaches.
- The approaches are validated under near-realistic conditions.

The following weakness of the approach can be stated:

- The definition of the interpolation function in accordance to the available reference setup may be a critical task. However, an individual reference design for the investigated structure and its qualitative parameter depending behavior can optimize the damage detection performance.

Outlook

It was in the scope of this thesis to contribute to automated damage detection methods with regard to the special requirements of engineering structures. The methods were derived theoretically and were validated on numerical and experimental data. While the developed methods have improved robustness for real-world applications, they also arise further research questions.

For practical applications it would be important to investigate in more detail the estimation of the residual covariance matrix. In the present applications to experimental

data this was always a critical task, since the covariance estimation from relatively few data blocks in comparison to the residual dimension may be challenging and can lead to numerical problems in its inversion for the statistical test. This is also important when the threshold of the non-parametric test should be derived from the (theoretical) rank of the residual covariance matrix. Another subject that should be addressed is the further investigation of the effect of the weighting functions for robustness to environmental variation and their optimal choice. In this context also applications for multivariate dependencies should be considered. This is a structure-depending task and thus data from various, more complex structures would be desirable. Moreover, the validation on data that was recorded under realistic conditions, i.e. traffic and wind, long term monitoring etc., should be performed in the next steps.

From a technical point of view the residual covariance related to the parameter adapted null space corresponding to the regression approach should be derived and evaluated with respect to the interpolation approaches. Furthermore, the developed strategies for damage detection under environmental variation should be extended to damage localization and quantification [DMZ16], as well as to rigorous evaluation of the methods' sensitivity to damage [MDV21], to provide solutions for the further steps in the damage diagnosis. This requires the derivation of a parametric version of the robust approach with the need of corresponding, parameter dependent sensitivities.

Resume in French

Introduction

Contexte

La recherche sur les méthodes automatisées de diagnostic d'endommagements basées sur les mesures vibratoires pour la surveillance de l'intégrité des ouvrages d'art (Structural Health Monitoring, SHM) a pris de l'ampleur au cours des dernières décennies, car de nombreuses structures ont atteint la fin de leur cycle de vie et se détériorent. Ces méthodes sont basées sur le fait que le comportement dynamique d'une structure peut être modifié par un ou des endommagements. Elles comparent les données mesurées dans un état de référence (sain) à celles de l'état actuel.

Des conditions particulières doivent être prises en compte pour l'application des méthodes de SHM aux ouvrages d'art : Comme l'excitation de la structure n'est généralement pas mesurée, les méthodes basées uniquement sur l'excitation ambiante sont particulièrement intéressantes. De plus, les caractéristiques calculées à partir de données mesurées ont une variabilité statistique intrinsèque, qui doit être prise en compte avant de décider si un changement dans une feature ou un paramètre est significatif, indiquant un endommagement. Lorsque des changements significatifs sont détectés, il faut distinguer entre les changements dus à des endommagements et ceux dus à la variabilité des conditions environnementales afin d'éviter les fausses alertes. Ces problématiques pour le traitement robuste des données sont au coeur de cette thèse, basée sur la méthodologie suivante.

Méthodologie

La méthode de détection stochastique des endommagements basée sur le sous-espace (SSDD) présentée dans [BAB00] s'applique aux mesures de sortie d'un système dynamique, représenté par un modèle d'espace d'état. Dans un résidu, le noyau gauche d'une matrice de Hankel construite à partir des covariances de mesures dans l'état de référence est confrontée à la matrice de Hankel calculée à partir de données du système actuel. Dans un test d'hypothèse le résidu est évalué statistiquement en tenant compte des

incertitudes des données dans l'état actuel dues aux bruits (excitations inconnues, bruits de mesure) par le biais de la matrice de covariance du résidu. Ainsi, les propriétés statistiques du test de détection d'endommagements peuvent être caractérisées précisément dans les conditions saines et endommagées d'une structure.

Contributions

La méthode SSDD existante jusqu'à présent ne répond pas à certaines exigences fondamentales concernant le traitement des incertitudes liées aux données de référence, ainsi que la prise en compte des changements dans les variables environnementales qui peuvent perturber la détection des endommagements. La contribution de cette thèse à ces problématiques peut être résumée comme suit :

(1) Détection d'endommagements avec incertitudes dans la référence Les algorithmes existants considèrent seulement les incertitudes du résidu qui sont liées aux données de test dans l'état actuel, et il est supposé que la référence est parfaitement connue. C'est vrai dans des cas académiques idéalisés, mais dans les applications réelles la référence est généralement estimée à partir de données et peut donc contenir des incertitudes considérables. Par conséquent, avec l'approche existante, les propriétés statistiques du résidu ne correspondent pas aux propriétés théoriques attendues. Le comportement du test devient imprévisible et les seuils pour la décision doivent être fixés empiriquement à partir d'études sur les données de référence. Pour lever ce verrou, les propriétés statistiques théoriques du résidu sont dérivées, conduisant au calcul de la covariance du résidu qui tient compte à la fois des incertitudes liées aux données de référence et de test. Le test d'hypothèse associé montre une très bonne conformité avec le comportement théorique attendu. Avec la nouvelle évaluation du résidu, un seuil peut maintenant être établi a priori basé sur la théorie, sans études empiriques approfondies sur les données de référence. De plus, le nouveau calcul améliore la sensibilité de test aux petits endommagements.

(2) Détection d'endommagements sous changements de paramètres environnementaux De nombreuses méthodes automatisées de détection d'endommagements basées sur les vibrations échouent en raison de la variabilité des conditions environnementales, car elles peuvent affecter le comportement dynamique des structures d'une manière similaire aux endommagements [Soh07]. Pour la SSDD, seuls quelques travaux ont été réalisés sur la robustesse aux changements des paramètres environnementaux tels que

la température. Toutes ces approches sont basées sur des études empiriques et ne sont pas optimales lorsque la température dans l'état actuel est différente de la température moyenne des ensembles de données de référence, ou bien elles nécessitent des ensembles de données de référence pour autant de scénarios de température que possible. Dans cette thèse, une approche robuste est dérivée qui s'inspire d'une approche d'interpolation de modèle. Des stratégies d'interpolation ou d'analyse de régression sont proposées pour calculer un noyau de référence adapté à la valeur du paramètre environnemental actuel, et ceci à partir de données dans l'état non endommagé à seulement quelques valeurs de paramètres environnementaux de référence. Le test de détection d'endommagements est développé en tenant compte des incertitudes liées au noyau de référence qui est basé sur l'interpolation ou la régression. Le test résultant s'avère être robuste et toujours sensible aux dommages. Pour la validation expérimentale, un pont d'essai équipé de plusieurs capteurs est construit dans le cadre de cette thèse sur un champ d'essai extérieur de l'Institut fédéral allemand de recherche et d'essai des matériaux (BAM).

Chapitre 1 – État de l'art

Habituellement, la détection d'endommagements est considérée comme un processus triple, comprenant l'extraction d'un résidu sensible aux endommagements à partir des données, la comparaison du résidu dans l'état de référence et l'état actuel, et enfin l'évaluation (statistique) de cette comparaison. Les concepts existants pour l'extraction des résidus utilisent des informations provenant des différentes étapes de la procédure d'identification du système et peuvent être classés en approches basées sur les paramètres modaux (par exemple, les fréquences et les déformées modales) et les paramètres associés, sur les paramètres des modèles de séries temporelles ou les caractéristiques dans le domaine fréquentiel, ou sur le signal ou les fonctions de traitement du signal. Les stratégies d'évaluation existantes vont des méthodes graphiques, telles que les cartes de contrôle, aux méthodes statistiques, telles que l'analyse des outliers ou les tests d'hypothèse, ces dernières permettant de prendre en compte mathématiquement les incertitudes intrinsèques des résidus (voir Fig. 1.2).

Les méthodes automatisées de détection d'endommagements par vibration qui sont robustes aux changements des conditions environnementales prennent en compte les paramètres environnementaux mesurés, par exemple en utilisant des approches de régression ou d'interpolation ou des méthodes de classification ; soit elles omettent la prise en compte

explicite des paramètres environnementaux en utilisant des résidus et des indicateurs d'endommagements robustes, ou des modèles de conditions normales de grande taille, représentant l'influence des paramètres sur les résidus sensibles aux endommagements.

Chapitre 2 – Contexte des méthodes

Les développements de cette thèse sont basés sur la détection stochastique des endommagements basée sur le sous-espace (SSDD) [BAB00; DMH14]. Cette méthode est basées sur les propriétés des l'identification sous-espace stochastique (SSI) basée sur les covariance des données, à l'issue d'un modèle d'espace d'état représentant une structure mécanique linéaire invariante dans le temps (LTI). Le résidu utilise des matrices de Hankel contenant des covariances des mesures et est défini comme le produit du noyau gauche de la matrice de Hankel dans l'état de référence S et de la matrice de Hankel estimée à partir d'un ensemble de données de mesure actuelles de longueur N dans l'état actuel $\widehat{\mathcal{H}}$ par

$$\zeta \stackrel{\text{def}}{=} \sqrt{N}\,\mathrm{vec}(S^T\widehat{\mathcal{H}}).$$

Sa distribution asymptotique est Gaussienne, avec une moyenne nulle dans l'état sain et une moyenne différente de zéro dans l'état endommagé. Son évaluation statistique dans un test d'hypothèse donne une statistique de test de détection des endommagements, dont la distribution asymptotique est χ^2, prenant en compte les incertitudes du résidu liées aux données de test par la covariance du résidu Σ_ζ. Le teste s'écrit

$$t = \zeta^T\Sigma_\zeta^{-1}\mathcal{J}_\zeta\left(\mathcal{J}_\zeta^T\Sigma_\zeta^{-1}\mathcal{J}_\zeta\right)^{-1}\mathcal{J}_\zeta^T\Sigma_\zeta^{-1}\zeta.$$

$\mathcal{J}_\zeta$ est la sensibilité asymptotique du résidu par rapport aux paramètres du système dans l'état de référence. La covariance du résidu a un impact significatif sur la sensibilité du test. Son calcul est basé sur la covariance empirique de la covariance des sorties du système.

Chapitre 3 – Détection d'endommagements par méthodes sous-espaces tenant compte des incertitudes dans le noyau de référence

Jusqu'à présent, la covariance du résidu de la SSDD est dérivée à partir de l'incertitude de la matrice de Hankel, où le noyau gauche de de référence est supposé être parfaitement connu sans aucune contribution à l'incertitude du résidu. Ceci est vrai dans des cas idéaux, alors que dans les applications du monde réel, la référence S est généralement estimée à partir de données. Négliger ses incertitudes dans la covariance du résidu a pour conséquence que le test ne suit plus sa distribution théoriquement attendue de χ^2. Cela devient particulièrement pertinent pour l'application en pratique lorsque peu de données du système de référence sont disponible, ne permettant pas le calcul d'un seuil empirique, ou donc un seuil théorique est désirable.

Dans ce chapitre, la théorie pour le résidu de la SSDD sous incertitudes du noyau de référence est dérivée. Le résidu est nouvellement évalué en le considérant comme une fonction des deux variables aléatoires $\widehat{S}$ et $\widehat{\mathcal{H}}$. Les perturbations de ces deux variables sont propagées au résidu, conduisant au calcul de sa covariance asymptotique et au test d'hypothèse associé. L'application du nouveau test aux données numériques montre un comportement statistique correct et prévisible, permettant également le calcul d'un seuil théorique a priori comme illustré dans la Fig. 1 (droite), alors qu'au contraire, le test conventionnel qui néglige les incertitudes de référence s'écarte significativement des valeurs attendues (gauche). Dans des études ultérieures, le nouveau test montre une plus grande sensibilité aux petits endommagements (Fig. 2, à gauche), son indépendance vis-à-vis de la longueur des données (Fig. 2, à droite) et d'autres paramètres de la procédure de calcul.

Chapitre 4 – Détection d'endommagements par méthodes sous-espaces sous conditions environnementales variées

L'application du diagnostic automatisé des endommagements basé sur les vibrations à la surveillance de l'intégrité des ouvrages d'art (SHM) échoue souvent en raison de l'évolution des conditions environnementales, car le comportement dynamique des struc-

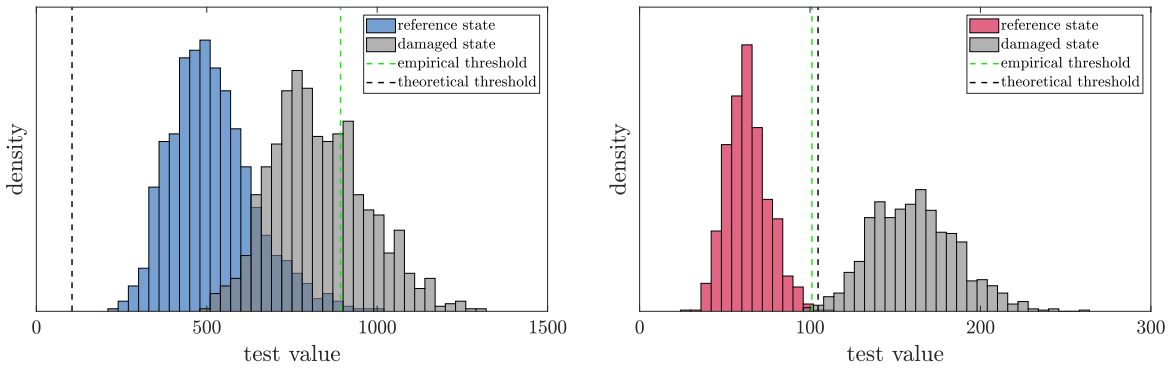

Figure 1 – Histogrammes du test dans les états de référence et endommagé, pour le test conventionnel (gauche) et le nouveau test (droite).

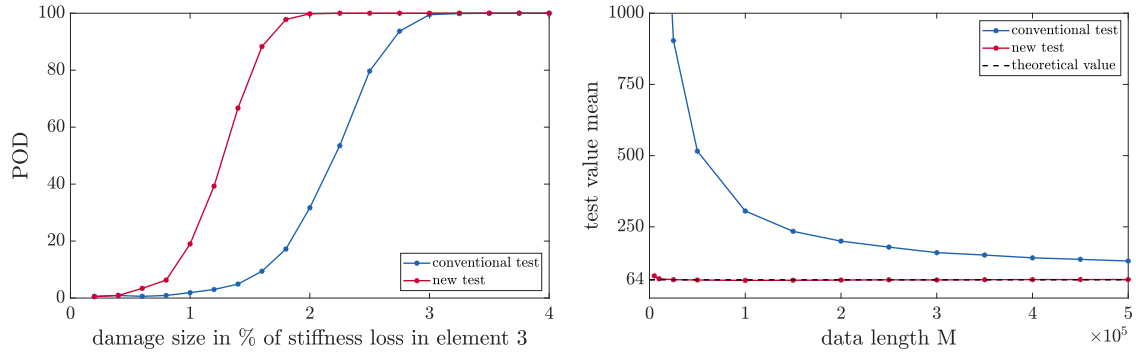

Figure 2 – Probabilité de détection (gauche) and dépendance du test de la longueur de données M dans l'état de référence (droite).

tures est affecté [Soh07]. Le résidu de la SSDD est également sensible à de tels changements. Nous développons la théorie d'une procédure SSDD robuste à la variabilité environnementale, inspirée de l'interpolation du modèle de [Zha18]. Les données enregistrées à quelques températures de référence seulement sont utilisées pour créer un noyau gauche de référence adapté à la température actuelle. Trois stratégies de calcul du noyau de référence sont proposées. La première stratégie utilise un noyau de référence calculé à partir d'une matrice de Hankel interpolée. La deuxième stratégie interpole les paramètres modaux conduisant à une matrice d'observabilité interpolée, à partir de laquelle le noyau de référence est calculé. Dans la troisième stratégie, un noyau gauche est calculé à partir d'une matrice d'observabilité qui est basée sur les paramètres modaux obtenus à partir d'une analyse de régression. Conformément au chapitre précédent, la théorie pour le calcul de la covariance du résidu où le noyau est adapté à la température est dérivée. La méthode est validée dans une étude numérique. Par rapport à une approche existante de

[Bal+08a] qui échoue lorsque l'effet de la température est plus élevé que l'effet dû aux endommagements, la nouvelle approche est robuste et toujours sensible aux endommagements comme le montre la Fig. 3. En utilisant le noyau gauche de référence adapté à la température, le taux de fausses alarmes peut être réduit de manière significative. Les stratégies basées sur la matrice d'observabilité sont plus performantes que l'interpolation directe de la matrice de Hankel.

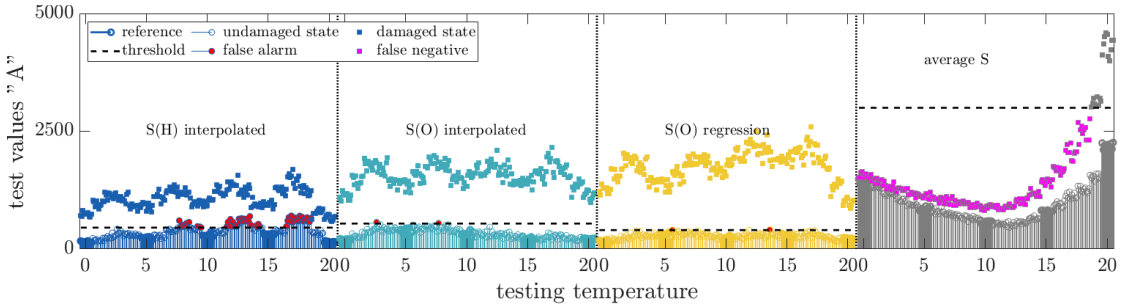

Figure 3 – Valeurs du test pour toutes les strategies développées, ainsi que pour l'approche existante [Bal+08a] aux températures de test variées et les références prises à 0, 5, 10, 15 and 20°C.

Chapitre 5 – Détection d'endommagements dans un cadre en acier en tenant compte des incertitudes dans la référence

La méthode de détection d'endommagements pour le résidu avec référence incertaine est validée sur des données expérimentales provenant d'un modèle de laboratoire d'une structure de fondation d'éolienne off-shore permettant des changements structurels réversibles. Les données ont été obtenues dans le cadre des travaux de Hille [Hil18] à l'Institut fédéral de recherche et d'essais des matériaux (BAM). Une procédure de test non paramétrique est utilisée pour éviter l'identification des modes sensibles aux endommagements.

Les résultats correspondent aux conclusions de l'étude numérique. Dans l'état de référence, le test conventionnel conduit à des valeurs d'essai plus élevées en raison d'un biais qui est introduit en négligeant les incertitudes dans l'état de référence (Fig. 4, à gauche). Le nouveau test, au contraire, montre une bonne conformité aux valeurs théoriquement attendues (droite), ce qui permet d'utiliser un seuil calculé sur une base

théorique. De plus, le nouveau test a une meilleure sensibilité aux endommagements que le test conventionnel, et des études plus poussées ont confirmé que le nouveau test est très robuste aux changements de longueur des données. Avec le test conventionnel, les valeurs et les performances du test ne sont pas prévisibles et nécessitent donc une étude approfondie de l'état de référence basée sur des données suffisamment longues pour, par exemple, dériver des seuils fiables.

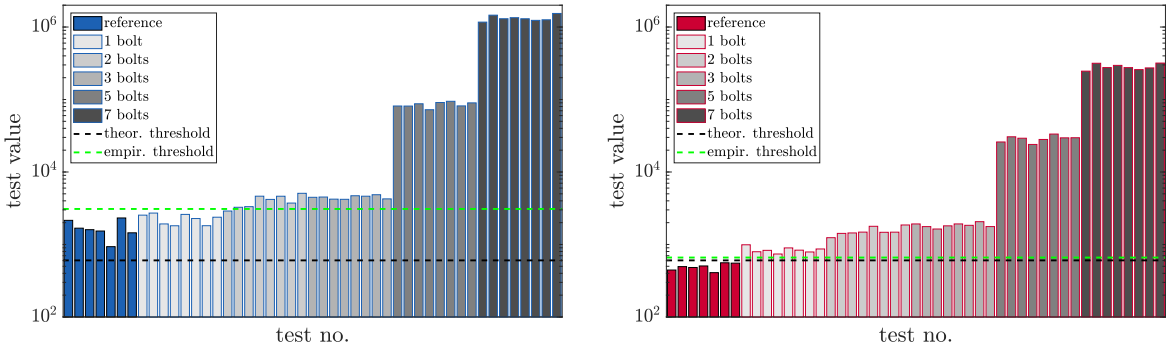

Figure 4 – Valeurs du test conventionnel (gauche) et du nouveau test (droite) dans l'état de réference et plusieurs états endommagés.

Chapitre 6 – Détection d'endommagements d'une poutre en laboratoire affectée par la température

Une première application des méthodes robustes du chapitre 4 sur les données réelles d'une poutre en béton testée dans une chambre climatique est effectué. La poutre est soumise à cinq températures différentes et à trois états de système différents dans le cadre des travaux de Simon et al. [Sim+20] dans le hall d'essai de l'Institut fédéral de recherche et d'essai des matériaux (BAM). La procédure de détection d'endommagements non paramétrique et entièrement basée sur les données est appliquée en utilisant l'interpolation directe de la matrice de Hankel pour calculer le noyau de référence adapté à la température.

Les résultats correspondent aux conclusions de l'étude numérique. L'approche d'interpolation est capable de distinguer de manière fiable les états sains et endommagés, en évitant les fausses alarmes comme le montre la Fig. 5 (en haut), alors que les méthodes précédentes ne parviennent pas à classer correctement l'état sain lorsque la température dans l'état de test

est différente des températures pour lesquelles des données de référence sont disponibles, comme l'illustre l'image du bas.

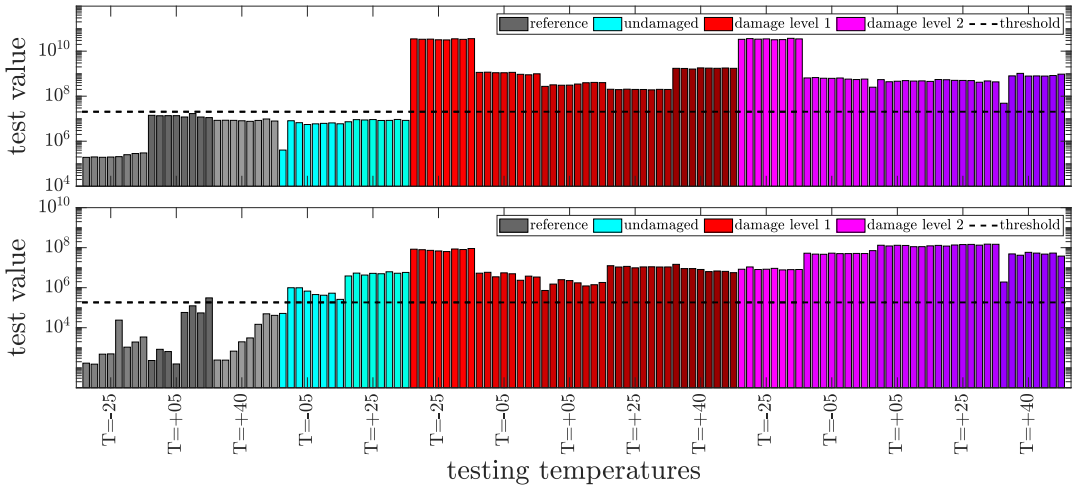

Figure 5 – Valeurs du test avec la stratégie d'interpolation des matrices Hankel (en haut), et avec l'approche existante [Bal+08a] (en bas). Les données de référence ont été utilisées à -25°C, 5°C, et 40°C.

Chapitre 7 – Détection d'endommagements sur un pont d'essai exposé à des variations de température ambiante

Les approches robustes aux changements de température pour la SSDD sont appliquées aux données expérimentales d'un pont d'essai (Fig. 6) situé sur un terrain d'essai extérieur de l'Institut fédéral de recherche et d'essai des matériaux (BAM) exposé à des conditions environnementales réelles. Les expériences incluant la conceptualisation du pont ont été réalisées dans le cadre de cette thèse.

Les nouvelles méthodes avec le noyau de référence adapté à la température permet une détection fiable des endommagements avec une réduction significative du taux de fausses alarmes par rapport à d'autres approches, comme l'illustre la Fig. 7. En particulier, lorsque des données de référence sont disponibles dans une plage de température et que la structure est testée à une température en dehors de cette plage, la méthode proposée permet de résoudre correctement ce problème par extrapolation à partir des points de référence.

Dans des études ultérieures, l'effet de la conception de la fonction de pondération est analysé, ce qui permet d'améliorer les performances du test en choisissant des fonctions de pondération adaptées au comportement dépendant de la température.

Figure 6 – Testing bridge.

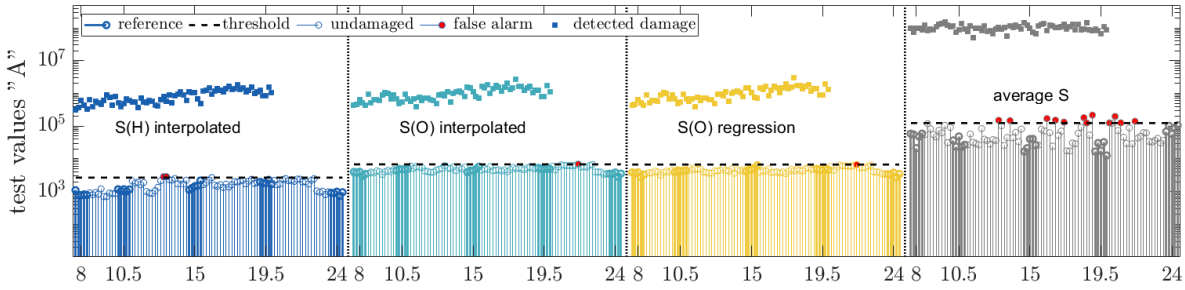

Figure 7 – Test values of the 4 algorithms for different testing temperatures in the undamaged and the damaged case, computed for reference setup A.

Conclusions

Dans cette thèse, des développements ont été réalisés dans le but d'améliorer la robustesse et la sensibilité de la SSDD pour une application sur les ouvrages d'art.

Jusqu'à présent, dans la procédure SSDD existante, les incertitudes liées aux modèles de référence estimés n'ont pas été prises en compte, ce qui entraînait un biais inhérent et un comportement imprévisible du test. Cette lacune a été comblée et l'évaluation de la covariance du résidu a été effectuée en tenant compte des incertitudes liées aux données d'essai et à la référence estimée. La partie cruciale de la définition d'un seuil entre l'état sain et l'état endommagé peut maintenant être faite a priori sur la base de considérations théoriques sans études empiriques approfondies sur les données de référence. La méthode

développée a été validée sur des données numériques et expérimentales montrant une bonne conformité avec le comportement théorique attendu et conduisant à une sensibilité de test plus élevée. Cependant, une estimation minutieuse de la matrice de covariance des données est nécessaire, car sa qualité affecte la quantification de l'incertitude du résidu.

Deuxièmement, une approche pour la SSDD a été dérivée qui est robuste aux changements environnementaux. La méthode s'inspire d'une approche d'interpolation de modèle conduisant à un noyau gauche de référence adapté aux paramètres (de température) sans connaissance explicite de la dépendance de la structure du paramètre. Trois stratégies différentes ont été proposées, basées sur des approches d'interpolation ou de régression de la matrice de Hankel ou des paramètres modaux. Les incertitudes du noyau de référence adapté aux paramètres ont été quantifiées, et il a été montré comment les calculer en fonction de la stratégie choisie. La validation sur des données numériques et expérimentales a montré une sensibilité de test significativement plus élevée que les approches précédentes, et les fausses alarmes dues à des changements dans les conditions environnementales ont pu être évitées en grande partie. L'approche nécessite une conception minutieuse de la fonction d'interpolation.

L'estimation de la matrice de covariance du résidu devrait faire l'objet d'une étude plus approfondie dans le futur, car dans une application pratique, l'estimation de la covariance à partir d'un nombre relativement faible de blocs de données par rapport à la dimension du résidu peut être difficile et entraîner des problèmes numériques. Un autre sujet qui devrait être abordé, bien qu'il s'agisse d'une tâche dépendant de la structure, est l'évaluation de l'effet des fonctions de pondération pour la robustesse aux variations environnementales et leur choix optimal. En outre, une version paramétrique de l'approche robuste est nécessaire pour l'extension à la localisation et à la quantification des endommagements [DMZ16] et l'évaluation rigoureuse de la sensibilité des méthodes aux endommagements [MDV21].

BIBLIOGRAPHY

[AB82] R.J. Allemang and D.L. Brown. « A correlation coefficient for modal vector analysis ». In: *Proceedings of the 1st International Modal Analysis Conference*. Orlando, Florida, USA, 1982, pp. 110–116.

[Ad99] M.M. Abdel Wahab and G. de Roeck. « Damage detecion in bridges using modal curvatures: application to a real damage scenario ». In: *Journal of Sound and Vibration* 226.2 (1999), pp. 217–235.

[Ada+78] R.D. Adams, P. Cawley, C.J. Pye, and B.J. Stone. « A vibration technique for non-destructively assessing the integrity of structures ». In: *Journal of Mechanical Engineering Science* 20.2 (1978), pp. 93–100.

[All+19] S. Allahdadian, M. Döhler, C. Ventura, and L. Mevel. « Towards robust statistical damage localization via model-based sensitivity clustering ». In: *Mechanical Systems and Signal Processing* 134 (2019), p. 106341.

[All03] R.J. Allemang. « The modal assurance criterion – Twenty years of use and abuse ». In: *Sound and Vibration* 37 (2003), pp. 14–23.

[Avc+21] O. Avci, O. Abdeljaber, S. Kiranyaz, M. Hussein, M. Gabbouj, and D.J. Inman. « A review of vibration-based damage detection in civil structures: From traditional methods to Machine Learning and Deep Learning applications ». In: *Mechanical Systems and Signal Processing* 147 (2021), p. 107077.

[BAB00] M. Basseville, M. Abdelghani, and A. Benveniste. « Subspace-based fault detection algorithms for vibration monitoring ». In: *Automatica* 36.1 (2000), pp. 101–109.

[Bal+08a] É. Balmès, M. Basseville, F. Bourquin, L. Mevel, H. Nasser, and F. Treyssède. « Merging sensor data from multiple temperature scenarios for vibration-based monitoring of civil structures ». In: *Structural Health Monitoring* 7.2 (2008), pp. 129–142.

[Bal+08b] É. Balmès, M. Basseville, L. Mevel, H. Nasser, and W. Zhou. « Statistical model-based damage localization: a combined subspace-based and substructuring approach ». In: *Structural Control and Health Monitoring* 15.6 (2008), pp. 857–875.

[Bal+09] É. Balmès, M. Basseville, L. Mevel, and H. Nasser. « Handling the temperature effect in vibration-based monitoring of civil structures: a combined subspace-based and nuisance rejection approach ». In: *Control Engineering Practice* 17.1 (2009), pp. 80–87.

[Bas+10] M. Basseville, F. Bourquin, L. Mevel, H. Nasser, and F. Treyssède. « Handling the temperature effect in vibration monitoring: two subspace-based analytical approaches ». In: *Journal of Engineering Mechanics* 136.3 (2010), pp. 367–378.

[BB15] L. Balsamo and R. Betti. « Data-based structural health monitoring using small training data sets ». In: *Structural Control and Health Monitoring* 22.10 (2015), pp. 1240–1264.

[BBM87] A. Benveniste, M. Basseville, and G.V. Moustakides. « The asymptotic local approach to change detection and model validation ». In: *IEEE Transactions on Automatic Control* 32.7 (1987), pp. 583–592.

[Ber02] D. Bernal. « Load vectors for damage localization ». In: *Journal of Engineering Mechanics* 128.1 (2002), pp. 7–14.

[Ber10] D. Bernal. « Load vectors for damage location in systems identified from operational loads ». In: *Journal of Engineering Mechanics* 136.1 (2010), pp. 31–39.

[Ber13] D. Bernal. « Kalman filter damage detection in the presence of changing process and measurement noise ». In: *Mechanical Systems and Signal Processing* 39.1-2 (2013), pp. 361–371.

[BF85] A. Benveniste and J.-J. Fuchs. « Single sample modal identification of a nonstationary stochastic process ». In: *IEEE Transactions on Automatic Control* 30.1 (1985), pp. 66–74.

[BHS16] M. Baeßler, F. Hille, and S. Said. « Bauwerksüberwachung von Brücken im Kontext saisonaler Einflüsse ». In: *Proceedings of Messen Im Bauwesen*. Berlin, Germany, 2016.

[Bhu+19] M.D.H. Bhuyan, G. Gautier, N. Le Touz, M. Döhler, F. Hille, J. Dumoulin, and L. Mevel. « Vibration-based damage localization with load vectors under temperature changes ». In: *Structural Control and Health Monitoring* 26.11 (2019), e2439.

[BM07] A. Benveniste and L. Mevel. « Nonstationary Consistency of Subspace Methods ». In: *IEEE Transactions on Automatic Control* 52.6 (2007), pp. 974–984.

[BMG04] M. Basseville, L. Mevel, and M. Goursat. « Statistical model-based damage detection and localization: subspace-based residuals and damage-to-noise sensitivity ratios ». In: *Journal of Sound and Vibration* 275.3 (2004), pp. 769–794.

[Bro+01] J.M.W. Brownjohn, P.-Q. Xia, H. Hao, and Y. Xia. « Civil structure condition assessment by FE model updating:: methodology and case studies ». In: *Finite Elements in Analysis and Design* 37.10 (2001), pp. 761–775.

[Bro+18] J.M.W. Brownjohn, S.-K. Au, Y. Zhu, Z. Sun, B. Li, J. Bassitt, E. Hudson, and H. Sun. « Bayesian operational modal analysis of Jiangyin Yangtze River Bridge ». In: *Mechanical Systems and Signal Processing* 110 (2018), pp. 210–230.

[CB02] G. Casella and R.L. Berger. *Statistical inference*. Pacific Grove, CA, USA: Duxbury Press, 2002.

[CB08] E.P. Carden and J.M.W. Brownjohn. « ARMA modelled time-series classification for structural health monitoring of civil infrastructure ». In: *Mechanical Systems and Signal Processing* 22.2 (2008), pp. 295–314.

[CF04] E.P. Carden and P. Fanning. « Vibration based condition monitoring: a review ». In: *Structural Health Monitoring* 3.4 (2004), pp. 355–377.

[CM11] E.P. Carden and A. Mita. « Challenges in developing confidence intervals on modal parameters estimated for large civil infrastructure with stochastic subspace identification ». In: *Structural Control and Health Monitoring* 18.1 (2011), pp. 53–78.

[Cro+12] E.J. Cross, G. Manson, K. Worden, and S.G. Pierce. « Features for damage detection with insensitivity to environmental and operational variations ». In: *Proceedings of the Royal Society A: Mathematical, Physical and Engineering Sciences* 468.2148 (2012), pp. 4098–4122.

[Der+08] A. Deraemaeker, E. Reynders, G. De Roeck, and Kullaa J. « Vibration-based structural health monitoring using output-only measurements under changing environment ». In: *Mechanical Systems and Signal Processing* 22.1 (2008), pp. 34–56.

[Der+15] N. Dervilis, I. Antoniadou, R.J. Barthorpe, E.J. Cross, and K. Worden. « Robust methods for outlier detection and regression for SHM applications ». In: *International Journal of Sustainable Materials and Structural Systems* 2.1-2 (2015), pp. 3–26.

[DFP98] S.W. Doebling, C.R. Farrar, and M.B. Prime. « A summary review of vibration-based damage identification methods ». In: *The Shock and Vibration Digest* 30.2 (1998), pp. 91–105.

[DM12] M. Döhler and L. Mevel. « Fast multi-order computation of system matrices in subspace-based system identification ». In: *Control Engineering Practice* 20.9 (2012), pp. 882–894.

[DM13a] M. Döhler and L. Mevel. « Efficient multi-order uncertainty computation for stochastic subspace identification ». In: *Mechanical Systems and Signal Processing* 38.2 (2013), pp. 346–366.

[DM13b] M. Döhler and L. Mevel. « Subspace-based fault detection robust to changes in the noise covariances ». In: *Automatica* 49.9 (2013), pp. 2734–2743.

[DMH14] M. Döhler, L. Mevel, and F. Hille. « Subspace-based damage detection under changes in the ambient excitation statistics ». In: *Mechanical Systems and Signal Processing* 45.1 (2014), pp. 207–224.

[DMZ16] M. Döhler, L. Mevel, and Q. Zhang. « Fault detection, isolation and quantification from Gaussian residuals with application to structural damage diagnosis ». In: *Annual Reviews in Control* 42 (2016), pp. 244–256.

[Döh+14] M. Döhler, F. Hille, L. Mevel, and W. Rücker. « Structural health monitoring with statistical methods during progressive damage test of S101 Bridge ». In: *Engineering Structures* 69 (2014), pp. 183–193.

[Döh+15] M. Döhler, L. Marin, L. Mevel, and D. Bernal. « Operational modal analysis with uncertainty quantification for SDDLV-based damage localization ». In: *MATEC Web of Conferences* 20 (2015).

[DVG12] J. Dong, M. Verhaegen, and F. Gustafsson. « Robust fault detection with statistical uncertainty in identified parameters ». In: *IEEE Transactions on Signal Processing* 60.10 (2012), pp. 5064–5076.

[Far+00] C.R. Farrar, P.J. Cornwell, S.W. Doebling, and M.B. Prime. *Structural health monitoring studies of the Alamosa Canyon and I-40 Bridges*. Tech. rep. Los Alamos National Lab. (LANL), Los Alamos, NM (United States), 2000.

[Far+94] C.R. Farrar, W.E. Baker, T.M. Bell, K.M. Cone, T.W. Darling, T.A. Duffey, A. Eklund, and A. Migliori. *Dynamic characterization and damage detection in the I-40 bridge over the Rio Grande.* Tech. rep. Los Alamos National Lab. (LANL), Los Alamos, NM (United States), 1994.

[FC03] P.J. Fanning and E.P. Carden. « Damage Detection based on Single-Input-Single-Output Measurements ». In: *Journal of Engineering Mechanics* 129.2 (2003), pp. 202–209.

[FDN01] C.R. Farrar, S.W. Doebling, and D.A. Nix. « Vibration-based structural damage identification ». In: *Philosophical Transactions: Mathematical, Physical and Engineering Sciences* 359.1778 (2001), pp. 131–149.

[FJ97] C.R. Farrar and G.H. James III. « System identification from ambient vibration measurements on a bridge ». In: *Journal of Sound and Vibration* 205.1 (1997), pp. 1–18.

[FK13] S.D. Fassois and F.P. Kopsaftopoulos. « Statistical time series methods for vibration based structural health monitoring ». In: *New Trends in Structural Health Monitoring*. Ed. by Wieslaw Ostachowicz and J. Alfredo Güemes. Vienna: Springer Vienna, 2013, pp. 209–264.

[FKB13] C.P. Fritzen, P. Kraemer, and I. Buethe. « Vibration-based damage setection under changing environmental and operational conditions ». In: *Advances in Science and Technology* 83 (2013), pp. 95–104.

[FKK13] C.P. Fritzen, M. Klinkov, and P. Kraemer. « Vibration-Based Damage Diagnosis and Monitoring of External Loads ». In: *New Trends in Structural Health Monitoring*. Ed. by Wieslaw Ostachowicz and J. Alfredo Güemes. Vienna: Springer, Vienna, 2013, pp 149–208. ISBN: 978-3-7091-1389-9.

[FM95] M. Friswell and J.E. Mottershead. *Finite element model updating in structural dynamics*. Springer Netherlands, 1995. ISBN: 978-90-481-4535-5.

[FMG03] C. P. Fritzen, G. Mengelkamp, and A. Güemes. « Elimination of temperature effects on damage detection within a smart structure concept. » In: *Proceeings of 4th International Workshop on Structural Health Monitoring*. Stanford, CA, USA, 2003, pp. 1530–1538.

[Fri07] M. Friswell. « Damage identification using inverse methods ». In: *Philosophical Transactions of the Royal Society A: Mathematical, Physical and Engineering Sciences* 365.1851 (2007), pp. 393–410.

[FSF01] M.L. Fugate, H. Sohn, and C.R. Farrar. « Vibration-based damage detection using statistical process control ». In: *Mechanical systems and signal processing* 15.4 (2001), pp. 707–721.

[FW07] C.R. Farrar and K. Worden. « An introduction to structural health monitoring ». In: *Philosophical Transactions of the Royal Society A: Mathematical, Physical and Engineering Sciences* 365.1851 (2007), pp. 303–315.

[FW12] C.R. Farrar and K. Worden. *Structural health monitoring: A machine learning perspective*. Chichester, West Sussex, U.K: Wiley, 2012. ISBN: 978-1-119-99433-6.

[Gau+17] G. Gautier, L. Mevel, J.-M. Mencik, R. Serra, and M. Döhler. « Variance analysis for model updating with a finite element based subspace fitting approach ». In: *Mechanical Systems and Signal Processing* 91 (2017), pp. 142–156.

[GDM20] S. Greś, M. Döhler, and L. Mevel. « Variance computation for system matrices and transfer function from input/output subspace system identification ». In: *IFAC-PapersOnLine* 53.2 (2020). 21st IFAC World Congress, pp. 933–938.

[GDM21] S. Greś, M. Döhler, and L. Mevel. « Uncertainty quantification of the modal assurance criterion in operational modal analysis ». In: *Mechanical Systems and Signal Processing* 152 (2021), p. 107457.

[GGW17] J. Gu, M. Gul, and X. Wu. « Damage detection under varying temperature using artificial neural networks ». In: *Structural Control and Health Monitoring* 24.11 (2017), e1998.

[GK17] Y. Goi and C.-W. Kim. « Damage detection of a truss bridge utilizing a damage indicator from multivariate autoregressive model ». In: *Journal of Civil Structural Health Monitoring* 7 (2017), pp. 153–162.

[GN09] M. Gul and F. Necati Catbas. « Statistical pattern recognition for Structural Health Monitoring using time series modeling: Theory and experimental verifications ». In: *Mechanical Systems and Signal Processing* 23.7 (2009), pp. 2192–2204.

[Gre+17] S. Greś, M.D. Ulriksen, M. Döhler, R.J. Johansen, P. Andersen, L. Damkilde, and S.A. Nielsen. « Statistical methods for damage detection applied to civil structures ». In: *Procedia Engineering* 199 (2017). X International Conference on Structural Dynamics, EURODYN 2017, pp. 1919–1924.

[Gre+21a] S. Greś, M. Döhler, P. Andersen, and L. Mevel. « Kalman filter-based subspace identification for operational modal analysis under unmeasured periodic excitation ». In: *Mechanical Systems and Signal Processing* 146 (2021), p. 106996.

[Gre+21b] S. Greś, M. Döhler, P. Andersen, and L. Mevel. « Subspace-based Mahalanobis damage detection robust to changes in excitation covariance ». In: *Structural Control and Health Monitoring* 28.8 (2021), e2760.

[Gre+21c] S. Greś, M. Döhler, P. Andersen, and L. Mevel. « Uncertainty quantification for the modal phase collinearity of complex mode shapes ». In: *Mechanical Systems and Signal Processing* 152 (2021), p. 107436.

[Han70] E.J. Hannan. *Multiple time series*. New York: Wiley, 1970.

[HF09] J. Hios and S. Fassois. « Stochastic identification of temperature effects on the dynamics of a smart composite beam: Assessment of multi-model and global approaches ». In: *Smart Materials and Structures* 18 (2009), p. 035011.

[Hil18] F. Hille. « Unterraumbasierte Detektion von Strukturschäden an Jacket-Gründungen von Offshore-Windenergieanlagen ». Doctoral Thesis. Berlin: Technische Universität Berlin, 2018.

[HO14] S. Hoell and P. Omenzetter. « Damage detection in a wind turbine blade based on time series methods ». In: *7th European Workshop on Structural Health Monitoring*. Nantes, France, 2014, pp. 237–244.

[Hu+15] W.-H. Hu, S. Said, R. Rohrmann, W. Rücker, A. Cunha, and A. Rogge. « Vibration-based structural health monitoring of a highway bridge based on continuous dynamic measurements during 14 years ». In: *Proceedings of SHMII-7 - 7th International conference on structural health monitoring of intelligent infrastructure*. Turin, Italy, 2015.

[Ike14] K. Ikeda. « Error analysis of state approaches in subspace identification methods ». In: *2014 Proceedings of the SICE Annual Conference (SICE)*. Sapporo, Japan, 2014, pp. 1685–1690.

[JC16] I.T. Jolliffe and J. Cadima. « Principal component analysis: a review and recent developments ». In: *Philosophical Transactions of the Royal Society A: Mathematical, Physical and Engineering Sciences* 374.2065 (2016), p. 20150202.

[JMM12] A. Jhinaoui, L. Mevel, and J. Morlier. « Subspace instability monitoring for linear periodically time-varying systems ». In: *16th IFAC Symposium on System Identification*. Brussels, Belgium, 2012, pp. 380–385.

[Jua94] J.-N. Juang. *Applied system identification*. Englewood Cliffs, NJ, USA: Prentice Hall, 1994.

[Kál63] R. Kálmán. « Mathematical description of linear dynamical systems ». In: *Journal of The Society for Industrial and Applied Mathematics, Series A: Control* 1 (1963), pp. 152–192.

[KBD13] S.M. Kojidi, D. Bernal, and M. Döhler. « Change detection under environmental variability ». In: *5th International Operational Modal Analysis Conference, IOMAC 2013* (2013), pp. 1–8.

[KF16] P. Kraemer and H. Friedmann. « Experimental validation of stochastic subspace algorithms for structural health monitoring of offshore wind turbine towers and foundations ». In: *8th European Conference în Structural Health Monitoring*. Bilbao, Spain, 2016.

[Kra91] M.A. Kramer. « Nonlinear principal component analysis using autoassociative neural networks ». In: *AIChE Journal* 37.2 (1991), pp. 233–243.

[Kul03] J. Kullaa. « Damage detection of the Z24 bridge using control charts ». In: *Mechanical Systems and Signal Processing* 17.1 (2003), pp. 163–170.

[Kul14] J. Kullaa. « Structural health monitoring under non-linear environmental or operational influences ». In: *Shock and Vibration* 2014 (2014).

[KWA19] T. Kernicky, M. Whelan, and E. Al-Shaer. « Vibration-based damage detection with uncertainty quantification by structural identification using nonlinear constraint satisfaction with interval arithmetic ». In: *Structural Health Monitoring* 18.5-6 (2019), pp. 1569–1589.

[KXY18] H. Kordestani, Y.-Q. Xiang, and X.-W. Ye. « Output-only damage detection of steel beam using moving average filter ». In: *Shock and Vibration* 2018 (2018).

[LD07] C. Y. Liu and J. T. DeWolf. « Effect of temperature on modal variability of a curved concrete bridge under ambient loads ». In: *Journal of Structural Engineering* 133.12 (2007), pp. 1742–1751.

[Le 56] L. Le Cam. « On the asymptotic theory of estimation and testing hypotheses ». In: *Berkeley Symposium on Mathematical Statistics and Probability*. 1956.

[Leo06] Cornelius T. Leondes, ed. *Mems/Nems, (1) Handbook Techniques and Applications Design Methods*. Springer, US, 2006.

[Lia+21] C.M. Liao, F. Hille, D. Fontoura Barosso, and E. Niederleithinger. « Monitoring of a prestressed bridge model by ultrasonic measurement and vibration recordings ». In: *Proceedings of 8th ECCOMAS Thematic Conference on Computational Methods in Structural Dynamics and Earthquake Engineering COMPDYN 2021*. Athens, Greece, 2021.

[Lim+21] M.P. Limongelli, E. Manoach, S. Quqa, P.F. Giordano, B. Bhowmik, V. Pakrashi, and A. Cigada. « Vibration Response-Based Damage Detection ». In: *Structural Health Monitoring Damage Detection Systems for Aerospace*. Ed. by Jasiūnienė E. Sause M.G.R. Springer Aerospace Technology, 2021.

[Lim10] M.P. Limongelli. « Frequency response function interpolation for damage detection under changing environment ». In: *Mechanical Systems and Signal Processing* 24 (2010), pp. 2898–2913.

[Lim19] M.P. Limongelli. « Vibration-based structural health monitoring: Challenges and opportunities ». In: *Advances in Engineering Materials, Structures and Systems: Innovations, Mechanics and Applications*. 2019, pp. 1999–2004.

[LLM08] J. Liu, X. Liu, and X. Ma. « First-order perturbation analysis of singular vectors in singular value decomposition ». In: *IEEE Transactions on Signal Processing* 56.7 (2008), pp. 3044–3049.

[LM11] X.-B. Lam and L. Mevel. « Uncertainty quantification for eigensystem-realization-algorithm, a class of subspace system identification ». In: *IFAC Proceedings Volumes* 44.1 (2011). 18th IFAC World Congress, pp. 6529–6534.

[LMK18] S. Liehr, S. Münzenberger, and K. Krebber. « Wavelength-scanning coherent OTDR for dynamic high strain resolution sensing ». In: *Optic Express* 26.8 (2018), pp. 10573–10588.

[Man02] G. Manson. « Identifying damage sensitive, environment insensitive features for damage detection ». In: *Proceedings of the International Conference on Identification in Engineering Systems*. Swansea, Wales, 2002, pp. 187–197.

[Mao12] Z. Mao. « Uncertainty quantification in vibration-based structural health monitoring for enhanced decision-making capability ». PhD thesis. University of California, San Diego, Jan. 2012.

[MCC12] F. Magalhães, A. Cunha, and E. Caetano. « Vibration based structural health monitoring of an arch bridge: From automated OMA to damage detection ». In: *Mechanical Systems and Signal Processing* 28 (2012), pp. 212–228.

[MDM16] P. Mellinger, M. Döhler, and L. Mevel. « Variance estimation of modal parameters from output-only and input/output subspace-based system identification ». In: *Journal of Sound and Vibration* 379 (2016), pp. 1–27.

[MDV21] A. Mendler, M. Döhler, and C. Ventura. « A reliability-based approach to determine the minimum detectable damage for statistical damage detection ». In: *Mechanical Systems and Signal Processing* 154 (2021), p. 107561.

[Men+20] A. Mendler, M. Döhler, C. Ventura, and L. Mevel. « Clustering of redundant parameters for fault isolation with Gaussian residuals ». In: *IFAC-PapersOnLine* 53 (2020). 21st IFAC World Congress, pp. 13727–13732.

[Men20] A. Mendler. « Minimum diagnosable damage and optimal sensor placement for structural health monitoring ». PhD thesis. University of British Columbia, 2020.

[Mig+12] L.F.F. Miguel, L.F.F. Miguel, J. Kaminski, and J.D. Riera. « Damage detection under ambient vibration by harmony search algorithm ». In: *Expert Systems with Applications* 39.10 (2012), pp. 9704–9714.

[NK07] K.K. Nair and A. Kiremidjian. « Time series based structural damage detection algorithm using Gaussian mixtures modeling ». In: *Journal of Dynamic Systems Measurement and Control* 129.3 (May 2007), pp. 285–293.

[Oli+18] G. Oliveira, F. Magalhães, Á. Cunha, and E. Caetano. « Vibration-based damage detection in a wind turbine using 1 year of data ». In: *Structural Control and Health Monitoring* 25.11 (2018), e2238.

[PB94] A.K. Pandey and M. Biswas. « Damage detection in structures using changes in flexibility ». In: *Journal of Sound and Vibration* 169.1 (1994), pp. 3–17.

[PBS91] A.K. Pandey, M. Biswas, and M.M. Samman. « Damage detection from changes in curvature mode shapes ». In: *Journal of Sound and Vibration* 145.2 (1991), pp. 321–332.

[PD00] B. Peeters and G. De Roeck. « One year monitoring of the Z24-bridge: Environmental influences versus damage events ». In: *Proceedings of SPIE - The International Society for Optical Engineering* 2 (2000).

[PD99] B. Peeters and G. De Roeck. « Reference-based stochastic subspace identification for output-only modal analysis ». In: *Mechanical Systems and Signal Processing* 13.6 (1999), pp. 855–878.

[Pee+04] B. Peeters, H. Van der Auweraer, P. Guillaume, and J. Leuridan. « The PolyMAX frequency-domain method: A new standard for modal parameter estimation? » In: *Shock and Vibration* 11 (2004), pp. 395–409.

[PGS07] R. Pintelon, P. Guillaume, and J. Schoukens. « Uncertainty calculation in (operational) modal analysis ». In: *Mechanical Systems and Signal Processing* 21.6 (2007), pp. 2359–2373.

[Pir+19] S. Pirskawetz, K.P. Gründer, D. Kadoke, and J. Unger. « Überwachung von Stahlbetonbrücken - Ein Modellprojekt ». In: *Proceedings of 22. Kolloquium Schallemission und 3. Anwenderseminar Zustandsüberwachung mit geführten Wellen*. Karlsruhe, Germany, 2019.

[PMD01] B. Peeters, J. Maeck, and G. De Roeck. « Vibration-based damage detection in civil engineering: excitation sources and temperature effects ». In: *Smart Materials and Structures* 10.3 (2001), pp. 518–527.

[Ram+10] L.F. Ramos, L. Marques, P.B. Lourenço, G. De Roeck, A. Campos-Costa, and J. Roque. « Monitoring historical masonry structures with operational modal analysis: Two case studies ». In: *Mechanical Systems and Signal Processing* 24.5 (2010), pp. 1291–1305.

[RF10] C. Rainieri and G. Fabbrocino. « Automated output-only dynamic identification of civil engineering structures ». In: *Mechanical Systems and Signal Processing* 24.3 (2010), pp. 678–695.

[Roh+00a] R. Rohrmann, M. Baeßler, S. Said, W. Schmid, and W. Rücker. « Structural causes of temperature affected modal data of civil structures obtained by long time monitoring, No.141 ». In: *Proceedings of SPIE - The International Society for Optical Engineering* 1 (2000).

[Roh+00b] R. Rohrmann, S. Said, W. Schmid, W. Rücker, and M. Baeßler. « Zustandsuntersuchung und Dauerüberwachung von Bauwerken mit Hilfe modaler Parameter ». In: *Vortragsband der VDI-Schwingungstagung Experimentelle und rechnerische Modalanalyse sowie Identifikation dynamischer Systeme*. Kassel, Germany, 2000, pp. 327–350.

[RPD08] E. Reynders, R. Pintelon, and G. De Roeck. « Uncertainty bounds on modal parameters obtained from stochastic subspace identification ». In: *Mechanical Systems and Signal Processing* 22.4 (2008). Special Issue: Crack Effects in Rotordynamics, pp. 948–969.

[RWD14] E. Reynders, G. Wursten, and G. De Roeck. « Output-only structural health monitoring in changing environmental conditions by means of nonlinear system identification ». In: *Structural Health Monitoring* 13.1 (2014), pp. 82–93.

[Ryt93] A. Rytter. « Vibrational based inspection of civil engineering structures ». English. PhD thesis. Aalborg, Denmark: Aalborg University, 1993.

[SCF00] H. Sohn, J. Czarnecki, and C.R. Farrar. « Structural health monitoring using statistical process control ». In: *Journal of Structural Engineering* 126 (11 2000), pp. 1356–1363.

[SCN09] F. Schoefs, A. Clément, and A. Nouy. « Assessment of ROC curves for inspection of random fields ». In: *Structural Safety* 31.5 (2009), pp. 409–419.

[SCS16] M.D. Spiridonakos, E.N. Chatzi, and B. Sudret. « Polynomial Chaos Expansion Models for the Monitoring of Structures under Operational Variability ». In: *ASCE-ASME Journal of Risk and Uncertainty in Engineering Systems, Part A: Civil Engineering* 2.3 (2016), B4016003.

[SDL15] E. Simoen, G. De Roeck, and G. Lombaert. « Dealing with uncertainty in model updating for damage assessment: A review ». In: *Mechanical Systems and Signal Processing* 56-57 (2015), pp. 123–149.

[SF01] H. Sohn and C.R. Farrar. « Damage diagnosis using time series analysis of vibration signals ». In: *Smart Materials and Structures* 10.3 (2001), pp. 446–451.

[Sim+20] P. Simon, R. Schneider, E. Viefhues, S. Said, R. Herrmann, and M. Baeßler. « Vibration-based structural health monitoring of a reinforced concrete beam subject to varying ambient temperatures using Bayesian methods ». In: *Proceedings of XI International Conference on Structural Dynamics EURODYN 2020*. Athens, Greece, 2020.

[SM13] S. Sankararaman and S. Mahadevan. « Bayesian methodology for diagnosis uncertainty quantification and health monitoring ». In: *Structural Control and Health Monitoring* 20.1 (2013), pp. 88–106.

[SMS99] R.P.C. Sampaio, N.M.M. Maia, and J.M.M. Silva. « Damage detection using the frequency-response-function curvature method ». In: *Journal of Sound and Vibration* 226.5 (1999), pp. 1029–1042.

[Soh+98] H. Sohn, M. Dzwonczyk, E.G. Straser, K.H. Law, T.H.-Y. Meng, and A.S. Kiremidjian. « Adaptive modeling of environmental effects in modal parameters for damage detection in civil structures ». In: *Smart Structures and Materials 1998: Smart Systems for Bridges, Structures, and Highways*. International Society for Optics and Photonics. 1998, pp. 127–138.

[Soh07] H. Sohn. « Effects of environmental and operational variability on structural health monitoring ». In: *Philosophical Transactions of the Royal Society A: Mathematical, Physical and Engineering Sciences* 365(1851) (2007), pp. 539–560.

[SSS10] M. Sun, W.J. Staszewski, and R.N. Swamy. « Smart sensing technologies for structural health monitoring of civil engineering structures ». In: *Advances in Civil Engineering* (2010).

[SW10] C. Surace and K. Worden. « Novelty detection in a changing environment: A negative selection approach ». In: *Mechanical Systems and Signal Processing* 24.4 (2010), pp. 1114–1128.

[SWF02] H. Sohn, K. Worden, and C.R. Farrar. « Statistical damage classification under changing environmental and operational conditions ». In: *Journal of Intelligent Material Systems and Structures* 13.9 (2002), pp. 561–574.

[TA18] A. Tributsch and C. Adam. « An enhanced energy vibration-based approach for damage detection and localization ». In: *Structural Control and Health Monitoring* 25.1 (2018), e2047.

[Tan+19] Z. Tang, Z. Chen, Y. Bao, and H. Li. « Convolutional neural network-based data anomaly detection method using multiple information for structural health monitoring ». In: *Structural Control and Health Monitoring* 26.1 (2019), e2296.

[Tan05] J. Tang. « Frequency response based damage detection using principal component analysis ». In: *2005 IEEE International Conference on Information Acquisition*. Hong Kong, China, 2005.

[Ube+17] F. Ubertini, G. Comanducci, N. Cavalagli, A. Laura Pisello, A. Luigi Materazzi, and F. Cotana. « Environmental effects on natural frequencies of the San Pietro bell tower in Perugia, Italy, and their removal for structural per-

formance assessment ». In: *Mechanical Systems and Signal Processing* 82 (Jan. 2017), pp. 307–322.

[Ulr+16] M.D. Ulriksen, D. Tcherniak, P.H. Kirkegaard, and L. Damkilde. « Operational modal analysis and wavelet transformation for damage identification in wind turbine blades ». In: *Structural Health Monitoring* 15.4 (2016), pp. 381–388.

[Ung+17] J. Unger, K.P. Gründer, F. Hille, S. Liehr, S. Maack, E. Niederleithinger, S. Piskawetz, A. Rogge, S. Said, E. Viefhues, and S. Zorn. « Innovative Messsysteme zum Brückenmonitoring am Beispiel einer Versuchsbrücke – vom Sensor bis zur Zustandsprognose ». In: *Proceedings of Messen im Bauwesen 2017*. Berlin, Germany, 2017.

[Van+05] S. Vanlanduit, E. Parloo, B. Cauberghe, P. Guillaume, and P. Verboven. « A robust singular value decomposition for damage detection under changing operating conditions and structural uncertainties ». In: *Journal of Sound and Vibration* 284.3 (2005), pp. 1033–1050.

[VD96] P. Van Overschee and B. De Moor. *Subspace identification for linear systems: theory, implementation, applications*. Dordrecht, The Netherlands: Kluwer, 1996.

[Ven+14] C. Ventura, P. Andersen, L. Mevel, and M. Döhler. « Structural health monitoring of the Pitt River Bridge in British Columbia, Canada ». In: *Proceedings of WCSCM - 6th World Conference on Structural Control and Monitoring*. Barcelona, Spain, July 2014.

[Vie+17] E. Viefhues, M. Döhler, F. Hille, and L. Mevel. « Stochastic subspace-based damage detection with uncertainty in the reference null space ». In: *IWSHM - 11th International Workshop on Structural Health Monitoring*. Stanford, United States, 2017.

[Vie+18] E. Viefhues, M. Döhler, F. Hille, and L. Mevel. « Asymptotic analysis of subspace-based data-driven residual for fault detection with uncertain reference ». In: *IFAC-PapersOnLine* 51.24 (2018). 10th IFAC Symposium on Fault Detection, Supervision and Safety for Technical Processes SAFEPROCESS 2018, pp. 414–419.

[Vie+19] E. Viefhues, M. Döhler, Q. Zhang, F. Hille, and L. Mevel. « Subspace-based damage detection with rejection of the temperature effect and uncertainty in the reference ». In: *Proceedings of IOMAC 2019 - 8th International Operational Modal Analysis Conference*. Copenhagen, Denmark, 2019.

[Vie+20] E. Viefhues, M. Döhler, F. Hille, and L. Mevel. « Fault detection for linear parameter varying systems under changes in the process noise covariance ». In: *IFAC-PapersOnLine* 53.2 (2020). 21th IFAC World Congress, pp. 13668–13673.

[Vie+21] E. Viefhues, M. Döhler, P. Simon, R. Herrmann, F. Hille, and L. Mevel. « Stochastic subspace-based damage detection of a temperature affected beam structure ». In: *Proceedings of SHMII-10 2021 - 10th International Conference on Structural Health Monitoring of Intelligent Infrastructure*. Porto, Portugal, 2021, pp. 1–6.

[Vie+22] E. Viefhues, M. Döhler, F. Hille, and L. Mevel. « Statistical subspace-based damage detection with estimated reference ». In: *Mechanical Systems and Signal Processing* 164 (2022).

[VSF14] K. Vamvoudakis-Stefanou, J. Sakellariou, and S. Fassois. « Output-only statistical time series methods for structural health monitoring: A comparative study ». In: *Proceedings of 7th European Workshop on Structural Health Monitoring, Nantes, France*. July 2014.

[Wae+16] J. Waeytens, B. Rosić, P.-E. Charbonnel, E. Merliot, D. Siegert, X. Chapeleau, R. Vidal, V. le Corvec, and L.-M. Cottineau. « Model updating techniques for damage detection in concrete beam using optical fiber strain measurement device ». In: *Engineering Structures* 129 (2016). SI: Structures Rehabilitation, pp. 2–10.

[WMF00] K. Worden, G. Manson, and N.R.J. Fieller. « Damage detection using outlier analysis ». In: *Journal of Sound and Vibration* 229.3 (2000), pp. 647–667.

[Wor+07] K. Worden, C.R. Farrar, G. Manson, and G. Park. « The fundamental axioms of structural health monitoring ». In: *Proceedings of the Royal Society A: Mathematical, Physical and Engineering Science* 463.2082 (2007), pp. 1639–1664.

[WSF02] K. Worden, H. Sohn, and C.R. Farrar. « Novelty detection in a changing environment: Regression and interpolation approaches ». In: *Journal of Sound and Vibration* 258.4 (2002), pp. 741–761.

[Yan+05a] A.-M. Yan, G. Kerschen, P. De Boe, and J.-C. Golinval. « Structural damage diagnosis under varying environmental conditions—Part I: A linear analysis ». In: *Mechanical Systems and Signal Processing* 19.4 (2005), pp. 847–864.

[Yan+05b] A.-M. Yan, G. Kerschen, P. De Boe, and J.-C. Golinval. « Structural damage diagnosis under varying environmental conditions—part II: local PCA for non-linear cases ». In: *Mechanical Systems and Signal Processing* 19.4 (2005), pp. 865–880.

[YDG04] A.-M. Yan, P. De Boe, and J.-C. Golinval. « Structural damage diagnosis by Kalman model based on stochastic subspace identification ». In: *Structural Health Monitoring* 3.2 (2004), pp. 103–119.

[YG06] A.-M. Yan and J.-C. Golinval. « Null subspace-based damage detection of structures using vibration measurements ». In: *Mechanical Systems and Signal Processing* 20.3 (2006), pp. 611–626.

[YK19] W.-J. Yan and L.S. Katafygiotis. « An analytical investigation into the propagation properties of uncertainty in a two-stage fast Bayesian spectral density approach for ambient modal analysis ». In: *Mechanical Systems and Signal Processing* 118 (2019), pp. 503–533.

[Zha18] Q. Zhang. « LPV system local model interpolation based on combined model reduction ». In: *IFAC-PapersOnLine* 51.15 (2018). 18th IFAC Symposium on System Identification SYSID 2018, pp. 1104–1109.

[ZR09] V. Zabel and W. Rücker. « Detection of a fatigue crack by vibration tests ». In: *Proceedings of 27th Intnational Modal Analysis Conference - IMAC-XXVII* (2009).

[ZU18] S. Zorn and J.F. Unger. « Probabilistic traffic load identification for concrete bridges ». In: *Proceeding of the 6th International Conference on Integrity-Reliability-Failure*. 2018.

DOCTORAT BRETAGNE LOIRE / MATHSTIC

UNIVERSITÉ DE RENNES 1

Titre : Détection statistique d'endommagements pour les ouvrages d'art par méthodes sous-espaces sous conditions environnementales

Mot clés : Détection d'endommagements, Méthodes sous-espaces, Vibrations, Quantification d'incertitude, Variation de température, Ouvrages d'art

Résumé : La détection automatisée d'endommagements basée sur les mesures vibratoires est pertinente pour la surveillance de l'intégrité des ouvrages d'art. Dans ce contexte, la détection basée sur les techniques sous-espace (SSDD) compare statistiquement les mesures à un modèle de référence. Dans cette thèse, une nouvelle approche est proposée pour améliorer la robustesse de la SSDD pour un usage applicatif réaliste. Tout d'abord, un test statistique est formulé tenant compte des incertitudes statistiques liées aux erreurs sur le modèle obtenu sur des données de référence. Cela conduit à une description précise des propriétés statistiques du test et des seuils d'alarme. Deuxièmement, une approche a été développée pour tenir compte des effets environnementaux sur la SSDD. A partir de mesures de référence dans plusieurs conditions environnementales différentes, un test est proposé détectant un défaut par rapport à une référence obtenue par interpolation. Les méthodes développées sont validées par des simulations numériques et appliquées à des données expérimentales obtenues en laboratoire et sur structures installées en extérieur.

Title: Subspace-based damage detection in engineering structures considering reference uncertainties and temperature effects

Keywords: Damage detection, Subspace methods, Vibrations, Uncertainty quantification, Environmental effects, Civil structures

Abstract: Automated vibration-based damage detection is of increasing interest for structural health monitoring of engineering structures. In this context, stochastic subspace-based damage detection (SSDD) compares measurements from a testing state to a data-driven reference model in a statistical framework. In this thesis theoretical developments have been proposed to improve the robustness of SSDD for realistic applications conditions. First, a statistical test has been proposed considering the statistical uncertainties about the model obtained from the reference data. This leads to a precise description of the test's distribution properties and damage detection thresholds. Second, an approach has been developed to account for environmental effects in SSDD. Based on reference measurements at few different environmental conditions, a test is derived with respect to an adequate interpolated reference. The proposed methods are validated in numerical simulations and applied to experimental data from the laboratory and outdoor structures.